THE UNIVERSITY *of* EDINBURGH

Imaging of abdominal aortic aneurysm disease activity and implications for endovascular aneurysm repair

by

Samuel Debono

MD, MRCS, PGCert Med Ed

A thesis presented for the degree of Doctor of Philosophy

The University of Edinburgh

2023

AD MAIOREM DEI GLORIAM

Lil missieri u ommi, Cost u Odette, u lil qalbi Eva

I dedicate this thesis to my parents:
through all my studies, and despite the distance,
you are my constant, and my very first,
source of support.

And to you, Eva,
for your unwavering belief in me.

Declaration

This thesis represents research that I undertook at The University of Edinburgh Centre for Cardiovascular Science, based at the Chancellor's Building, Edinburgh Imaging Facility and Clinical Research Facility at the University of Edinburgh and Royal Infirmary of Edinburgh between August 2020 and July 2023. The work has not been submitted for any other degree or professional qualification. All work contained herein is my own, except were indicated in the thesis and as summarised on this declarations page.

This thesis was financially supported by the British Heart Foundation Research Excellence Award (RE/18/5/34216) and a British Heart Foundation Project Grant (PG/21/10461). Tissue imaging was funded by the Royal College of Surgeons of Edinburgh research pump priming grant (SPPG/17/110).

I personally designed, drafted the protocol, obtained Research Ethics Committee and NHS research and development (R&D) and Caldicott approvals and undertook recruitment for the symptomatic patients in the retrospective observational study in Chapter 3. The data used for the control subjects and asymptomatic patients were part of a previous study at the University of Edinburgh led by Miss Rachael Forsythe (NCT02229006). Analysis of periaortic fat attenuation, the focus of this chapter, had not been previously performed. I performed all the image analysis, with assistance from Dr Evangelos Tzolos and Dr Michelle Williams, in developing the analysis method.

The repeatability study in Chapter 4 was performed using data from a previous study at the University of Edinburgh led by Miss Rachael Forsythe (NCT02229006). Analysis of sodium [^{18}F]fluoride uptake on volume-based regions of interest with segmentation of the abdominal aorta, the focus of this chapter had not been previously performed. I designed the study with assistance from Professor Marc Dweck and Professor David Newby and assistance from Mr Maaz Syed and Dr Alexander Fletcher in image analysis. I performed all the image analysis whilst Miss Jennifer Nash performed inter-observer image analysis.

I led the clinical studies in Chapters 5 and 6 (NCT04577716). I designed, drafted the protocol, obtained Research Ethics Committee and NHS R&D and Administration of Radioactive Substances Advisory Committee (ARSAC) approvals, undertook all recruitment, trial management, supervised the scanning and performed all image analysis. I was supported in this role by Professor David Newby as Chief Investigator, Miss Rachael Forsythe as Principal Investigator and Mr Maaz Syed and Miss Jennifer Nash as co-investigators. Radiotracer production was performed by the Radiochemistry team at the University of Edinburgh and radiotracer administration was performed by the radiographers at Edinburgh Imaging. The pre-operative imaging data in Chapter 5 were obtained as part of a previous study at the University of Edinburgh led by Miss Rachael Forsythe (NCT02229006).

Tissue sampling was obtained through the efforts of Mr Jakub Kaczynski and Miss Rachael Forsythe. Tissue sectioning, staining and slide-scanning was performed by the Shared University Research Facilities at the University of Edinburgh. Ex vivo imaging was performed by Dr Adriana Tavares' pre-clinical team mainly Mr Carlos Alcaide-Corral and Dr Mark MacAskill. I performed the quantitative image analysis with support from Dr Calum Gray, Dr Mark MacAskill and Dr Adriana Tavares. Histopathological analysis was performed by Dr David Dorward, from the Pathology department at the Royal Infirmary of Edinburgh.

At the time of writing, Chapters 1, 4 and 5 have been published in peer-reviewed journals and I am first author for these papers. Chapters 3 and 6 are currently under review with a peer-reviewed journal and I am first author. I have also led, performed and completed recruitment for the longitudinal clinical study for which clinical outcomes are awaited (Chapter 7).

All research was conducted within the principles of Good Clinical Practice, in accordance with the Declaration of Helsinki and the East Scotland and South-East Scotland Research Ethics Committees.

Mr Samuel Debono

13th October 2023

Abstract

Background

Abdominal aortic aneurysm treatment pathways are initiated when an aortic size threshold of 55 mm is reached as this signifies a high annual risk of rupture due to presumed active aneurysm disease. Endovascular aneurysm repair (EVAR) is one treatment modality which reduces the procedural morbidity and mortality associated with open surgical repair. However, EVAR patients can develop complications such as leaks behind their stent graft (endoleak) which reduces the long-term benefit of EVAR. Here, we explore the use of two potential imaging biomarkers, periaortic adipose tissue (on computed tomography) and sodium [^{18}F]fluoride positron emission tomography, in different abdominal aortic aneurysm disease states to better understand the disease process and to assess its implications in EVAR.

Methods

First, we assessed periaortic adipose tissue attenuation in 70 patients with untreated abdominal aortic aneurysm disease (asymptomatic, symptomatic and rupture patients) and 18 control subjects **(Chapter 3)**. Then, in 25 patients with an abdominal aortic aneurysm, we developed a method of quantifying sodium [^{18}F]fluoride uptake on positron emission tomography, which we termed aortic microcalcification activity (AMA) **(Chapter 4)**. We then considered sodium [^{18}F]fluoride uptake in 10 patients before and after their aneurysm was treated with EVAR **(Chapter 5)**. Following this, we assessed sodium [^{18}F]fluoride uptake in 37 patients whose aneurysm had been treated

with EVAR, in 15 of whom this had been complicated by endoleak formation **(Chapter 6)**.

Results

There were no differences in the periaortic adipose tissue attenuation in aneurysmal and non-aneurysmal segments of the aorta in asymptomatic patients (-81.4±7 versus -75.4±8 Hounsfield units, HU) and comparable segments in control subjects (-83.3±9 versus -78.8±6 HU, $p>0.05$ for all comparisons). However, symptomatic patients demonstrated higher periaortic adipose tissue attenuation in both aneurysmal (-57.9±7 HU, $p<0.0001$) and non-aneurysmal segments (-58.2±8 HU, $p<0.0001$).

There was moderate-to-good agreement between mean tissue-to-background ratio and aortic microcalcification activity (AMA) measurements (intraclass correlation co-efficient, 0.88). These, sequentially improved with the application of thresholding (intraclass correlation coefficient 0.93, 95% confidence interval 0.89–0.95) and variable diameter (intraclass correlation coefficient 0.97, 95% confidence interval 0.94–0.99) techniques. The optimised method had good intra-observer (mean 1.57 ± 0.42, bias 0.08, coefficient of repeatability 0.36 and limits of agreement -0.43 to 0.43) and inter-observer (mean 1.57 ± 0.42, bias 0.08, co-efficient of repeatability 0.47 and limits of agreement -0.53 to 0.53) repeatability.

We found that following EVAR, sodium [^{18}F]fluoride uptake was markedly reduced in the suprarenal (0.62 reduction, p=0.03), neck (0.72 reduction, p=0.02) and body of the aneurysm (0.69 reduction, p=0.02) while it remained unchanged in the thoracic aorta (0.11 reduction, p=0.41).

When compared to those without an endoleak, patients with an endoleak had higher AMA in the thoracic (1.22±0.2 versus 1.07±0.2, p<0.01), suprarenal (1.58±0.3 versus 1.36±0.2, p<0.05) and neck (1.40±0.3 versus 1.14±0.3, p<0.05) regions of the aorta but not within the aneurysm body (0.94±0.3 versus 1.08±0.3, p>0.05).

Conclusion

Periaortic adipose tissue attenuation is not increased in stable abdominal aortic aneurysm disease. The generalised increase in patients with symptomatic disease likely reflects the systemic consequences of acute rupture. Aortic microcalcification activity (AMA) provides repeatable measures of sodium [^{18}F]fluoride uptake that are comparable to established methods. EVAR is associated with a reduction in AMA within the stented aortic segment, whilst endoleaks after EVAR are associated with higher AMA in aortic regions outside the aneurysm. These findings suggest that whilst EVAR can modify aortic disease activity within the treated aneurysm, aortic degeneration appears to continue beyond the aneurysm. Aortic sodium [^{18}F]fluoride uptake is a promising non-invasive measure of aneurysm disease activity that may inform treatment strategies and provide additional prognostic information.

Lay Summary

The aorta is the main blood vessel which carries blood around the body. It can become diseased and increase in size. This enlargement is called an abdominal aortic aneurysm. The larger it gets, the higher the chance it has of bursting (rupture). Rupture can be fatal, so when aneurysms reach a certain size, they need to be repaired to prevent this from happening. A modern approach to treatment uses a metal scaffolding, called a stent graft, to protect the weak diseased aneurysm wall from the blood pressure. This procedure is called Endovascular Aneurysm Repair (EVAR). Whilst this is a safe operation in the short term, in the longer term, blood can leak behind the stent and cause an endoleak. Endoleaks happen either because the stent graft has moved or because the aorta continues to increase in size. These two mechanisms appear to be directed by ongoing aneurysm disease activity within the aorta.

This thesis looked at using new scanning techniques to better understand aneurysm disease activity, to understand why in certain patients EVAR treatment can result in endoleaks.

We looked at computed tomography (CT) scans performed in routine and emergency clinical practice. We selected different parts of the fat around the aorta to get more information about the aneurysm. We found that aortas that are going to or have burst, have changes in this fat not just in the aneurysm but through the whole of the aorta.

Then, we used a research scan, called sodium [^{18}F]fluoride positron emission tomography (PET) combined with CT. This technique uses a small radioactive dye to identify areas of the aorta with high levels of aneurysm disease activity. These areas are called microcalcification and are not visible on CT. We refined our method of analysis to split the aorta and to obtain several measures of microcalcification in different parts of the aorta. First, we found that after EVAR is performed, there is a reduction in the disease activity in the aneurysm and in other parts covered by the stent graft. Then, we also found that after EVAR, patients with an endoleak have higher levels of microcalcification, not necessarily in the aneurysm itself but in other parts of the aorta away from the aneurysm.

These results could have implications for the future treatment of patients with abdominal aortic aneurysm because, by helping us to understand the change in aneurysm disease activity in patients treated with EVAR, these scanning techniques could help us select the most appropriate treatment for individual patients.

Acknowledgements

My time in clinical research and this thesis would not have been possible without the support of a large group of people, and for this I owe them thanks and gratitude.

My primary supervisor Professor David Newby, whose knack at making what seem like unsurmountable challenges look simpler, and his open-door policy provided me with reassurance and guidance. My secondary supervisors, Professor Marc Dweck, who has a great understanding of PET image analysis, and Miss Rachael Forsythe, whose research groundwork made my PET study possible. Lynn McKinlay, Prof. Newby's personal assistant who was crucial in helping me navigate the administrative aspects of university research. She also made me feel welcome when I first started in the middle of the Covid-19 pandemic, where multiple new meetings with research staff had to happen virtually.

The Centre for Cardiovascular Science is composed of various teams who ensured that my research could take place: the staff at the Clinical Research Facility and the staff at the Imaging Facility. These include the administrative, IT support, radiotracer production team, physicists and the clinical radiographers.

The vascular surgery teams at the study site and the three patient identification centres, without them recruitment would never have been completed: the

Royal Infirmary of Edinburgh, Queen Elizabeth University Hospital in Glasgow, University Hospital Hairmyres and Ninewells Hospital.

The study patients, who voluntarily gave up their time, sometimes travelling for long distances, this research would not have been possible without you.

Through these three years I have met some wonderful people in the “Barn”: The encouragement, enthusiasm, sense-checking, long commutes, lunch in the CB café, laughter and friendships made all difference. In particular, Maaz you are an R-wizard, Alex your scientific mind is exceptional, Jen your humour and chats brightened up my days.

My parents, you were the first to ignite in me a thirst for knowledge, I wouldn’t have come this far without your support. And finally, my fiancée Eva, you patiently had to sit and listen to my research ups and downs through the last three years. You always believed I would get to the end.

Thank you.

Contents

DECLARATION III

ABSTRACT VI

LAY SUMMARY IX

ACKNOWLEDGEMENTS XI

CONTENTS XIII

ABBREVIATIONS XVII

CHAPTER 1: INTRODUCTION 1

1.1 The abdominal aorta **2**
1.1.1 Histology and embryology 2

1.2 Abdominal aortic aneurysms **3**
1.2.1 Pathological mechanisms associated with aortic aneurysm disease 4
1.2.2 Risk factors, prevalence and screening 6
1.2.3 Aneurysm growth and repair thresholds 7

1.3 Treatment of abdominal aortic aneurysms **9**
1.3.1 Open surgical repair 9
1.3.2 Endovascular aneurysm repair 10
1.3.2.1 Endoleaks 15
1.3.3 Clinical trials and practice guidelines 21
1.3.4 Emergency treatment 26

1.4 Imaging the aorta **27**
1.4.1 Surveillance following EVAR 29
1.4.2 Outcome risk prediction 32

1.5 Biomarkers of aortic disease activity **33**
1.5.1 Periaortic adipose tissue 35
1.5.2 Positron emission tomography 37
1.5.2.1 2-[^{18}F]fluoro-2-deoxyglucose 38
1.5.2.2 Sodium [^{18}F]fluoride 40

1.6 Aim and hypothesis **42**

CHAPTER 2: METHODS 44

2.1 Study populations **45**

2.2 Study regulations **47**

2.3 Recruitment **49**

2.4 Study visit **51**

2.5 Computed tomography **52**
2.5.1 Periaortic adipose tissue study 54
2.5.1.1 Adipose tissue assessment 54

2.6 Sodium [^{18}F]fluoride positron emission tomography and computed tomography **58**
2.6.1 Image acquisition 59
2.6.2 Image analysis 61
2.6.2.1 Radiotracer uptake quantification 61

2.7 Ex vivo study **65**

2.8 Statistical analysis **68**

CHAPTER 3: PERIAORTIC ADIPOSE TISSUE IN ABDOMINAL AORTIC ANEURYSMS 71

3.1 Abstract **72**
3.1.1 Background 72
3.1.2 Methods 72
3.1.3 Results 72
3.1.4 Conclusion 73

3.2 Introduction **73**

3.3 Methods **74**

3.4 Results **77**
3.4.1 Periaortic adipose tissue attenuation 77
3.4.2 Visceral and subcutaneous fat attenuation 78

3.5 Discussion **79**

3.6 Clinical Perspectives **89**

CHAPTER 4: QUANTIFYING SODIUM [^{18}F]FLUORIDE UPTAKE IN ABDOMINAL AORTIC ANEURYSMS 90

4.1 Abstract **91**
4.1.1 Background 91
4.1.2 Methods 91
4.1.3 Results 91
4.1.4 Conclusion 92

4.2 Introduction **92**

4.3 Methods **93**
4.3.1 Sodium [^{18}F]fluoride PET-CT 94
4.3.2 Image Analysis 94
4.3.3 Background blood pool 95
4.3.4 Volumes of interest within the aorta 95
4.3.5 Tissue to background ratio 95
4.3.6 Abdominal aortic microcalcification activity 96
4.3.7 Intra-observer and inter-observer repeatability 100
4.3.8 Ex vivo tissue 100
4.3.9 Statistical analysis 102

4.4 Results **103**
4.4.1 Abdominal aortic aneurysm sodium [^{18}F]fluoride uptake 103
4.4.1.1 Maximum Values 103
4.4.1.2 Mean Values 103
4.4.2 Enhanced image analysis technique 104
4.4.2.1 Maximum Threshold 104
4.4.2.2 Aneurysm variable radius 104
4.4.3 Intra-observer and inter-observer repeatability 115
4.4.4 Ex vivo tissue 115

4.5 Discussion **124**

4.6 Clinical Perspectives **128**

CHAPTER 5: AORTIC SODIUM [^{18}F]FLUORIDE UPTAKE FOLLOWING ENDOVASCULAR ANEURYSM REPAIR 130

5.1 Abstract **131**
5.1.1 Background 131
5.1.2 Methods 131
5.1.3 Results 131
5.1.4 Conclusion 132

5.2 Introduction **132**

5.3 Methods **133**
5.3.1 Study assessments 134
5.3.2 Image Analysis 135
5.3.2.1 Aortic morphology and calcium score 135
5.3.2.2 Aortic microcalcification activity 135
5.3.3 Statistical Analysis 136

5.4 Results **136**
5.4.1 Aortic morphology 138
5.4.2 Aortic microcalcification activity 138

5.5 Discussion **143**

5.6 Clinical Perspectives **151**

CHAPTER 6: AORTIC DISEASE ACTIVITY IN PATIENTS WITH ENDOLEAK AFTER ENDOVASCULAR ANEURYSM REPAIR 152

6.1 Abstract **153**
6.1.1 Background 153
6.1.2 Methods 153
6.1.3 Results 153
6.1.4 Conclusion 154

6.2 Introduction **154**

6.3 Methods **155**
6.3.1 Study population 156
6.3.2 Positron emission tomography and computed tomography 156
6.3.3 Image analysis 157
6.3.4 Statistical analysis 158

6.4 Results **158**
6.4.1 Aortic microcalcification activity 162

6.5 Discussion **170**

6.6 Clinical Perspectives **174**

CHAPTER 7: CONCLUSIONS AND FUTURE DIRECTIONS 175

7.1 Main findings **176**
7.1.1 Periaortic adipose tissue 177
7.1.2 Sodium [^{18}F]fluoride PET-CT 178

7.2 Future directions **180**
7.2.1 Perivascular adipose tissue in patients with peripheral arterial disease 181
7.2.2 Aortic radiotracer quantification 182
7.2.3 Predicting endoleaks following EVAR using sodium [^{18}F]fluoride 183
7.2.4 Other radiotracers 187

7.3 Conclusion **190**

JOURNAL PUBLICATIONS AND PRIZES 191

REFERENCES 193

Abbreviations

[^{18}F]FDG	2-[^{18}F]fluoro-2-deoxyglucose
AMA	aortic microcalcification activity
ANOVA	analysis of variance
CT	computed tomography
DICOM	Digital Imaging and Communications in Medicine
EDTA	ethylene diamine tetra-acetic acid
EVAR	endovascular aneurysm repair
HbA1c	glycated haemoglobin
HU	Hounsfield units
MBq	megabecquerel
MDT	multidisciplinary team
microPET	micro-positron emission tomography
MRI	magnetic resonance imaging
mSv	milliSieverts
PACS	Picture Archiving and Communications System
PET	positron emission tomography
PET-CT	positron emission tomography-computed tomography
PET-EVAR	Predicting Endoleaks Following Endovascular Aortic Aneurysm Repair Using Sodium [^{18}F]Fluoride
SoFIA^3	Sodium [^{18}F]Fluoride Imaging of Abdominal Aortic Aneurysms
SUV	standard uptake values
TBR	tissue-to-background ratios
USPIO	ultrasmall superparamagnetic particles of iron oxide

Chapter 1: Introduction

Published by **Debono S**, Nash J, Tambyraja AL, Newby DE, Forsythe RO. Endovascular repair for abdominal aortic aneurysms. *Heart*. 2021 Nov;107(22):1783-1789. doi: 10.1136/heartjnl-2020-318288. Epub 2021 Mar 4. PMID: 33674354.

1.1 The abdominal aorta

The aorta is the largest blood vessel in the body. It delivers blood from the left ventricle to the rest of the body and the limbs. As it makes its way along from its origin to the end it is given different names depending on which anatomical structures it has passed through or which branches are given off. The abdominal aorta begins at the aortic hiatus of the diaphragm when the descending thoracic aorta enters the abdomen at approximately the lower level of the 12^{th} thoracic vertebra. It ends when it divides into the right and left common iliac arteries at approximately the 4^{th} lumbar vertebra (Drake et al., 2005).

Within the abdomen, the abdominal aorta gives off several branches which supply the abdominal viscera. Originating sequentially from the anterior surface are the coeliac trunk and the superior mesenteric artery (which supply the foregut and midgut respectively). Below these are the two renal arteries which originate from the lateral surface and further down is the anteriorly originating inferior mesenteric artery (which supplies the hindgut). Along the length of the abdominal aorta, there are also several posterior branches which supply the diaphragm and body wall (inferior phrenic arteries), and the spinal cord (four pairs of lumbar arteries) (Drake et al., 2005).

1.1.1 Histology and embryology

The aortic wall is comprised of three layers: the tunica intima, media and adventitia. The innermost (luminal) layer is the intimal layer and it is made up

of endothelial cells in direct contact with the blood on one side and with the internal elastic lamina on the other (containing elastin-rich collagen, fibroblasts and smooth muscle cells). The medial layer is made up of spirally-arranged smooth muscle cells, and structural proteins such as elastic tissue and collagen and this gives the aorta its mechanical properties. These components are arranged together as lamellar units (concentric layers of elastin with interspersed cells and collagen). The outermost layer, the adventitia, is mainly composed of collagen and serves to anchor the aorta in place in relation to adjacent structures (Boron & Boulpaep, 2005; Singh et al., 2018).

Whilst the ascending aorta and the arch are embryologically derived from the neural crest, the thoracic aorta originates from mesodermal somites and the abdominal aorta from the splanchnic mesoderm. The abdominal aorta is subsequently less distensible, has less lamellar units than the thoracic aorta and has an avascular media (Singh et al., 2018).

1.2 Abdominal aortic aneurysms

An arterial aneurysm is dilatation of the blood vessel when compared to its original diameter. The abdominal aorta is defined as being aneurysmal when its diameter is at least one and a half times the normal aortic diameter at the level of the renal arteries, this would be greater than 30 mm (Aggarwal et al., 2011).

Abdominal aortic aneurysms are progressive, and as the aorta enlarges the vessel wall becomes weaker, increasing its risk of rupture. Rupture refers to acute haemorrhage from the aneurysm beyond the true aortic wall. Aortic rupture is a surgical emergency which if left untreated, invariably results in death. The current best clinical predictor of aneurysm rupture is its size and therefore patients with an abdominal aortic aneurysm undergo regular surveillance with assessment of the aneurysm diameter using ultrasound (Sakalihasan et al., 2005). In the United Kingdom, when an abdominal aortic aneurysm reaches a threshold diameter of 55 mm or expands by more than 10 mm in a year, surgical repair is considered to prevent the risk of aneurysm rupture.

1.2.1 Pathological mechanisms associated with aortic aneurysm disease

The pathophysiology of abdominal aortic aneurysms is not completely understood. There appears to be a reduction of smooth muscle cells as a result of apoptosis and degeneration of the aortic media (Carmo et al., 2002; López-Candales et al., 1997). Inflammation, production of reactive oxygen species and endoplasmic reticulum stress have been associated with smooth muscle atrophy (Qin et al., 2017). It is therefore plausible that this atrophy may be triggered by an initial inflammatory response secondary to exposure to common cardiovascular risk factors such as smoking, dyslipidaemia, and hypertension. This leads to endothelial dysfunction and the production of vasoactive substances. These stimuli trigger an immune-mediated response,

leading to neutrophil infiltration at the junction between the media and adventitia (M. B. J. Syed et al., 2019).

The principal immune mediator in aneurysm disease appears to be CD4+ T-lymphocytes through the production of interferon-alpha (Xiong et al., 2004). T helper 2 (Th2) cells, which produce interleukin-4, interleukin-5 and interleukin-13, are also strongly implicated (Shen & LeMaire, 2017). The local production of interleukins affects the media directly by reducing vascular smooth muscle cells and increasing breaks in elastin. Downstream activation of macrophages and natural killer cells stimulate the production of matrix metalloproteinases (MMP). In particular, the local production of MMP-9 accelerates the degradation of the intracellular matrix and causes further weakening of the arterial wall (Bersi et al., 2017). This process results in aortic remodelling which leads to a reduction in elastin, collagen, glycosaminoglycans, and an imbalance of matrix metalloproteinases, reducing the amount of connective tissue protein content and aortic wall strength which results in loss of structural integrity and aortic dilatation (Quintana & Taylor, 2019).

The atrophic activity within the media leads to the release of free extracellular calcium (New et al., 2013). This stimulates a phenotypic change in vascular smooth muscle cells that mimics osteoblastic function (Fuery et al., 2018). The extracellular calcium is then deposited as microscopic hydroxyapatite crystals (containing calcium phosphate) within the extracellular space. This microcalcification is a marker of active disease (Joshi et al., 2014). In contrast,

macroscopic plaque formation occurs when medial calcium amalgamates into larger lesions. Established calcified plaque which is visible on conventional CT, is a late change and signifies chronic healed inflammation. Meanwhile, microcalcification is beyond the resolution of CT and is thought to be indicative of more active disease (M. B. J. Syed et al., 2019).

1.2.2 Risk factors, prevalence and screening

The strongest modifiable risk factor in abdominal aortic aneurysm disease is cigarette smoking. In a screening and validation study of United States veterans, smoking habit increased the odds of having an abdominal aortic aneurysm five-fold (Lederle et al., 2000), whereas a healthier lifestyle (consisting of weekly exercise, and consumption of fruit and vegetables) reduced the risk (Kent et al., 2010). Hypertension and atherosclerosis are similarly associated conditions, however patients with diabetes mellitus appear to be less likely to develop an aneurysm (Jahangir et al., 2015; Lederle et al., 2000). This difference in risk factors underscores some important differences between the pathophysiology of atherosclerotic and aneurysmal disease.

Non-modifiable risk factors include male sex, increasing age, family history, concomitant peripheral artery aneurysms, and white ethnicity (Jahangir et al., 2015). It is unclear why women are less likely to develop aneurysms, however they do have higher rates of ruptures and higher 30-day mortality and more complications after treatment (Johansson & Harris, 2017). These

considerations should therefore be taken into account both when considering size thresholds but also treatment strategies.

The prevalence of abdominal aortic aneurysms is extremely low before the age of 55 years but increases after this: it is present in up to 2.3% in the 75 to 79-year age group (2275 per 100,00 population) (Sampson et al., 2014). Prevalence data in 65-year-old men suggest that aneurysms are present in 1.5% of the Swedish (2006 to 2014) (Wanhainen et al., 2016) and 1.34% of the English (2009 to 2013) screening programmes (Jacomelli et al., 2016).

In Sweden and the United Kingdom, abdominal aortic aneurysm screening programmes only cover men, where patients are invited for an abdominal ultrasound scan at the age of 65 years. In the United States, screening is recommended for men aged 65 to 74 years with a past or current smoking habit. Screening programmes reduce all-cause and disease-specific mortality due to early detection and treatment (Takagi et al., 2018).

1.2.3 Aneurysm growth and repair thresholds

Individual patient data meta-analysis of 15,475 individuals with a small aneurysm (30 to 54 mm diameter) showed a growth rate of 2.2 mm per year (Sweeting et al., 2012). This is higher in current smokers (2.6 mm per year) and lower in patients with diabetes (1.7 mm per year). Rupture rate is strongly associated with smoking and the female sex. The use of common cardiovascular drugs (beta-blocker, calcium channel blocker, antiplatelet or

antihypertensive therapies) does not correlate with growth rates, except for statin therapy which is associated with lower growth rates (Salata et al., 2018). In randomised controlled trials, angiotensin converting enzyme inhibitor therapy (Golledge et al., 2020) and doxycycline (Baxter et al., 2020) have no effect on aneurysm growth. An observational cohort study found that there was a lower incidence of abdominal aortic aneurysm related events in patients with diabetes who were prescribed metformin than those who weren't prescribed metformin compared to those who were not diabetic (Golledge et al., 2019). Studies exploring the effect of metformin therapy are currently ongoing (ClinicalTrials.gov numbers NCT04224051 and NCT04500756).

Since patients with abdominal aortic aneurysms are also at high risk of all cardiovascular events, five-year survival rates are higher in those taking antiplatelet, statin or antihypertensive therapies (Bahia et al., 2016). Adequate drug therapy management of these medical conditions is therefore recommended on recent abdominal aortic aneurysm guidelines (Wanhainen et al., 2019).

Most aneurysms are considered for repair after a diameter of 55 mm is reached, or when rapid growth occurs (more than 10 mm per year) (Chaikof et al., 2018; NG156, 2020; Wanhainen et al., 2019). A size of 55 mm was agreed upon because less than 50 mm had such a low rupture risk which then greatly increased between 50 and 60 mm. In fact, a Cochrane review summarised the four trials on which size threshold recommendations are based. The annual

risk of rupture when comparing surveillance versus repair was found to be less than 1% below 50 mm, 10% between 50-60 mm, and 20% above 60 mm. Furthermore, endovascular treatment of patients with a diameter of 40 to 55 mm showed no survival advantage and is not recommended at these small sizes (Ulug et al., 2020).

1.3 Treatment of abdominal aortic aneurysms

Abdominal aortic aneurysms can be treated by performing open surgical repair or endovascular aneurysm repair (EVAR). EVAR use has increased as technique and technology have developed. In the United States, EVAR was performed in 76% of all aneurysm repairs in 2013 (Suckow et al., 2018). This proportion was 58% in Sweden in repairs performed between 2010 to 2014 (Lilja et al., 2017). In the United Kingdom, having been 61% before the Covid-19 pandemic in 2019, it was 59% in 2021 (Waton et al., 2020; Waton et al., 2022).

1.3.1 Open surgical repair

Open surgical repair is performed through either a midline vertical or a transverse abdominal incision. A textile polyester graft such as Dacron is used to replace the diseased aorta. After the aorta is cross-clamped, the proximal anastomosis is sutured as close to the renal arteries as possible to prevent later aneurysm formation in the remaining infrarenal aortic neck. Aneurysm anatomy dictates whether the graft is a simple tube or bifurcated “trouser” graft. The distal anastomoses are completed at either common iliac, external iliac,

or femoral arteries as necessary. Open repair is a high-risk operation, with reported inpatient mortality as high as 10% (Holt et al., 2007) but greatly reduced (3.1%) in higher volume centres (Waton et al., 2022). Apart from mortality, a range of long-term serious complications can occur in both open repair and EVAR (Table 1).

1.3.2 Endovascular aneurysm repair

EVAR involves the insertion of a stent graft within the abdominal aortic aneurysm. It works by reinforcing the diseased aortic wall by excluding the dilated aneurysm sac from the circulation from the inside of the artery (Parodi et al., 1991). The proximal and distal aspects of the stent need to provide an adequate seal with the native arterial wall so that blood cannot leak around the endograft and enter the aneurysm sac. If this does happen, ongoing sac expansion and secondary aneurysm rupture can occur.

The stent is made of nitinol (a nickel-titanium alloy) covered with polytetrafluoroethylene. It has its own delivery system and is self-expanding. The proximal part of the graft is held in place by barbs or anchors at its proximal end to ensure adequate fixation. The repair is planned according to each individual's aneurysm anatomy. The complete endograft is comprised of modular parts of at least two or three separate components including a bifurcate main body and limb components. The modular parts provide a degree of flexibility in size selection, although the physical overlap between each component must be sufficient to ensure that no intervening leaks occur.

Table 1. **Long-term complications common to endovascular and open aneurysm repair**

Complication	**Estimated incidence**		**Details**
	EVAR	**Open**	
Limb kinking and/or occlusion	1.4-8%	1-5%	Kinks within the graft limbs can be asymptomatic, but occlusions can present with symptoms of new onset (acute) or worsening limb ischaemia. These should be imaged and treated as clinically necessary. In EVAR, the biggest risk for limb occlusion is landing the limb in the external iliac artery and the landing artery diameter (Conway et al., 2012; Faure et al., 2015).
Graft infection	0.2-1%	0.3-6%	Graft infection is more likely to occur if prosthetic material is present in the groin. Treatment includes surgical excision of the graft and debridement of the operative field. It has a high morbidity, with a 25% risk of re-infection, and a 54% five-year mortality (Charlton-Ouw et al., 2014).
Secondary aorto-enteric fistula	0.3-0.5%	0.3-0.5%	Rare but serious. This usually presents with significant gastrointestinal bleeding. Removal of all infected material with concurrent surgical reconstruction is necessary for definite treatment, but bridging endovascular therapy is sometimes performed in the immediate setting to prevent catastrophic haemorrhage and death.

Secondary aortic rupture	1-5%	<1%	Rupture secondary to clinical failure of the stent graft e.g., due to untreated endoleak. In open repair this may be secondary to aneurysm formation in the infrarenal aortic segment or graft infection.
Sexual dysfunction	16%	27%	Sexual dysfunction can occur in both types of repairs and although risk factors and therapeutic options are as yet undefined. Certain operative factors may play a role e.g., dissection close to the pelvic nerve plexus in tube graft open repair or bilateral occlusion of internal iliac arteries in EVAR. Discussion at the consent process is therefore important.

EVAR, endovascular aneurysm repair.

The effectiveness of EVAR is dependent on achieving a good seal with the native arteries at the proximal and distal sealing zones, i.e., the infrarenal aortic neck and (usually) the common iliac arteries. Manufacturers' 'Instructions for Use' refer to endograft-specific anatomical requirements which aneurysm anatomy must adhere to, in order to reduce the risk of stent migration, endoleak formation and late aneurysm rupture. Instructions for Use give recommended morphological features at the sealing zones and outline the hostile neck features that are incompatible with the use of a specific endograft (Table 2). Additionally, there must be adequate femoral access, and no substantial or circumferential calcification or thrombus in the landing zones (Wanhainen et al., 2019). If one of the iliac seal zones is of insufficient quality i.e., too short or aneurysmal, other options are available. The iliac artery can be occluded with a plug and a surgical femoro-femoral crossover graft is fashioned to perfuse the leg in question after insertion of an aorto-uni-iliac stent. Alternatively, an iliac branch device may be used. This involves inserting a further bifurcated endograft into the common iliac artery, with limbs into the internal and external iliac arteries.

The stent graft is delivered into the aneurysm under fluoroscopic guidance through sheaths inserted into the femoral arteries (Figure 1). Open cut-down onto the femoral arteries may be required, although percutaneous EVAR with sheath insertion using ultrasound and fluoroscopic guidance is increasingly performed. This requires pre-deploying closure devices into the common femoral artery before sheath insertion and fully deploying them upon sheath

Table 2. **Features of a hostile neck which can preclude use of a 'standard' stent graft**

Hostile Neck Features
Short neck of less than 10 mm
Infrarenal angulation of more than 60°
Conical or reverse tapered
Infrarenal diameter of more than 28 mm
Circumferential mural thrombus or calcification

(Stather et al., 2013)

removal to close the arterial puncture site. A systematic review found that percutaneous access is associated with a lower frequency of post-operative groin infection and lymphocoele formation, and a reduction in procedure time and hospital stay. There was no additional risk of haematoma formation, pseudoaneurysm, or arterial thrombosis (Hajibandeh et al., 2016). This approach is less invasive and allows EVAR to be performed under local anaesthesia, sometimes even as a day case procedure.

EVAR has a shorter post-procedural hospital stay and improved 30-day survival when compared to open surgery. However, EVAR is associated with a higher rate of reintervention and over time the early survival advantage gained is lost (Greenhalgh, Brown, Powell, Thompson, Epstein, et al., 2010).

1.3.2.1 Endoleaks

The effectiveness of an EVAR stent graft to maintain a proximal seal is dependent on the quality of aortic tissue to maintain its position. Long-term EVAR durability is compromised by endoleak formation. Endoleak is the presence of persistent blood flow within the aneurysm sac but outside of the stent graft. It can be observed either immediately following stent graft delivery (early) or it can develop months or years after the procedure (late). There are five types of endoleaks, and they are classified by their origin (Figure 2).

Inflow of blood around the stent graft can result in a pressurised aneurysm sac which may lead to rupture (Fransen et al., 2003). Therefore, an obvious type

Figure 1. **Operative imaging of an abdominal aortic aneurysm**

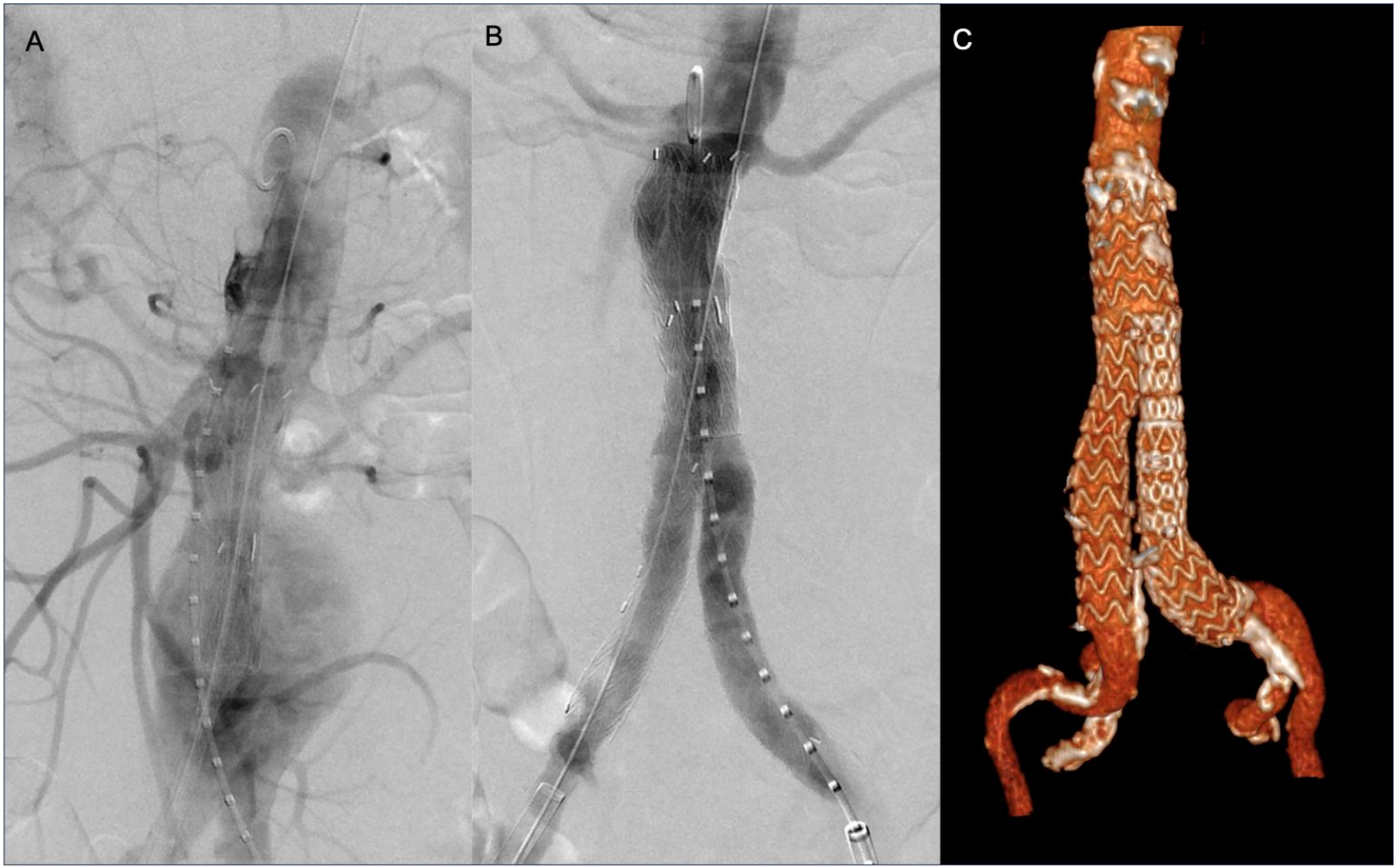

A. Intraoperative fluoroscopy showing digital subtraction angiography of the non-deployed stent graft within the abdominal aorta and aneurysm. Contrast can be seen within the aortic branches and the aneurysm sac and the aortic bifurcation.
B. Digital subtraction angiography after the stent graft was deployed demonstrating correct position and absence of endoleaks.
C. Three-dimensional reconstruction of a post-operative computed tomography angiography showing a stent graft in place.

Figure 2. **Types of endoleak**

A. Type I: This results from loss of seal at the proximal or distal sealing zones. It is further categorised depending on location of seal loss. IA, proximal seal loss; IB, distal seal loss; IC, an iliac plug (not shown).
B. Type II: Blood flow within the sac from patent collateral arteries arising from the aneurysm itself, such as the inferior mesenteric artery (type IIA) or lumbar arteries (type IIB).
C. Type III: Loss of seal arising from either around the junctions of the different modular parts (type IIIA) or due to holes in the graft fabric (type IIIB).

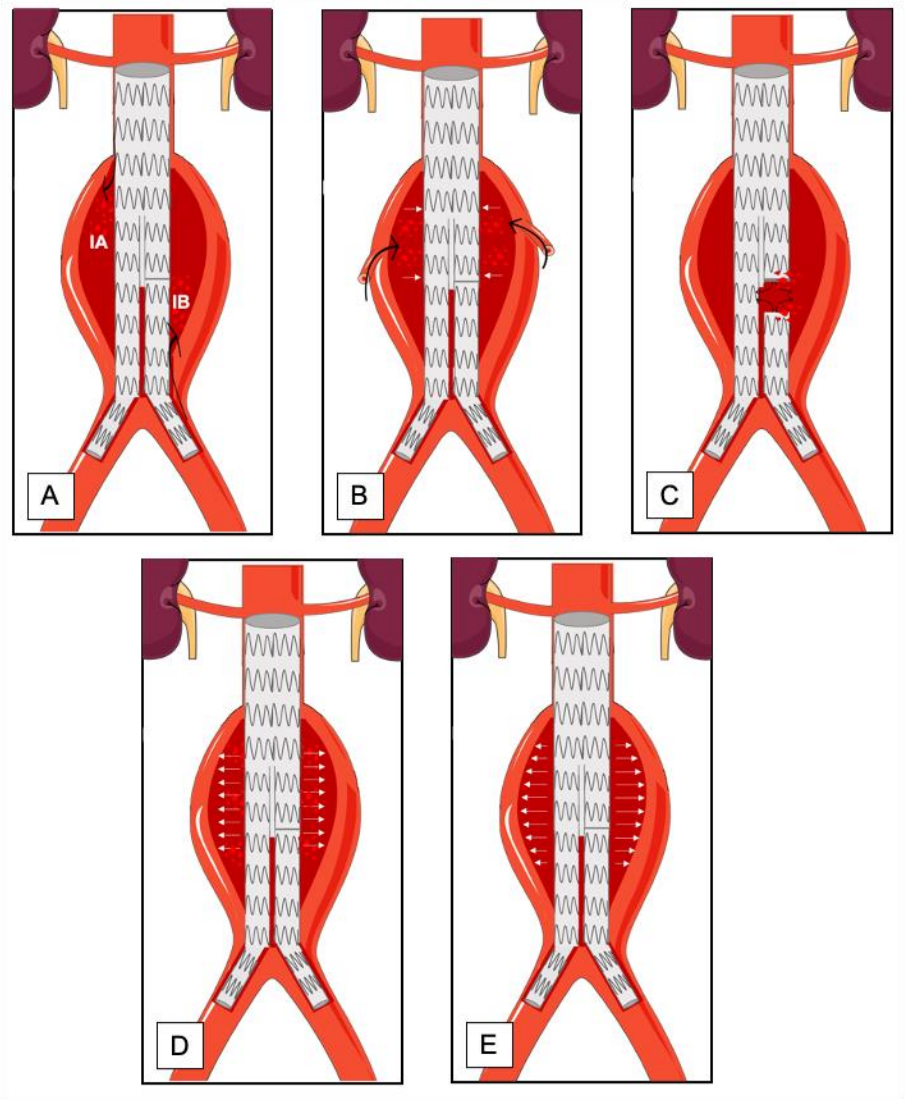

D. Type IV: This occurs due to graft porosity and used to be more common with older generation stent grafts.
E. Type V: Sometimes described as endotension, this refers to sac enlargement on serial imaging in the absence of a visualised endoleak. Other types of endoleaks should be completely excluded first.

Black arrows indicate direction of blood and white arrows indicate pressure within the sac.

IA or type III endoleak which is noted on completion angiography at the end of the procedure requires immediate treatment. Type IA endoleak occurs more frequently when the aforementioned hostile neck features are present (Table 2) (Chaikof et al., 2018). In contrast, around half of early type II endoleaks appear to follow a more benign course and tend to be managed conservatively unless there is aneurysm sac growth. Surveillance of type II endoleaks without intervention is not associated with an increased risk of aneurysm-related mortality, all-cause mortality, sac expansion, or type I endoleak development (Sidloff et al., 2014).

Type II endoleaks, which arise from collateral vessels are the most common type of endoleak. However, a proportion of endoleaks occur as a consequence of progression of aneurysmal disease and continued changes in aortic morphology, or components of the stent may dissociate leading to loss of proximal or distal sealing zones of the stent graft and perfusion of the aneurysm sac (Lal et al., 2015). The presence of the defective pre-existing aortic stent graft can make the repair of a ruptured aorta even more technically challenging and sometimes impossible.

Stent graft migration is defined as more than a 10-mm movement of the graft or stent resulting in symptoms or the need for re-intervention (Chaikof, Blankensteijn, et al., 2002). Stent migration can result in a type I endoleak, separation of modular components or graft occlusion. Similar to type IA endoleak, stent migration is more likely to occur when hostile neck features

are present (Stather et al., 2013). Device adjuncts have been developed with the aim of reducing the risk of type I endoleak and migration, especially in short necks. These include circumferentially deploying helically shaped anchors (EndoAnchors) to tack the endograft to the wall of the aortic neck (Jordan et al., 2016).

1.3.3 Clinical trials and practice guidelines

Four major randomised controlled trials have compared EVAR and open surgical repair (Table 3). A further meta-analysis of the individual patient data (2,783 patients) at 5 years confirmed the original trial findings. The early (0 to 6 months) reduction in EVAR group mortality (pooled hazard ratio 0.61; confidence interval 0.42 to 0.89; p=0.010) changed within 3 years and the survival rates converged. Beyond this, aneurysm-related mortality was higher in the EVAR group (pooled hazard ratio 5.16; confidence interval 1.49 to 17.89; p=0.010). There was no early survival advantage with EVAR in patients with moderate renal dysfunction or coronary artery disease (Powell et al., 2017). Long term follow-up of these trials has shown that EVAR is not associated with a higher risk of death due to cancer, but a greater need for re-intervention (hazard ratio 2.13; confidence interval 1.69 to 2.68; p<0.001) (Antoniou et al., 2020).

The risk of increased risk of cancer was specifically looked at since it had been thought that radiation associated with the EVAR procedure and subsequent

Table 3. **Summary of the randomised control trials comparing open surgical repair and endovascular aneurysm repair for unruptured abdominal aortic aneurysm**

Study name	**Recruitment period**	**Aneurysm Size**	**Patient numbers**	**Duration of follow up**	**Main findings**
Endovascular Aneurysm Repair 1 Trial (EVAR-1) (Patel et al., 2016)	1999-2004	>55 mm	1252 626 EVAR 626 Open	15 years	No all-cause mortality difference between the two groups. Beyond 8 years, higher all-cause mortality and aneurysm-related mortality in the EVAR group. Higher re-intervention rate in the EVAR group.
Open versus Endovascular Repair (OVER) (Lederle et al., 2019)	2002-2008	>50 mm	881 444 EVAR 437 Open	13 years	No significant difference in all-cause mortality between the two groups. A higher number of secondary therapeutic interventions in the EVAR group.
Dutch Randomised Endovascular Aneurysm Management (DREAM) (van Schaik et al., 2017)	2000-2003	>50 mm	351 173 EVAR 178 Open	12 years	No survival difference was observed between the two groups, this despite an increasing number of re-interventions within the EVAR group.

Anevrysme de l'aorte abdominale: Chirurgie versus Endoprothese (ACE) (Becquemin et al., 2011)	2003-2008	>50 mm	316 150 EVAR 149 Open	5 years	No difference in the cumulative survival, free of death and major adverse event rates. Higher reintervention rates in the EVAR group at 3 years.

EVAR, endovascular aneurysm repair.

cross-sectional imaging might put patients at a higher risk of cancer in the abdomen (Markar et al., 2019).

The increasing re-interventions with EVAR highlight concerns over endograft durability and the need for ongoing post-operative surveillance. These contrasting findings of early benefit with endovascular treatments, but later benefits from open surgery, strike a chord with the experience of coronary revascularisation where percutaneous coronary intervention is associated with better short-term outcomes but coronary artery bypass surgery reduces longer term mortality (Gaudino et al., 2020).

A further trial (Greenhalgh, Brown, Powell, Thompson, & Epstein, 2010) randomised 404 patients with large abdominal aortic aneurysm but who weren't eligible for open repair to undergo either EVAR or no repair. Aneurysm-related mortality was lower in the EVAR group (adjusted hazard ratio, 0.53; 95% confidence intervals, 0.32 to 0.89; p=0.02), however there was no overall mortality benefit observed (adjusted hazard ratio, 0.99; 95% confidence interval, 0.78 to 1.27; p=0.97). This was compounded by the fact that patients in the EVAR group (48%) had EVAR-related complications including requiring re-interventions.

These EVAR trials have informed the recommendations in clinical practice guidelines published by the Society for Vascular Surgery, the European

Society for Vascular Surgery, and the National Institute for Health and Care Excellence. However, each came to different conclusions. The Society for Vascular Surgery recommends an assessment of operative risk and life expectancy when contemplating repair, arguing that a patient who is at high risk for open surgery may be at a lower risk for EVAR (Chaikof et al., 2018). The European Society for Vascular Surgery recommends EVAR as the preferred treatment modality where anatomically suitable, but open repair in patients with longer life expectancies (more than 10 to 15 years) (Wanhainen et al., 2019). The National Institute for Health and Care Excellence recommends open surgical repair unless contraindicated due to a hostile abdomen, anaesthetic risks, or comorbidities when EVAR is recommended but notes that this needs balancing with the uncertain benefit of EVAR in these patients (NG156, 2020).

There are many critics of the differences in the recommendations. Some argue that the quoted trials were performed with either older generation endografts or ones which are not commercially available anymore. Newer generation grafts appear to have fewer re-intervention rates than their older counterparts in more recent studies (IMPROVE Trial Investigators, 2017). Endovascular experience amongst clinicians has also continued to increase and imaging technology and devices to develop. In contrast, the surgical technique for open repair has remained more or less unchanged since the 1950s. Similar arguments have been previously advanced for percutaneous and open

surgical approaches for coronary revascularisation and yet open surgery continues to have the best long-term outcomes (Gaudino et al., 2020).

The European Society for Vascular Surgery took into consideration more contemporary population-based registries, some of which reported improved short-term outcomes that are sustained for at least five years (Lilja et al., 2017). Others would argue that the conclusions by the National Institute for Health and Care Excellence are more valid since they only considered higher quality evidence (in the form of randomised control trials). They also looked at cost-effectiveness in more detail and used United Kingdom-specific economic modelling. It concluded that despite the short-term benefit, EVAR's higher net costs and lower net benefits than open repair, put it above the range of what would normally be considered a cost-effective use of National Health Service resources. This lack of consensus has even led some to suggest that new randomised controlled trials are required (Spanos et al., 2020).

1.3.4 Emergency treatment

A ruptured abdominal aortic aneurysm refers to acute haemorrhage from the aneurysm beyond the true aortic wall. It is a surgical emergency which invariably results in death if left untreated. The National Institute for Health and Care Excellence guidelines suggest that EVAR *should be considered*, but both the Society and European Society for Vascular Surgery suggest that when anatomically suitable, a ruptured abdominal aortic aneurysm *should be* repaired by EVAR. The largest randomised trial comparing open aneurysm

repair versus EVAR in ruptured abdominal aortic aneurysms (the IMPROVE Trial - Immediate Management of Patients with Ruptured Aneurysm: Open vs Endovascular repair) recruited 613 patients with a clinical diagnosis of rupture in the United Kingdom and Canada. There were no mortality differences at 30 days (37.4% versus 35.4%) or 1 year (45.1% versus 41.1%) between the two groups (IMPROVE Trial Investigators, 2015; Powell et al., 2014). Three-year outcomes however suggest that the endovascular strategy was associated with a survival advantage, a gain in quality-adjusted life years, similar levels of re-intervention and reduced costs (IMPROVE Trial Investigators, 2017).

1.4 Imaging the aorta

Abdominal aortic aneurysms are asymptomatic unless they are close to have ruptured. Imaging therefore plays a central role in diagnosis and treatment. Ultrasound scan is the clinical standard for diagnosis. It has a high sensitivity and specificity which makes it ideal for screening and surveillance (Wilmink et al., 2002). However, ultrasound is operator-dependent and cannot penetrate bony structures so visualising other parts of the aorta requires cross-sectional imaging. Ultrasound is also not sensitive enough to detect retroperitoneal haemorrhage as a result of aneurysm rupture, so computed tomography (CT) is required in an emergency setting.

CT and magnetic resonance imaging (MRI) are well-suited to visualising the aortic anatomy since their high spatial resolution allows easy assessment of aortic pathology. CT is particularly sensitive at detecting calcified plaque within

the vasculature. Modern assessment of mature plaques can offer an objective approach at analysing calcified lesions and allows quantification of vessel calcification. Calcium scores refer to this total burden of calcification and can provide a powerful marker of cardiovascular risk (Agatston et al., 1990; Osborne-Grinter et al., 2022). MRI is perhaps more ideal when frequent imaging is required since it does not expose patients to repeated ionising radiation. However, its use in aortic aneurysm disease has been less favoured because it does not visualise calcification well and because the metal in the stent graft leads to an inhomogenous magnetic field which results in significant image degradation (Koch et al., 2010; Saida et al., 2012).

CT combined with iodinated contrast, CT angiography, has a central role in the elective management and intervention planning of abdominal aortic aneurysm disease because visualising the whole aorta allows accurate objective anatomical assessments to be performed. CT angiography can define arterial tributaries, renal vein anatomy and neck and aneurysm morphology. This is crucial information for planning of both open and endovascular repairs. In open repair, the operating surgeon needs to be aware of how much healthy aorta is available and if clamping can be done below or above the renal arteries to allow suturing of the graft. They would need to be aware of which back-bleeding vessels need to be tied off, and at which level the distal anastomosis can be performed. In endovascular repair, pre-operative planning needs to confirm that the neck is healthy enough for an adequate seal (Table 2), what diameter and lengths of the different parts of the graft are required, what

angles of the fluoroscopy C-arm best visualise the anatomy, and if the access vessels are adequate. During an EVAR, CT imaging can even be fused with real-time angiography for intraoperative use for greater accuracy.

1.4.1 Surveillance following EVAR

Because most endoleaks are asymptomatic, patients managed with EVAR are enrolled in life-long surveillance to detect, prevent and treat subsequent complications. European guidelines suggest that only CT angiography can be used as a solitary imaging modality for EVAR surveillance. CT angiography is accessible, sensitive, and reproducible, and it is particularly well suited to detect the EVAR stent, luminal blood flow, aortic morphology and established calcified plaque (Wanhainen et al., 2019). However, because of cost and the risks of contrast nephropathy and ionising radiation from serial CT scans, duplex ultrasound or contrast-enhanced duplex ultrasound also form part of current surveillance strategies. Duplex ultrasound-based surveillance may be used if CT angiography performed within the first post-operative year is reassuring. However, whilst duplex ultrasound can reliably detect the presence of type I endoleaks, it is less sensitive in detecting type II endoleaks. An EVAR surveillance programme could therefore take the form of a CT angiogram at 30 days post-operatively, proceeding to annual ultrasound surveillance. An increase in aneurysm sac diameter or an endoleak on surveillance would then trigger early cross-sectional imaging, otherwise a CT angiogram could be repeated after five years (Figure 3) (Wanhainen et al., 2019).

Figure 3. **An approach to the elective management of patients with an abdominal aortic aneurysm**

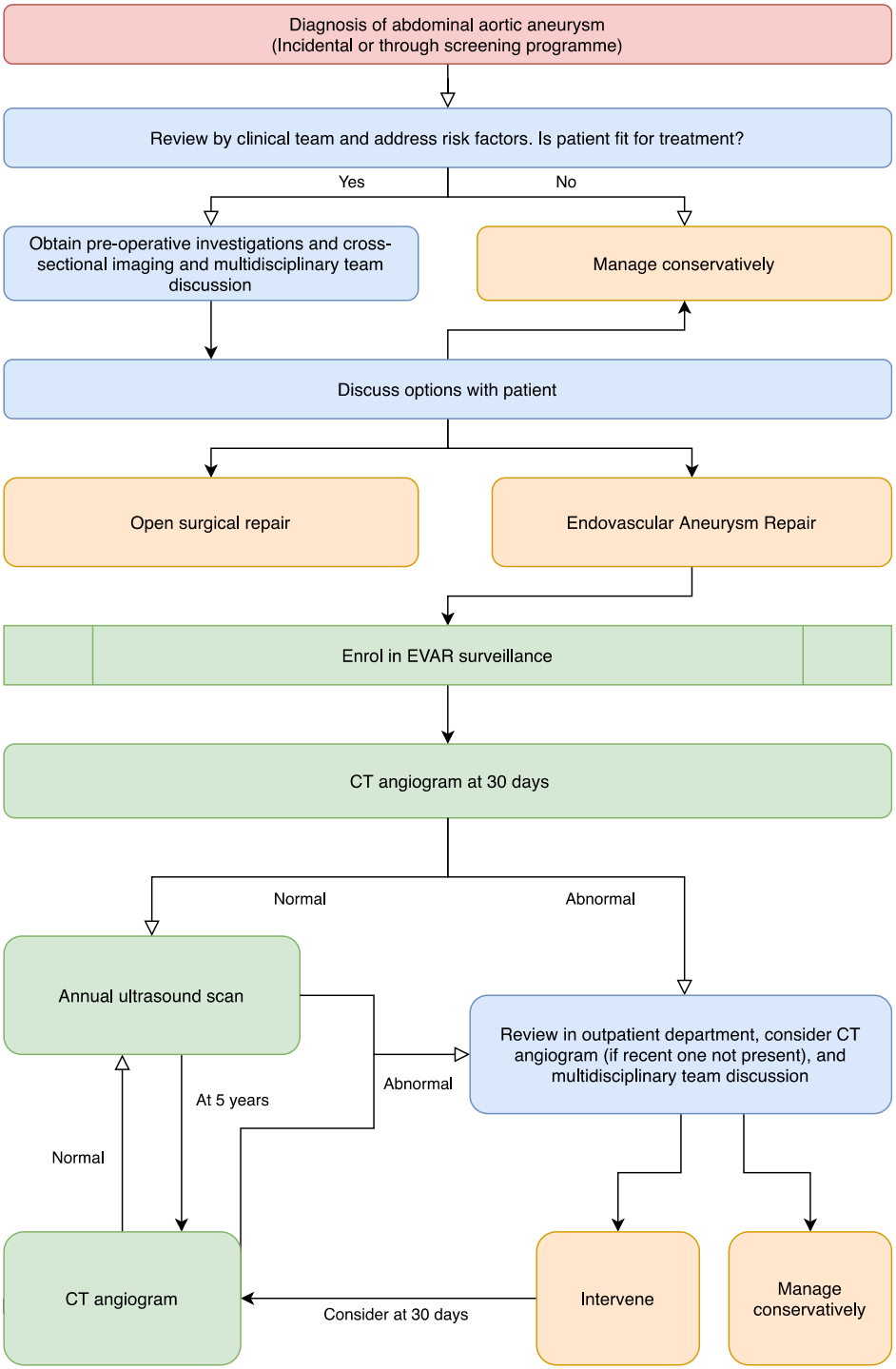

After diagnosis of an abdominal aortic aneurysm at size-threshold, the patient should be reviewed by a member of the clinical team. If obvious contra-

indications to treatment are present e.g., active malignancy with a reduced life-expectancy, it may be more prudent for the patient to be managed conservatively from the outset. If not, cross-sectional imaging in the form of a computed tomography (CT) angiogram should be sought to provide anatomical details on aneurysm morphology. Pre-operative investigations which assess the patient's aerobic capacity may be performed at this point. The case should be discussed at a multidisciplinary team (MDT) level, usually consisting of vascular surgeons, interventional radiologists and vascular anaesthetists. The outcome of the meeting should then be discussed with the patient and a treatment decision reached. If conventional endovascular aneurysm repair (EVAR) is performed, a normal post-operative CT angiogram would lead to enrolment in a post-operative EVAR surveillance programme (e.g., an annual ultrasound scan). Abnormal scans at any point would trigger more detailed imaging which can also be discussed at an MDT level if required. If required, interventions can be planned depending on what abnormality is identified.

1.4.2 Outcome risk prediction

The imaging work-up for treatment of an abdominal aortic aneurysm and post-operative surveillance after EVAR generate a substantial amount of imaging data. There has therefore been a drive to use this data to allow improved predictions of EVAR outcomes and to reduce the dependency on annual surveillance. Being able to predict which patients will develop endoleaks after EVAR would mean that not all patients need to be put under surveillance.

Table 2 (Section 1.3.2.1) already alludes to some of the anatomical features in the aneurysm neck which preclude insertion of a standard EVAR stent graft – this is based upon adverse outcome data when such stent grafts were used in these situations (Oliveira et al., 2018; Wanhainen et al., 2019).

Other information obtained from spatially-correct three-dimensional CT angiography data can be used to try to predict EVAR outcomes (Chaikof, Fillinger, et al., 2002; Chew et al., 2019; Fujii et al., 2020; Oliveira-Pinto et al., 2020; Schanzer et al., 2011). Adverse features described include:

- A high (>1.2) aortic tortuosity index, described as the distance along a central luminal line between the lowest renal artery and the aortic bifurcation divided by the straight-line distance from these two anatomical markers.
- An acute (<120°) aortic angle, the most acute angle in the pathway between the lowest renal artery and the aortic bifurcation.

- The presence, size and patency of the aortic branch vessels, i.e., lumbar arteries, the inferior mesenteric artery and accessory renal arteries.
- Adverse iliac artery morphology pertaining to the distal seal zone such as calcification, small luminal diameter, acute angulation, high tortuosity and short length.
- A large aneurysm luminal volume and the presence of aneurysm sac thrombus.

Despite these descriptions, a sub-analysis of the second-largest EVAR randomised control trial found no evidence that these aneurysm-related anatomical features differed between patients who did or did not develop endoleaks on follow up (Lal et al., 2015).

1.5 Biomarkers of aortic disease activity

Elective repair of an abdominal aortic aneurysm is usually triggered by an increase in the aneurysm diameter (Section 1.2.3) but no other measure or indicator of risk of aortic rupture is available. Medical treatments which reduce or slow down aortic growth are also unknown. Unsurprisingly, because as with natural aneurysm growth rate being so low (Section 1.2.3), clinical trials would take too long to reach these endpoints. Section 1.4.2 also discusses the absence of robust prediction methods of EVAR failure. Clinical research, which can include morphology, bio-markers or functional imaging could increase our understanding of abdominal aortic aneurysm disease and could help us develop such predictive tools (Wanhainen et al., 2019).

One attractive prospect as a method of tracking disease by predicting aneurysm disease development or progression could be serum biomarkers. These may be used to evaluate the global burden of aneurysm-related inflammatory and degenerative activity. Various markers of inflammation such as certain cytokines, C-reactive protein, and osteopontin have been considered. However, it is uncertain whether these mediate the disease process or are simple bystander markers of disease progression (Hellenthal et al., 2009). No serum biomarkers for abdominal aortic aneurysm disease are presently known.

Our increased understanding of cardiovascular disease processes and the development in available technology has led to imaging biomarkers being increasingly explored for use as surrogate markers of disease progression. These could even serve as endpoints for clinical research: Certainly, non-invasive imaging could monitor or identify disease activity occurring locally in the tissue. Such disease activity may not be apparent from biomarkers within the systemic circulation (Ishizaka et al., 2012). Using imaging biomarkers, biological activity within the aortic wall could be detected to identify pathology even prior to a morphological change (e.g., increase in diameter) taking place (M. B. J. Syed et al., 2019). These molecular imaging techniques can target specific biological pathways which are known to have a role in disease activity.

1.5.1 Periaortic adipose tissue

One promising imaging biomarker that uses imaging data collected on routine CT angiography is the attenuation of adipose tissue around a blood vessel. Perivascular adipose tissue is crudely defined as any adipose tissue surrounding a blood vessel including both periaortic and pericoronary deposits (Britton & Fox, 2011). This tissue is metabolically active and secretes several bioactive substances termed ‘adipokines’. Excessive caloric intake causes adipose tissue remodelling through a process of adipocyte hyperplasia and hypertrophy, subsequent adipocyte dysfunction and apoptosis followed by inflammatory cell infiltration and fibrosis. This results in a chronic low-grade inflammatory state (Mancio et al., 2018).

Analysis of adipose tissue attenuation in the coronary circulation (pericoronary adipose tissue) has shown its ability to predict myocardial infarction and all-cause and cardiac mortality on retrospective analyses of CT coronary angiograms (Oikonomou et al., 2018; Tzolos et al., 2022). This imaging biomarker demonstrates a difference in CT-measured adipose tissue attenuation purported to occur as a result of a shift in lipophilic content within the adipose tissue, possibly due to the presence of inflammation (Figure 4) (Antonopoulos et al., 2017).

This technique has also garnered interest in vessels larger than the coronary arteries such as the aorta, since a potentially larger effect could be observed

Figure 4. **Change in adipose tissue driving changes in tissue attenuation.**

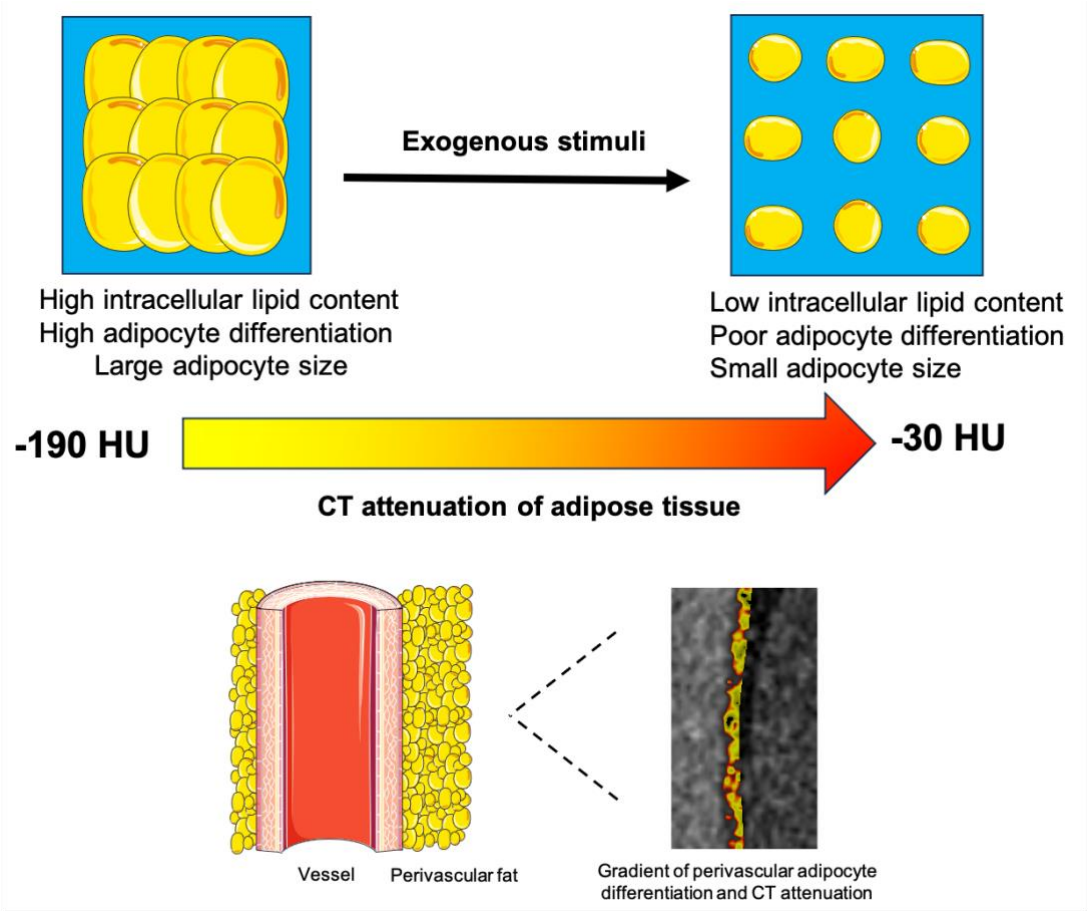

In the presence of exogenous stimuli, adipocytes lose their intracellular lipid content, become less differentiated and smaller in size. This correlates to a shift in the makeup of the adipose tissue, from having greater lipophilic content to greater aqueous content. This change corresponds to a change in the computed tomography (CT) attenuation of the tissue, from more negative to less negative Hounsfield units (HU). The change in adipocytes can therefore be detected by assessing the gradient of the adipose tissue attenuation around the blood vessels on CT (adapted from Mancio et al., 2018).

due to the larger amount periaortic adipose tissue present. In patients with Takayasu arteritis, a large-vessel vasculitis characterised by pan-arterial granulomatous inflammation, periaortic adipose tissue density was higher when compared to patients with atherosclerotic coronary artery disease or control subjects. There was also an association with clinical and biochemical markers of inflammation and a moderate association was also observed between the pericoronary adipose tissue and [^{68}Ga]-DOTATATE coronary positron emission tomography (Wall et al., 2021).

Periaortic adipose tissue has also been assessed in abdominal aortic aneurysm disease and compared with occlusive aorto-iliac disease and control subjects. Here, the presence of an abdominal aortic aneurysm was found to be an independent predictor of higher perivascular adipose tissue attenuation around the aneurysm sac and demonstrated a relationship with aortic volume (Dias-Neto et al., 2018).

1.5.2 Positron emission tomography

Positron emission tomography (PET) is a molecular imaging modality that produces a topological map of the body using biologically compatible compounds which bind to specific targets within the tissue. These compounds are called radioactive tracers (or radiotracers) and have one or more atoms replaced with a radioisotope through which radioactive decay can then be detected by the PET scanner (Section 2.6). Radiotracer uptake on PET can be quantified, and this can serve as a measure of the molecular mechanisms

occurring in the target tissue. When PET is combined with CT angiography (PET-CT), radiotracer uptake in very specific anatomic locations of interest can be assessed.

1.5.2.1 2-[^{18}F]fluoro-2-deoxyglucose

One of the most commonly used PET radiotracers is 2-[^{18}F]fluoro-2-deoxyglucose ([^{18}F]FDG), a glucose analogue. In the body, it is taken up by cells that metabolise glucose and its intracellular distribution is associated with the degree of metabolic activity and inflammation in regions of uptake (Tarkin et al., 2016).

Multiple pre-clinical and clinical studies have explored the role of [^{18}F]FDG as a marker of inflammation in abdominal aortic aneurysm disease (Gandhi et al., 2021). McBride and colleagues found high [^{18}F]FDG uptake in the aortic wall of patients in 13 out of 15 patients with an abdominal aortic aneurysm under surveillance. However, only a weak correlation between [^{18}F]FDG uptake and MRI with ultrasmall superparamagnetic particles of iron oxide (USPIO; a marker of phagocytic activity) was found (McBride et al., 2016). Kotze and colleagues meanwhile found an inverse trend between [^{18}F]FDG uptake and future aneurysm expansion in a study of 25 patients under surveillance (Kotze et al., 2011). Marini and colleagues showed that reduced radiotracer uptake in aneurysmal aortic segments was correlated with a reduction in cell density in the diseased aortic wall on histology (Marini et al., 2012).

Within patients who have been treated with EVAR, Courtois and colleagues showed increased uptake in 6 out of 17 patients before EVAR. Furthermore, post-operative PET only showed a moderate association with sac growth and only in the presence of an endoleak (Courtois et al., 2019). In contrast, in 33 patients having an EVAR there was low pre-operative radiotracer uptake in the aneurysm sac followed by increased uptake at 6 months which was associated with reduced sac shrinkage (Marie et al., 2018).

[^{18}F]FDG has been a successful radiotracer in imaging atherosclerosis that is driven by local and systemic inflammation and it may have a role in prediction of future cardiovascular events (Figueroa et al., 2013; Tarkin et al., 2016). However, [^{18}F]FDG appears to highlight all regions of active glucose metabolism and increased tissue glycolysis which is not disease-specific (Vaidyanathan et al., 2015). This is in fact the basis of its use as a diagnostic tool for graft infections in the abdominal aortic aneurysm patient (Sah et al., 2015). However, its uptake can be inconsistent as it appears to be greatly influenced by local tissue environments such as hypoxia or microvascular permeability (Taqueti et al., 2014; Wu & Nguyen, 2011).

The studies mentioned above appear to provide a conflicting picture of [^{18}F]FDG as a radiotracer for abdominal aortic aneurysm disease and therefore its use does not appear to have a clear decisive role in monitoring disease progression.

1.5.2.2 Sodium [^{18}F]fluoride

Sodium [^{18}F]fluoride is another PET radiotracer. It was originally developed for skeletal imaging, in particularly bony metastases (Ahuja et al., 2020). It has now been shown to also bind selectively, specifically and with high affinity to calcified deposits within atherosclerotic plaque and distinguish between areas of macro- and microcalcification (Irkle et al., 2015). In arterial atherosclerotic plaques, the presence of calcified vesicles, the precursors to microcalcification, make it more susceptible to rupture (New et al., 2013). As discussed above (Section 1.2.1), microcalcification within the aortic wall represents deposition of hydroxyapatite crystals formed of calcium phosphate within the extracellular matrix as part of abdominal aortic aneurysm pathology. Sodium [^{18}F]fluoride also co-localises to increased medial microcalcification which is associated with ascending thoracic aneurysms (Fletcher, Nash, et al., 2022). Microcalcification can therefore serve as an important marker of the abdominal aortic aneurysm disease process which can be detected by sodium [^{18}F]fluoride.

The Sodium [^{18}F]Fluoride Imaging of Abdominal Aortic Aneurysms (SoFIA^{3}) study, was a prospective observational study in a population of 76 patients with a sub-threshold abdominal aortic aneurysm. Aortic sodium [^{18}F]fluoride uptake localised specifically to the aneurysm and was associated with more rapid aneurysm expansion. This was independent of age, sex, baseline diameter, body mass index, blood pressure, smoking, renal function or peripheral arterial disease. During follow up, aneurysms with the highest

sodium [^{18}F]fluoride uptake expanded more rapidly and patients were most likely to require elective abdominal aortic aneurysm repair (because they reached the threshold of 55 mm) or to have experienced aneurysm rupture (Forsythe et al., 2018). In abdominal aortic aneurysms, sodium [^{18}F]fluoride PET-CT appears to be able to predict aortic expansion and rupture.

The use of sodium [^{18}F]fluoride as a PET radiotracer still has some remaining challenges. It is physiologically taken up by bone with a significant spill-over and contamination of signal from the vertebrae into the aneurysm. Background correction techniques have been attempted to address this (Akerele et al., 2019). The different aortic aneurysm anatomy between patients and the variable aneurysm diameters also mean that quantification must be standardised to allow accurate comparison between different patients and to reduce the potential for error between observers.

The SoFIA^3 study demonstrated that sodium [^{18}F]fluoride PET-CT can detect aortic aneurysm-specific microcalcification and predict aneurysm-related events in untreated abdominal aortic aneurysms. This knowledge is transferable to patients treated with EVAR. Unlike traditional open surgery, the diseased vascular tissue is retained intact in EVAR, this has the potential for ongoing perfusion of the tissue, particularly in the event of endoleak formation. The potential for continued aortic degeneration remains unknown. The main conflict in recommending EVAR is between the short-term benefit of minimally invasive surgery versus the risks of ongoing surveillance, endoleak formation,

re-intervention and delayed sac rupture in the longer term. Imaging using sodium [^{18}F]fluoride holds the promise to bridge this gap in our knowledge, by exploring its use to evaluate changes in the aorta which evolve over time, and explore this in relation to future complications.

1.6 Aim and hypothesis

The overarching aim of this thesis was to investigate methods of non-invasive imaging of abdominal aortic aneurysm disease activity and relate the findings to endovascular aneurysm repair.

Specifically, I had the following objectives:

1. To assess whether periaortic adipose tissue attenuation is associated with aneurysm disease activity in different disease states (**Chapter 3**).
2. To develop an analysis method for quantifying aortic sodium [^{18}F]fluoride uptake in patients with abdominal aortic aneurysms (**Chapter 4**).
3. To investigate aortic sodium [^{18}F]fluoride uptake in patients before and after undergoing EVAR (**Chapter 5**).
4. To investigate aortic sodium [^{18}F]fluoride uptake in patients with and without endoleak after EVAR (**Chapter 6**).

I sought to address the following hypotheses:

1. Periaortic adipose tissue attenuation is related to the severity of different abdominal aortic aneurysm disease states.

2. Current measurements of sodium [^{18}F]fluoride uptake in the abdominal aorta can be improved upon whilst accounting for vertebral bone signal spill-over in a comparable and time-efficient manner.
3. Aortic sodium [^{18}F]fluoride uptake is reduced after successful EVAR treatment.
4. Aortic sodium [^{18}F]fluoride uptake is increased in patients with an active endoleak after EVAR treatment.

Chapter 2: Methods

2.1 Study populations

The populations studied consist of patients with abdominal aortic aneurysms in different disease states and control subjects. The study populations of the individual studies are further described in each chapter.

The periaortic adipose tissue study (Chapter 3) had three patient cohorts: control subjects, patients with an asymptomatic abdominal aortic aneurysm and patients with a symptomatic abdominal aortic aneurysm. The control subjects and the asymptomatic patients were part of a historical cohort from the Sodium [^{18}F]Fluoride Imaging of Abdominal Aortic Aneurysms (SoFIA^{3}) study (NCT02229006), conducted by Miss Rachael Forsythe, Dr Jenny Robson and Professor David Newby. The symptomatic cohort consisted of patients identified through operative and clinical records of patients presenting with a ruptured abdominal aortic aneurysm or undergoing repair. Their electronic health record was retrospectively interrogated for the relevant clinical parameters.

The quantification of sodium [^{18}F]fluoride uptake study (Chapter 4) consisted of consecutive patient imaging from the historical cohort of the Sodium [^{18}F]Fluoride Imaging of Abdominal Aortic Aneurysms (SoFIA^{3}) study (NCT02229006), conducted by Miss Rachael Forsythe, Dr Jenny Robson and Professor David Newby.

The sodium [^{18}F]fluoride uptake following EVAR study (Chapter 5) consisted of the original patients from the cohort of the Sodium [^{18}F]Fluoride Imaging of Abdominal Aortic Aneurysms (SoFIA^{3}) study (NCT02229006) who had subsequently undergone an EVAR operation. These patients were recruited as part of the cross-sectional component of the PET-EVAR study (see below).

The Predicting Endoleaks Following Endovascular Aortic Aneurysm Repair Using Sodium [^{18}F]Fluoride (PET-EVAR) study (NCT04577716) is a prospective observational study for which I am the Principal Investigator, supervised by Miss Rachael Forsythe, Professor Marc Dweck and Professor David Newby. I was responsible for writing the protocol, obtaining the relevant approvals, recruiting and running the patients through the study visits and image and data analysis. Here, only the cross-sectional components of the study are being reported, because the patients recruited into the longitudinal component are still undergoing follow up visits. The cross-sectional case control study (Chapter 6) consisted of patients who had undergone an EVAR operation, recruited into the PET-EVAR study. The objective of this study was to investigate the sodium [^{18}F]fluoride uptake in patients with and without an endoleak after EVAR, and therefore patients who had a documented endoleak and patients who did not have a documented endoleak after EVAR, were invited to participate.

The aortic tissue for the ex vivo study (Chapter 6) was collected from patients undergoing open abdominal aortic aneurysm repair at the Edinburgh Vascular

Service, Royal Infirmary of Edinburgh, NHS Lothian. Control aortic tissue was obtained from the Edinburgh Brain and Tissue Bank, University of Edinburgh.

2.2 Study regulations

The Sodium [^{18}F]Fluoride Imaging of Abdominal Aortic Aneurysms (SoFIA^3) study, whose imaging data were used for parts of Chapters 3, 4 and 5, had previously obtained ethical approval by the South East Scotland Research Ethics Committee (South East Scotland 01 Committee, 14/SS/0080) and registered on a public database (NCT02229006).

The periaortic adipose tissue study was sponsored and approved by the Academic and Clinical Central Office for Research and Development (ACCORD) which represents both the University of Edinburgh and NHS Lothian (AC21019). It had ethical approval from the East of Scotland Research Ethics Service (21/ES/0044). Since patient informed consent was waived due to the retrospective nature of the study, further Caldicott approval (CRD21102) from the NHS Lothian Research & Development Department (2021/0066) was also obtained.

The Predicting Endoleaks Following Endovascular Aortic Aneurysm Repair Using Sodium [^{18}F]Fluoride (PET-EVAR) study was also sponsored and approved by the Academic and Clinical Central Office for Research and Development (ACCORD) which represents both the University of Edinburgh and NHS Lothian (AC20136). Ethical approval was obtained from the South

East Scotland Research Ethics Committee (South East Scotland 02 Committee, 20/SS/0119). Further approval by the Administration of Radioactive Substances Advisory Committee (ARSAC) was obtained (AA-746). The study also received approval from NHS Lothian Research and Development with the Royal Infirmary of Edinburgh being the research site (2021/0012). Further approvals for patient identification centres were obtained from the respective research and development departments at NHS Greater Glasgow and Clyde, NHS Lanarkshire and NHS Tayside (GN20CA566, L20123_PIC, 2020CV05 respectively). Furthermore, the study was registered on a public database (NCT04577716), with the Central Portfolio Management System (48641) for the National Institute for Health and Care Research (NIHR) and NHS Research Scotland (NRS20/254718).

Tissue governance approval for the ex vivo study was obtained from NHS Lothian Research and Development (2017/0246/SR859) with ethical approval covered under BioResource (15/ES/0094) and the Edinburgh Brain Bank (16/ES/0084).

This rigorous study regulation ensured that the research was conducted in accordance with the principles of the International Conference on Harmonisation Tripartite Guideline for Good Clinical Practice (ICH GCP). All studies were conducted in accordance with the declaration of Helsinki. Apart from where indicated above, informed patient consent was obtained for all patient participation in the research.

2.3 Recruitment

Recruitment of patients with a symptomatic abdominal aortic aneurysm in the periaortic adipose tissue study, although prospective, was performed using retrospective health records and imaging. The necessary detail regarding this is included in Section 2.1 and in Chapter 3.

Patients were recruited into the Predicting Endoleaks Following Endovascular Aortic Aneurysm Repair Using Sodium [^{18}F]Fluoride (PET-EVAR) study in the manner described below.

Patients who had undergone an EVAR operation were identified either by the research team using contemporaneous databases held by the relevant regional health board or by their health care team. The electronic health record was scanned for an obvious exclusion criterion, or departure from the inclusion criteria.

These were the inclusion criteria: A diagnosis of an abdominal aortic aneurysm as defined by the European Society of Vascular Surgery guidelines on the management of aorto-iliac artery aneurysms (Wanhainen et al., 2019); EVAR performed within manufacturers' 'Instructions for Use'; a minimum age of 50 years and patients having the capacity to give informed consent. For the endoleak group, any type of documented endoleak or stent graft migration.

These were the exclusion criteria: Patient unable to undergo PET-CT scanning; severe chronic kidney disease (estimated glomerular filtration rate ≤30 mL/min/1.73 m^2); major or untreated cancer reducing life expectancy to below 2 years; pregnancy or breastfeeding; an allergy or contra-indication to iodinated contrast; inability or unwillingness to give informed consent; a life-expectancy of less than two years and a known history of connective tissue disease.

After the potential study participant was identified, an approved letter and participant information sheet was sent to them for consideration. Contact by phone was then made, with an explanation of what participation would involve and potential risks. Potential participants had an opportunity to ask questions and it was made clear that study involvement was on a voluntary basis. If the patient agreed, then arrangements for the study visit were made. Every effort was made to minimise bias based on the patient's geographical location; if the patient had issues with travelling to the study site, expense reimbursement or arrangement of private transport was offered. Despite these efforts, at certain points, recruitment proved tricky as some potential patients were not keen on travelling into, and arranging visits in a hospital during a pandemic. Covid-19 therefore had an impact on the original recruitment timelines which had to be adapted to this new reality.

2.4 Study visit

Chapters 3 and 4 involve the use of retrospective data and image analysis which is discussed in the relevant sections. The study visit discussed here is for patients in Chapters 5 and 6 who attended a study visit as part of recruitment in the PET-EVAR study.

The study visit took place at the Edinburgh Imaging Facility at the Queen's Medical Research Institute, University of Edinburgh. Patients were not fasted. The nature of the study was once again explained to patients on the day of the visit. Any remaining questions or queries about the study were answered, after which patients signed a consent form.

A medical, surgical and medication history was taken. Parameters including height, weight, oxygen saturations, heart rate and blood pressure were measured. A peripheral vascular examination was performed. These were all recorded in a data collection sheet.

A 20-G peripheral cannula was inserted and venesection performed for blood sample collection. Four samples were sent to the Royal Infirmary of Edinburgh clinical laboratories for immediate processing and the following tests were performed: full blood count, urea and electrolytes, bone profile, liver function tests, C-reactive protein, coagulation screen and glycated haemoglobin (HbA1c).

Three samples were taken to the Clinical Research Facility, Royal Infirmary of Edinburgh for processing. The serum gel bottle was centrifuged at 2500 *g* for 10 min at 20°C and serum was stored in 1 mL aliquots. Samples collected with ethylene diamine tetra-acetic acid (EDTA) were centrifuged at 2000 *g* for 10 min at 20°C and plasma was stored 1 mL aliquots. The third EDTA sample was not centrifuged and was stored for potential genetic analysis. All samples were stored at -80°C.

The cannula was then flushed with 10 mL of normal saline prior to intravenous administration of sodium [^{18}F]fluoride by the radiographers.

At the end of the PET scan, the cannula was removed and patients were allowed to go home. Contact with patients pertaining to the blood tests and scan results was made within the following 2 weeks and the patient's general practitioner and the vascular team in the tertiary setting were informed of the study visit.

2.5 Computed tomography

A computed tomography (CT) scan is an X-ray examination where a series of X-ray exposures are rotated around an area of interest in the body and cross-sectional images are generated following computer processing. The X-ray source and detectors rotate around the patient, who is slowly moved up or down the table in relation to the X-ray source. Two-dimensional image slices are constructed. Slice thickness refers to the thickness of each slice which

forms the computerised three-dimensional reconstruction image (Patel & De Jesus, 2023).

The radiodensity or photon attenuation of the different body tissues, using Hounsfield units (HU), then creates the different pixels which form the image. For example, bone (400-2000 HU) appears white and air (-1000 HU) appears black (Patel & De Jesus, 2023). Contrast can be used to better visualise tissue by altering its radiodensity, e.g., iodinated-contrast is radio-dense and appears white. Arterial vessels can be visualised better by timing the scan to when intravenously administered an iodine-based contrast reaches the arterial system (CT angiogram). Abdominal viscera can be visualised better by delaying the time of the scan for when contrast reaches the portal-venous system (delayed-phase CT).

CT scans involve ionising radiation and this has the potential to cause biological harm to tissue. A radiation dose of 100 milliSieverts (mSv) is typically thought to have a 0.5 % risk of cancer (ICRP, 2007). Contrast agents can cause allergic reactions or damage the kidneys especially in those who already have renal impairment. The total research protocol dose for the PET-EVAR study was calculated at up to 46.2 mSv. The inclusion and exclusion criteria for the study aimed to minimise study participants' exposure to the above risks.

Image acquisition and analysis for Chapter 3 is addressed in the section below. Details for CT image acquisition and analysis when combined with PET, for Chapters 4, 5 and 6, are discussed in the PET section of this chapter.

2.5.1 Periaortic adipose tissue study

Asymptomatic patients and control subjects underwent contrast-enhanced CT angiography (120 kV, 145 mAs, 3/3 mm, field of view 400; and 1/1 mm, field of view 300; triggered at 181 HU) at their study visit.

Symptomatic patients underwent CT imaging according to local Emergency Department and Radiology protocols. Antero-posterior aortic diameter was measured in the orthogonal plane using Picture Archiving and Communications System (PACS, Carestream Health).

2.5.1.1 Adipose tissue assessment

Data were exported in Digital Imaging and Communications in Medicine (DICOM) format. Assessment of visceral and subcutaneous adipose tissue attenuation was performed using OsiriX (version 13.0.0; OsiriX Imaging Software, Geneva, Switzerland). For each scan, four circular regions of interest were drawn in both the visceral fat and the subcutaneous fat at the mid-level of the third lumbar vertebra (Figure 5) (Derstine et al., 2022; Gleinert-Rożek et al., 2020). The mean attenuation values were then calculated for each patient.

Figure 5. **Regions of interest in visceral and subcutaneous fat**

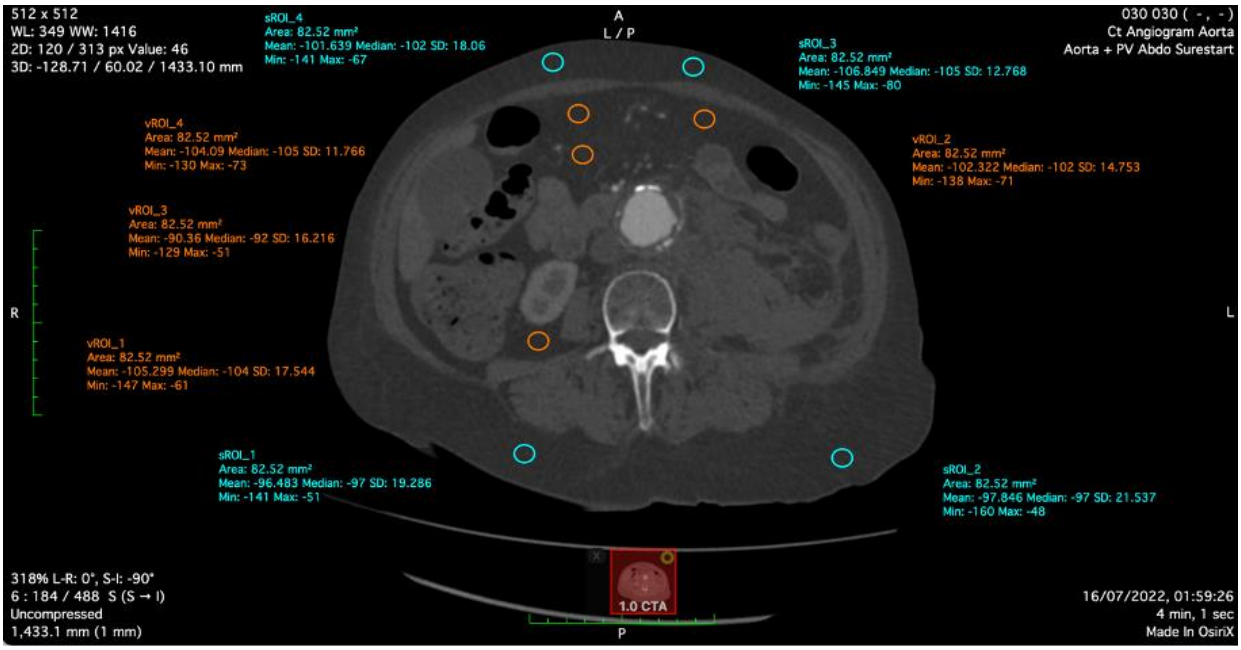

Four regions of interest were drawn in the visceral fat (orange circles) and the subcutaneous fat (cyan circles) on OsiriX. A mean value was obtained for each. Although all efforts were made to keep the regions of interest in the same CT slice, sometimes lower or higher slices had to be chosen due to reduced subcutaneous fat or the presence of high-density fluid (blood) within the visceral fat.

Periaortic adipose tissue attenuation assessment was performed using semi-automated software (Autoplaque, version 2.5, Cedars-Sinai Medical Center, Los Angeles) (Williams et al., 2020). Analysis for each subject was performed in two aortic regions (Figure 6):

- The abdominal aorta - from just below the lower-most renal artery until the aortic bifurcation.
- The normal aorta - a 20-mm straight segment of non-aneurysmal aorta, usually in the suprarenal abdominal aorta.

The mean tissue attenuation at a 2-mm distance from the vessel wall was considered (Goeller et al., 2019; Tzolos et al., 2022). Conversion factors were used on the attenuation values to adjust for different scans having been performed at different tube voltages (Etter et al., 2023; Ma et al., 2020).

Autoplaque is an analytical tool developed by Cedars-Sinai Medical Center, Los Angeles, United States. It is a semi-automated image analysis programme primarily designed to quantify non-calcified and calcified coronary plaque on CT angiography (Dey et al., 2009). This has been shown to be excellent when compared with intravascular ultrasound quantification (Dey et al., 2010). Its use has since been expanded to include assessment of pericoronary adipose tissue attenuation and this has demonstrated excellent inter- and intra-observer repeatability in the coronary arteries (Tzolos, McElhinney, et al., 2021).

Figure 6. **Analysis of periaortic adipose tissue attenuation**

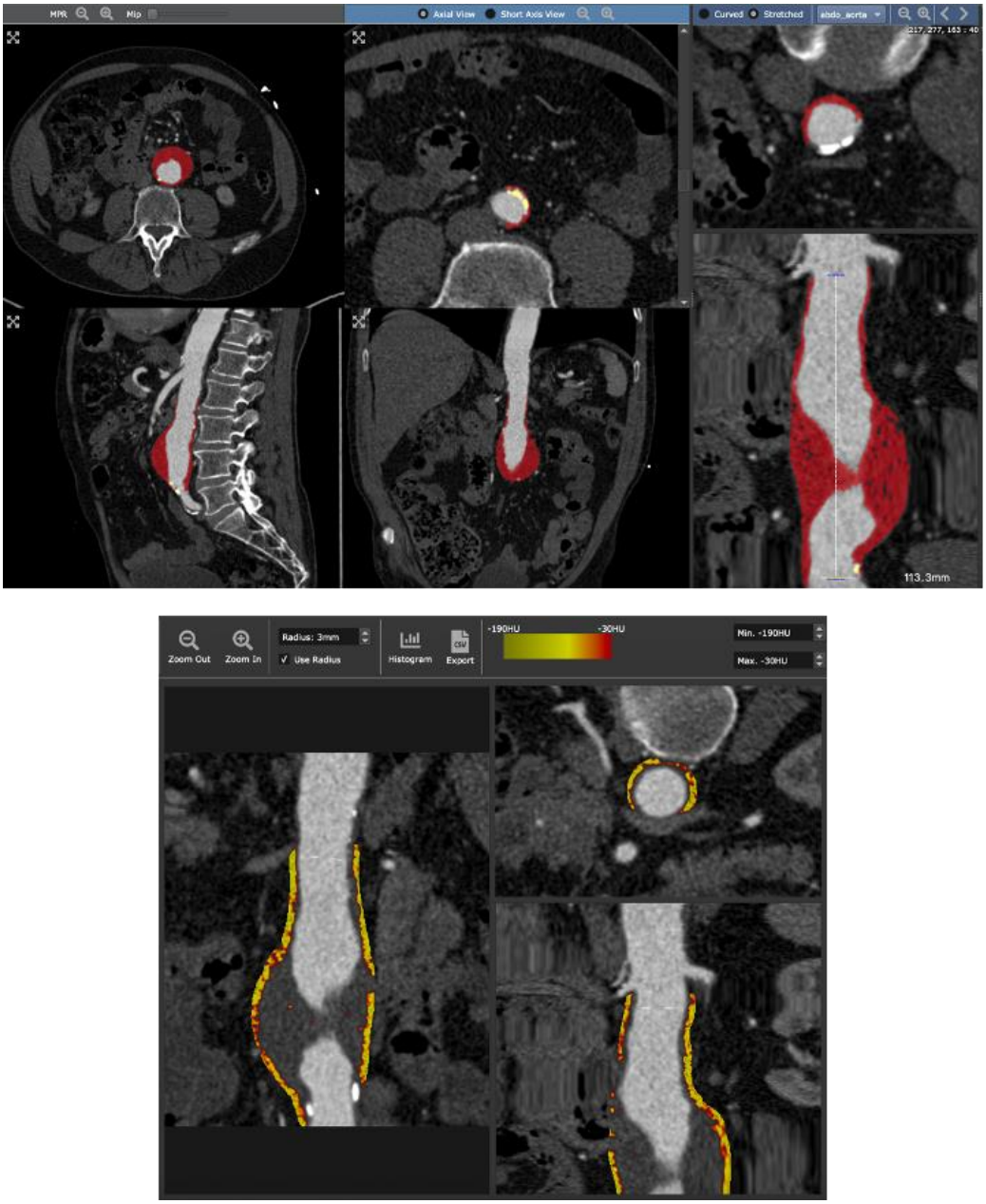

Images were loaded onto a multiplanar image viewer using Autoplaque. The lesion in question is first defined (red). Periaortic adipose tissue attenuation can then be viewed (yellow scale range). Numerical values can be automatically exported by the analysis programme.

2.6 Sodium [^{18}F]fluoride positron emission tomography and computed tomography

Positron emission tomography (PET) allows three-dimensional mapping of positron-emitting radiopharmaceuticals which are administered in very small quantities. When the data are combined with detailed morphological CT images, the capabilities of PET can be further enhanced by allowing accurate co-registration of the two imaging modalities.

The PET scanner contains a ring of γ-ray (gamma-ray) detectors which can detect simultaneous pairs of γ-photons. Positron-emitting radioisotopes, such as fluorine-18, undergo radioactive decay where a proton converts to a neutron and emits a positron (the positively charged antiparticle of the electron), and a neutrino (a chargeless particle). The emitted positron almost instantaneously interacts with a nearby electron to cause an annihilation event whereby matter ceases and is replaced by a pair of two photons (γ-rays) which travel in equal and diametrically opposite directions to be detected by the scanner. If these opposing detectors detect the pair of photons within a specific time frame (coincidence time window), a coincidence event is recorded and the annihilation event is considered to have occurred along the line of response between the two detectors. However, if one of the photons is not detected (e.g., because it was absorbed by the tissue) then that is not considered to be a coincidence event (Lameka et al., 2016). These data acquired by the γ-ray detectors are then used to form the PET images.

Misrepresentation of coincidence events can occur and this degrades the acquired image (termed random scatter and dead time). During data processing, modern PET scanners can correct for such errors and improve on image accuracy. Furthermore, PET data are attenuation-corrected, this refers to the fact that photons released from the centre of the body are attenuated (undergo a reduction in their signal) to a greater extent than photons released from the periphery or body surface. Attenuation correction of the data, usually made using attenuation data from the CT scan, can further improve the accuracy of quantification (Lameka et al., 2016).

The radiotracer sodium [^{18}F]fluoride is produced after irradiating ^{18}O-water with 10 to 18 megaelectron volt (MeV) protons through a carbonate-type anion exchange resin column within a cyclotron (Koukourakis et al., 2009). The sodium salt of [^{18}F]fluoride is a colourless liquid which can then be administered intravenously. It has a half-life of 110 minutes, and at least 60 minutes are usually allowed after intravenous administration to achieve the optimal uptake time within the body.

2.6.1 Image acquisition

For Chapters 4 and 5, patients were administered a target dose of 125 megabecquerels (MBq) of sodium [^{18}F]fluoride intravenously and imaged after 60 minutes on a hybrid 128–slice PET-CT scanner (Biograph mCT, Siemens Healthineers, Erlangen, Germany). An attenuation correction CT scan was performed (120 kV, 50 mAs, 5/3 mm), followed by acquisition of PET data at

10-min intervals in three bed positions. Contrast-enhanced CT angiography (120 kV, 145 mAs, 3/3 mm, field of view 400; and 1/1 mm, field of view 300; triggered at 181 HU), centred on the abdominal aortic aneurysm and extended to the aortic bifurcation, was performed on the same scanner immediately after PET acquisition.

The major difference in PET imaging for the PET-EVAR study was that four bed positions were used here rather than three, this was to ensure full image capture of the abdominal aorta. Otherwise, it used a similar protocol from that described above. Imaging was performed on a hybrid 128–slice PET-CT scanner (Biograph mCT, Siemens Healthineers, Erlangen, Germany). Patients were administered a target dose of 125 MBq of sodium [^{18}F]fluoride intravenously and imaged after 60 minutes of uptake time. A low-dose attenuation correction CT scan was performed (120 kV, 50 mAs, 5-mm thickness, 3-mm increments), followed by acquisition of PET data at 10-min intervals in four bed positions to ensure coverage of the thoracic and abdominal aorta. Static PET-CT images were reconstructed with correction applied for attenuation, dead-time, scatter, and random coincidences, using an optimised iterative reconstruction algorithm (ultra-High Definition; TrueX + Time-of-Flight, 2 iterations and 21 subsets, matrix 200, zoom 1; Gaussian filter 5 mm). Immediately after PET acquisition, a non-contrast aortic CT calcium score was performed, followed by arterial and delayed-phase contrast-enhanced aortic CT angiograms (120 kV, 145 mAs, 3-mm thickness, 3-mm

increments, field of view 400; and 1/1 mm, field of view 300; triggered at 181 HU).

2.6.2 Image analysis

Pre-operative CT angiograms were accessed through a national PACS (PACS, Carestream Health). This allowed pre-operative measurements relating to aneurysm morphology, aortic sac size, neck length and length of common iliac arteries. The obtained post-operative CT angiograms confirmed the presence or absence of an active endoleak through an independent vascular multidisciplinary team meeting. Antero-posterior aortic diameter was measured in the orthogonal plane.

For Chapter 5, calcium score was measured in the descending thoracic aorta and in the suprarenal aorta using dedicated software (Vitrea Advanced, Toshiba Systems). It was quantified as calcium score (AU), calcium volume (mm^3) and calcium mass (mg). The threshold for calcification was set at a computed tomographic density of 130 HU having an area $\geq$1 mm^2 (Agatston et al., 1990). Care was taken to avoid the vertebrae being counted as calcification.

2.6.2.1 Radiotracer uptake quantification

PET quantification in regions of interest has previously been performed using maximum tissue-to-background ratios (TBRs). TBR is calculated by dividing standard uptake values (SUVs) (the decay-corrected tissue concentration

divided by the injected dose/body weight) by the mean SUV in the blood pool. The blood pool SUV can be obtained from the superior vena cava or the right atrium. This method of sodium [^{18}F]fluoride quantification was advanced in coronary arterial vessels and aortic valve leaflets with favourable reproducibility and repeatability (Dweck et al., 2012; Joshi et al., 2014; Pawade et al., 2016). It has also been used to quantify uptake in abdominal aortic aneurysms (Forsythe et al., 2018). This is an accurate but time-intensive process which also requires the manual exclusion of areas affected by the spill-over effect created by physiological radiotracer uptake within the vertebrae.

Sodium [^{18}F]fluoride uptake quantification was performed using FusionQuant, a custom-validated PET quantification tool developed by Cedars-Sinai Medical Center (Fusion Quant v1.21.0421, Cedars-Sinai Medical Center, Los Angeles, United States) (Massera et al., 2020). It has previously been used to quantify sodium [^{18}F]fluoride uptake in the coronary circulation and in the thoracic aorta (Syed et al., 2022; Tzolos et al., 2020).

The methodical development of sodium [^{18}F]fluoride uptake quantification for abdominal aortic aneurysms on PET is explored in Chapter 4. Below, is a brief overview of the method used for PET analysis.

The background blood pool activity was determined by placing two 8-mm radius spheres in the centre of the right and left atria. The cumulative SUV

within the spheres were then corrected for the spheres' total volume (2.1 cm^3) and a mean background pool activity calculated.

Four aortic regions were considered separately in the analysis (Figure 7):

- The 'descending thoracic aorta' was defined as the region where the first trans-axial slice of the descending aorta starts until the aortic hiatus at the diaphragm (Joshi et al., 2015).
- The 'suprarenal aorta' was defined as the origin of the coeliac artery down to the origin of the upper most renal artery.
- The 'neck' was defined as the origin of the lower most renal artery until the abdominal aorta became aneurysmal, or there was a definite change in vessel calibre (the latter applied to cases where the neck was ectatic).
- The 'aneurysm body' was defined as where the neck ended until the aortic bifurcation.

FusionQuant's centreline function, using a multiplanar reconstruction viewer, allows the creation of a volume of interest with an adjustable radius and length along a centreline which can be adjusted for the vessels' shape and angulation as necessary (Figure 8). The created volume of interest included the aortic lumen, any thrombus present and the aortic wall. The diameter for each volume of interest matched that of the maximal aortic luminal diameter at that point in the centreline. Four different centrelines were drawn for each of the aortic segments described above. The mean cumulative SUV of each volume

Figure 7. **Regional analysis of aortic microcalcification activity**

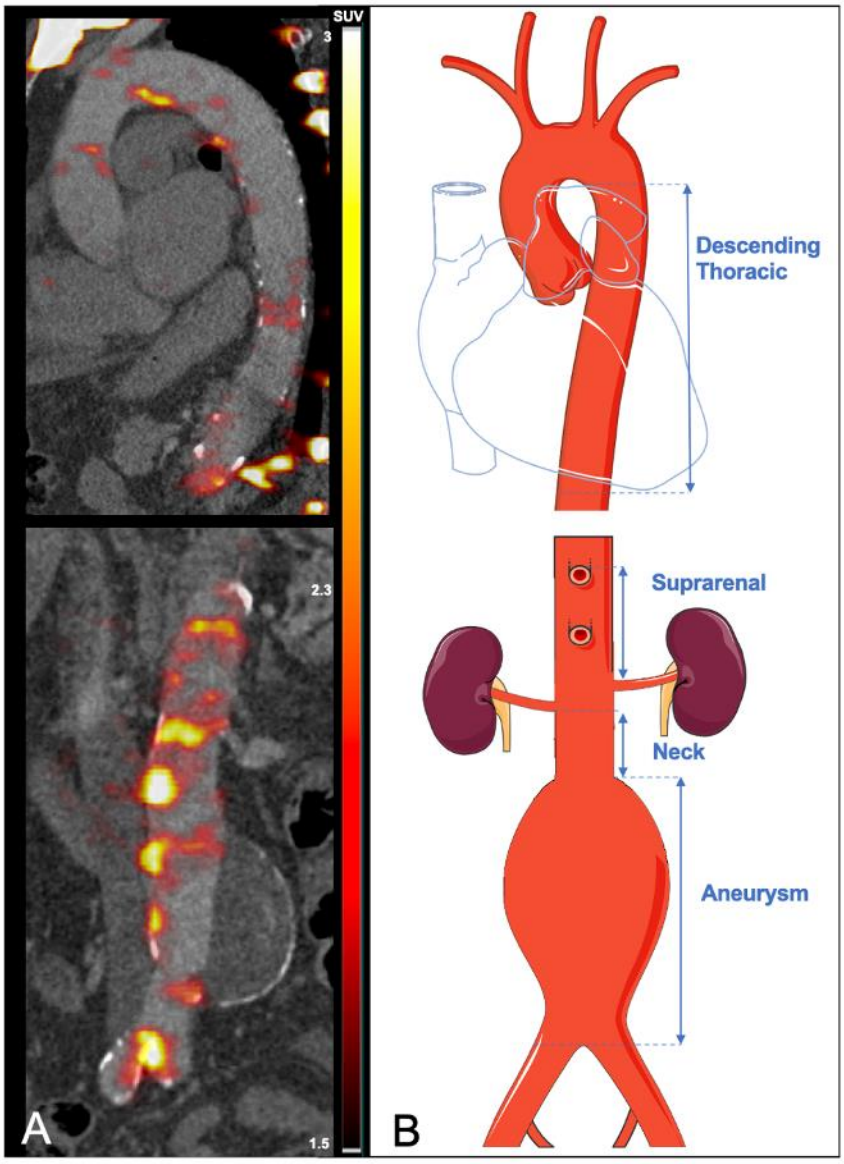

A. Pre-operative positron emission tomography (PET) and computed tomography (CT) with a colour scale bar in standard uptake values (SUV).
B. Schematic representation demonstrating the analysed aortic regions (vertical arrows: descending thoracic, suprarenal, neck, and aneurysm body).

of interest created and its volume were thus obtained. The cumulative SUV for each of the aortic segments was then divided by the volume and the mean background pool activity to obtain what was termed the aortic microcalcification activity (AMA) (Fletcher et al., 2021).

AMA can therefore provide a summary measure of mean aortic sodium [^{18}F]fluoride uptake in a three-dimensional volume. Within the thoracic aorta, this technique has demonstrated very good repeatability and reproducibility with the SUV method of quantification (Fletcher et al., 2021). Such a technique should include within it a threshold technique to correct for the spill-over effect created by physiological radiotracer uptake in the vertebrae.

The comparability of the established SUV method with AMA in the abdominal aorta is explored in Chapter 4.

2.7 Ex vivo study

Using similar principles to PET, micro-positron emission tomography (microPET) is an established preclinical non-invasive imaging tool for studying disease development and progression in small animal models (McDougald et al., 2020). This technique can also be expanded to study ex vivo human tissue. Meanwhile, autoradiography allows the study of radiotracer distribution using imaging plates which can detect radioactivity. Radiotracer exposure can be performed on either pre-made tissue slices or on a whole animal model (Bergström et al., 2003).

Figure 8. **Image analysis on a multiplanar viewer**

FusionQuant can view computed tomography with positron emission tomography imaging as overlay in three orthogonal planes. The acquisition of all imaging data in the same session ensures accurate co-registration, this was ensured prior to any analysis. Here, a three-dimensional region of interest created as a centreline around the abdominal aortic aneurysm is displayed (green).

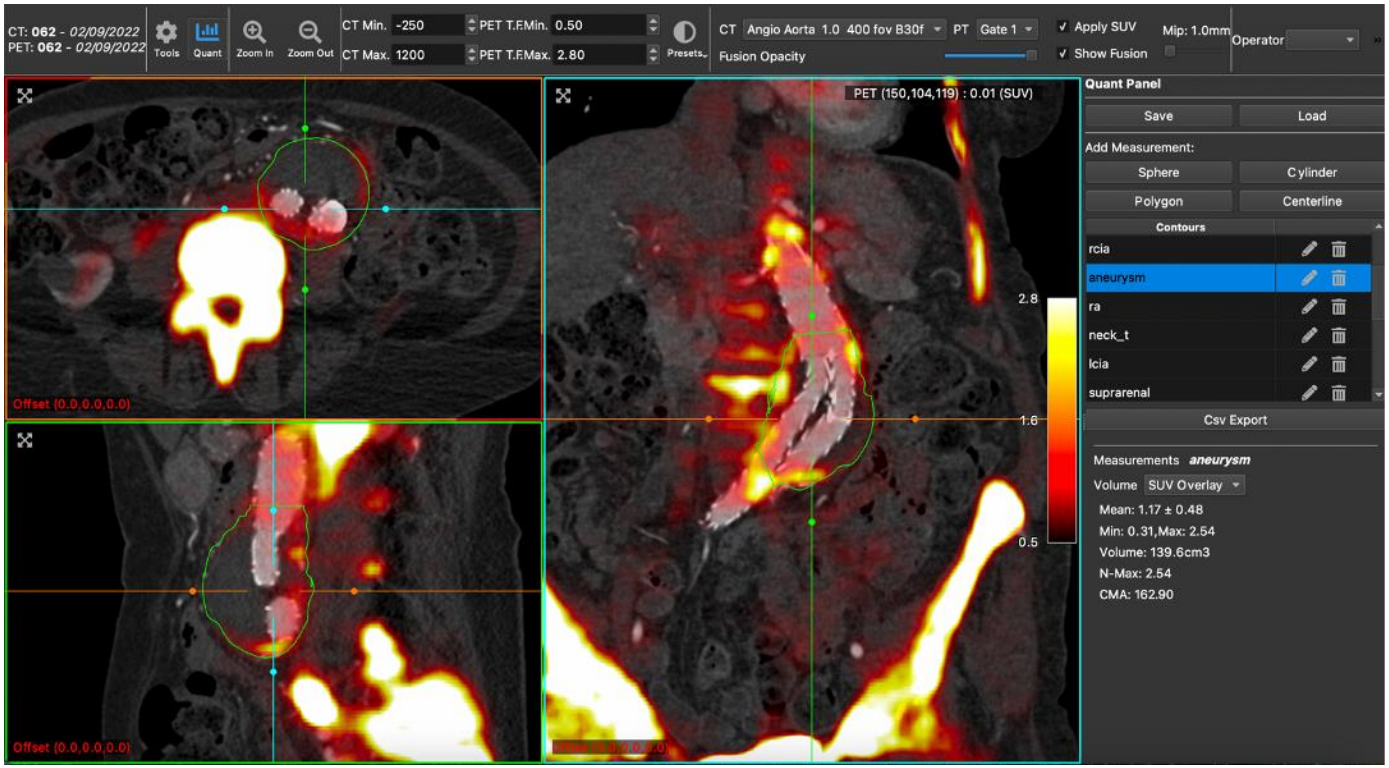

Intact tissue underwent microPET with sodium [^{18}F]fluoride. Following a 30-minute incubation with the radiotracer, PET data was acquired using a nanoPET-CT scanner (Mediso, Hungary) over 30 minutes, followed by an attenuation correction CT. Image analysis on reconstructed three-dimensional PET data was performed using PMOD 4.2 (PMOD Technologies LLC, Zurich, Switzerland).

Analysis on whole tissue considered the tissue as one volume of interest. Regional analysis involved drawing three equally sized spherical volumes of interest in the three areas of visually highest and lowest uptake. Average radiotracer uptake values (kBq/cm^3) across each volume of interest were obtained. All values were then normalised for the radiotracer incubation concentration by dividing the obtained value by the corrected radiotracer concentration (kBq/mL) for each study scan. This allowed comparison between different scans.

Guided by areas of high radiotracer uptake, the tissue was then sectioned at 4-µm thickness after being embedded in paraffin blocks. Slides were stained with Haematoxylin and Eosin, von Kossa, Picrosirius Red, elastic Van Giesen's and Alizarin Red S stains. Images were captured using Axioscan slide scanner (Zeiss, Germany). At room temperature, slides were incubated with 100 kBq/mL of sodium [^{18}F]fluoride in a phosphate buffered saline for 60 minutes and a blocking control (10 µmol/L sodium fluoride). This was followed by two 5-minute washes in phosphate buffered saline and one in deionised

water. Autoradiography imaging (Amersham Typhoon IP Biomolecular Imager, Cytiva) was then performed after the slides were exposed to a high-resolution autoradiography plate (BAS-IP-SR 2040; Cytiva) (Fletcher, Nash, et al., 2022). Radiotracer content quantification was performed using FIJI software (v2.0.0, open source) by drawing regions of interest around the tissue and on empty glass slide thus obtaining a ratio of mean background activity.

Histopathologic aneurysm disease severity scoring was performed by an experience pathologist blinded to the results of microcalcification imaging and patient status. The scoring system was adapted from a previously described system by Bruijn and colleagues (Bruijn et al., 2021). In brief, samples were scored on the following 10 categories of disease activity: mesenchymal cell loss, intimal or medial fibrosis, elastin degradation, aorta wall thickness, inflammation measured as transmural lymphoid infiltrates and tertiary lymphoid organs-like structures in the adventitia, neovascularisation, atherosclerotic lesion, microcalcification and adventitial adipocytic degeneration. The total histopathology scores of each sample were then compared according to their tissue type status.

2.8 Statistical analysis

All statistical analysis was performed in RStudio (V2022.02.3+492, RStudio, PBC). Shapiro-Wilk test was used to assess the normality distribution of data. Continuous variables with normal distribution are presented as mean ± standard deviation and skewed continuous variables are presented as median

[interquartile range]. Categorical variables are presented as number (percentage).

In Chapter 3, periaortic adipose tissue attenuation values between the three groups were first assessed using Student t tests and Wilcoxon rank sum tests. Following this, a multi-regression model was used with periaortic adipose tissue attenuation as the independent variable and age, hypertension and hypercholesterolemia as the independent variables. Subcutaneous and visceral adipose tissue attenuation was assessed using Wilcoxon rank sum tests.

Within Chapter 4, associations between quantification methods were evaluated as a continuous variable (Pearson's correlation coefficient). Quantification methods were compared using intraclass correlation coefficient (consistency and 2-way random effects model) and Bland-Altman plots (Bland & Altman, 1986; Koo & Li, 2016). Reliability of intraclass correlation coefficient values are described as: poor when less than 0.5; moderate when 0.5 to 0.75; good when 0.75 to 0.9; and excellent when greater than 0.9 (Koo & Li, 2016). Intra- and inter-observer repeatability were similarly assessed using mean bias, 95% limits of agreement and coefficient of repeatability (Vaz et al., 2013).

A simple main effect one-way model was used to assess regional difference in the aortic microcalcification activity (AMA) between pre-operative and post-operative PET quantification data in Chapter 5. A Kruskal-Wallis rank sum test

was used to assess regional differences in the AMA between the two timepoints. Wilcoxon signed-rank test was used to test pre-operative and post-operative calcium scores.

A two-way repeated measures analysis of variance (ANOVA) was used to assess regional differences in the AMA between endoleak and no endoleak groups in Chapter 6. P-values were adjusted using the Bonferroni multiple testing correction method. Change in aneurysm sac size was corrected for the interval distance between the pre-operative and post-operative scan (mm/year). Pearson's correlation coefficient was used to assess the association between change in aneurysm sac size and AMA ratio.

Other statistical significance was assessed using Pearson's Chi-squared test, Fisher's exact test, Students t-test, Kruskal-Wallis rank sum test or Wilcoxon rank sum test as appropriate. A two-sided $p < 0.05$ was considered statistically significant.

Chapter 3: Periaortic adipose tissue in abdominal aortic aneurysms

Published by **Debono S**, Tzolos E, Syed MBJ, Nash J, Fletcher AJ, Dweck MR, Newby DE, Dey D, Forsythe RO, Williams MC. CT Attenuation of Periaortic Adipose Tissue in Abdominal Aortic Aneurysms. *Radiol Cardiothorac Imaging*. 2024 Feb;6(1):e230250. doi: 10.1148/ryct.230250. PMID: 38329405.

3.1 Abstract

3.1.1 Background

Pericoronary adipose tissue attenuation on CT angiography has been associated with localised coronary inflammation that is predictive of adverse cardiac events and mortality. Adipose tissue also surrounds other vascular structures, including the abdominal aorta. The aim of the study was to assess periaortic adipose tissue attenuation on CT angiography in different abdominal aortic aneurysm disease states.

3.1.2 Methods

Periaortic adipose tissue attenuation was assessed on CT angiography in patients with asymptomatic or symptomatic (including rupture) abdominal aortic aneurysms, as well as control subjects without aneurysms. Periaortic adipose tissue attenuation was measured using semi-automated software in aneurysmal and non-aneurysmal segments of the abdominal aorta, and in subcutaneous and visceral adipose tissue.

3.1.3 Results

Eighty-eight participants were included: 70 patients with abdominal aortic aneurysms (40 asymptomatic and 30 symptomatic patients including 24 with acute rupture), and 18 control subjects. Participants had a median age of 70 [interquartile range 65 to 78] years and 89% (78/88) were male. There were no differences in the periaortic adipose tissue attenuation in aneurysmal and non-aneurysmal segments of the aorta between asymptomatic patients (-

81.4±7 versus -75.4±8 HU) and comparable segments in control subjects (-83.3±9 versus -78.8±6 HU, $p>0.05$ for all). However, symptomatic patients demonstrated much higher periaortic adipose tissue attenuation in both aneurysmal (-57.9±7 HU, $p<0.0001$) and non-aneurysmal segments (-58.2±8 HU, $p<0.0001$).

3.1.4 Conclusion

Periaortic adipose tissue attenuation is not increased in stable abdominal aortic aneurysm disease, although there is a generalised increase in patients with symptomatic disease likely reflecting the systemic consequences of acute rupture.

3.2 Introduction

As detailed in Section 1.5.1, perivascular adipose tissue refers to any adipose tissue surrounding a blood vessel including periaortic deposits and is metabolically active (Britton & Fox, 2011).

Dysfunction and remodelling of the adipocytes within this tissue can result in a low-grade inflammatory state with chronic inflammatory cell infiltration and fibrosis which leads to an increase in adipose tissue attenuation (measured in Hounsfield Units, HU) (Figure 4) (Mancio et al., 2018). Analysis of adipose tissue attenuation around the right coronary artery has been able to predict myocardial infarction and all-cause and cardiac mortality on retrospective

analyses of CT coronary angiograms (Oikonomou et al., 2018; Tzolos et al., 2022).

There are larger amounts of perivascular adipose tissue around the aorta when compared to the coronary vessels and therefore as an imaging biomarker, analysis of periaortic adipose tissue could have a role in aortic pathology. Previous work has reported that the presence of an abdominal aortic aneurysm was an independent predictor of higher perivascular adipose tissue attenuation around the aneurysm sac and demonstrated a relationship with aortic volume (Dias-Neto et al., 2018).

The aim of this study was to investigate periaortic adipose tissue attenuation on CT imaging within the abdominal aorta in patients with different abdominal aortic aneurysm disease states to assess whether periaortic adipose tissue attenuation is associated with aneurysm disease activity.

3.3 Methods

Further study methodology is outlined in Chapter 2. In brief however, this was a single centre observational study with a retrospective analysis of CT imaging.

The study population was comprised of three groups: (i) asymptomatic patients with an unruptured abdominal aortic aneurysm, (ii) symptomatic patients with CT evidence of a ruptured abdominal aortic aneurysm, or unruptured

abdominal aortic aneurysm proceeding to emergency repair, and (iii) control subjects with a normal calibre abdominal aorta.

Asymptomatic patients and control subjects were consecutive study participants recruited in the Sodium [^{18}F]Fluoride Imaging of Abdominal Aortic Aneurysms (SoFIA^{3}) study (NCT02229006), a prospective case-control observational cohort study of patients with asymptomatic abdominal aortic aneurysms under ultrasound surveillance and control subjects with normal calibre abdominal aortas (Forsythe et al., 2018).

Symptomatic participants were patients who had presented to their local Emergency Department with abdominal pain and a clinical suspicion of ruptured abdominal aortic aneurysm.

Asymptomatic patients and control subjects underwent a contrast-enhanced CT angiography and symptomatic patients underwent CT imaging according to local Emergency Department and Radiology protocols.

The aortic diameter was measured in the antero-posterior plane using the PACS (Carestream Health).

Assessment of visceral and subcutaneous adipose tissue attenuation was performed using OsiriX (version 13.0.0; OsiriX Imaging Software, Geneva, Switzerland). Mean attenuation values were calculated for each patient by

drawing four circular regions of interest in the visceral fat and the subcutaneous fat at the mid-level of the third lumbar vertebra (Derstine et al., 2022; Gleinert-Rożek et al., 2020) (Figure 5).

Periaortic adipose tissue attenuation assessments were performed using Autoplaque (version 2.5, Cedars-Sinai Medical Center, Los Angeles) (Williams et al., 2020). Two aortic regions were analysed: (i) the abdominal aorta (from just below the lowermost renal artery until the aortic bifurcation), and (ii) the normal aorta (a 20-mm straight segment of non-aneurysmal aorta, usually in the suprarenal abdominal aorta). In patients with rupture, the normal segment of the aorta excluded areas with CT-evidence of haemorrhage. The mean tissue attenuation at a 2-mm distance from the vessel wall was considered and conversion factors were used on the attenuation values to adjust for different scans having been performed at different tube voltages (Etter et al., 2023; Ma et al., 2020) (Figure 6).

Continuous variables with normal distribution are presented as mean ± standard deviations, and skewed continuous variables are presented as medians (interquartile range). Categorical variables are presented as numbers (percentages). Periaortic adipose tissue attenuation values between the three groups were first assessed using Student t tests and Wilcoxon rank sum tests. A multi-regression model was then used with periaortic adipose tissue attenuation as the independent variable and age, hypertension and hypercholesterolemia as the independent variables. Subcutaneous and

visceral adipose tissue attenuation was assessed using Wilcoxon rank sum tests. A two-sided $p<0.05$ was considered statistically significant.

3.4 Results

The study population comprised of 88 participants: 40 had an asymptomatic unruptured abdominal aortic aneurysm, 30 had a symptomatic abdominal aortic aneurysm (6 of which were unruptured). Eighteen were control subjects with a normal aortic diameter. All symptomatic patients without aortic rupture presented with abdominal pain which was deemed to be due to an unruptured abdominal aortic aneurysm found on CT imaging. Symptomatic patients had a median C-reactive protein of 21 [6 to 54] mg/L. Control subjects were younger and had fewer medical co-morbidities than the other two groups (Table 4).

3.4.1 Periaortic adipose tissue attenuation

The periaortic adipose tissue attenuation in the aneurysmal aorta of asymptomatic patients (-81.44±7 HU) did not differ from that of control subjects (-83.27±9 HU; p=0.433) (Figure 9). Similarly, in the non-aneurysmal abdominal aorta, the periaortic adipose tissue attenuation of asymptomatic patients (-75.43±8 HU) did not differ from comparable segments in control subjects (-78.81±6 HU; p=0.188).

In symptomatic patients, both the aneurysmal abdominal aorta (-57.85±7 HU) and the non-aneurysmal abdominal aortic segment (-58.16±8 HU) demonstrated much higher periaortic adipose tissue attenuation values when

compared to the other two groups (p<0.0001; Figure 10). This was also true for separate analysis of symptomatic patients without rupture (aneurysmal segment -58.72±6 HU, p<0.0001; non-aneurysmal segment -60.84±9 HU, p<0.01) and rupture patients alone (aneurysmal segment -57.63±7 HU, p<0.0001; non-aneurysmal segment -57.47±7 HU, p<0.0001) (Figure 9).

In a multivariable regression analysis, acutely symptomatic aneurysms were associated with high periaortic adipose tissue attenuation values around the aneurysm as an independent variable (univariable ß estimate, 25.42 [95% CI: 21.12, 29.71]; p<0.0001) and when corrected for age, the presence of hypertension, and the presence of hypercholesterolemia (multivariable ß estimate, 25.39 [95% CI: 20.51, 30.27]; p<0.0001). Similar patterns were seen around segments of normal aorta (univariable ß estimate, 20.65 [95% CI: 16.20, 25.10]; p<0.0001 and multivariate ß estimate, 21.21 [95% CI: 16.33, 26.10]; p<0.0001) (Figure 9).

A weak positive correlation was observed between aortic diameter and the periaortic adipose tissue attenuation in symptomatic patients (r=0.29, p=0.025), but not in the other two groups. No relationship was observed between periaortic adipose tissue attenuation and C-reactive protein.

3.4.2 Visceral and subcutaneous fat attenuation

Over a median area of 82.5 mm^2, there were no demonstrable differences in adipose tissue attenuation values between visceral (-106.1 [-109.5 to -99.9]

HU) and subcutaneous (-108.2 [-112.2 to -101.3] HU) fat (p=0.057). Visceral fat attenuation was similar across the study groups (control subjects, -106.5 [-108.7 to -100.6]; asymptomatic patients, -106.2 [-109.9 to -102.1]; symptomatic non-rupture patients, -102.0 [-107.6 to -93.1]; and symptomatic rupture patients, -104.3 [-109.5 to -97.0] HU; p>0.05 for all comparisons, Figure 11).

The subcutaneous fat attenuation was slightly higher in the symptomatic patients (-102.1 [-111.6 to -96] HU) when compared to asymptomatic patients (-110.0 [-112.2 to -106.7] HU; p<0.005) but not when compared to control subjects (-107.8 [-112.2 to -102.7] HU; p=0.095). These differences were most apparent in the subgroup of symptomatic patients with ruptured aneurysms (Figure 11).

3.5 Discussion

In this case control study, we have assessed the periaortic adipose tissue attenuation in patients with abdominal aortic aneurysm disease. We found that periaortic adipose tissue attenuation is not directly influenced by the presence of abdominal aortic aneurysm disease per se, with similar values observed in participants with and without abdominal aortic aneurysms. Indeed, even within the same patient, we observed no differences in periaortic adipose tissue attenuation in areas with and without aneurysm disease. However, patients with symptomatic aneurysms had increased periaortic adipose tissue attenuation which was also present within non-aneurysmal segments of the

Table 4. **Patient characteristics for the periaortic adipose tissue assessment study**

	Patient groups			**p-values**		
Characteristic	**Control Subjects**	**Asymptomatic (Unruptured) Abdominal Aortic Aneurysm**	**Symptomatic Abdominal Aortic Aneurysm**	**Control versus Asymptomatic**[2]	**Control versus Symptomatic**[2]	**Asymptomatic versus Symptomatic**[2]
	N = 18[1]	N = 40[1]	N = 30[1]			
Age (years)	66 ± 2	72 ± 6	74 ± 9	<0.001	<0.001	0.3
Male	18 (100%)	35 (88%)	25 (83%)	0.3	0.14	0.7
Aortic diameter, mm	20 (19, 20)	49 (44, 55)	74 (62, 89)	<0.001	<0.001	<0.001
Medical History						
Hypertension	5 (28%)	23 (57%)	22 (73%)	0.036	0.002	0.2
Cerebrovascular accident	0 (0%)	4 (10%)	4 (13%)	0.3	0.3	0.7
Ischaemic heart disease	1 (5.6%)	7 (18%)	11 (37%)	0.4	0.018	0.069
Peripheral arterial disease	0 (0%)	7 (18%)	2 (6.7%)	0.087	0.5	0.3
Diabetes	1 (5.6%)	6 (15%)	2 (6.7%)	0.4	>0.9	0.5

Hypercholesterolaemia	6 (33%)	32 (80%)	21 (70%)	<0.001	0.013	0.3
Current or ex-smoker	3 (21%)	12 (31%)	21 (81%)	0.7	<0.001	<0.001
Medications						
Antiplatelet agents	2 (11%)	26 (65%)	19 (63%)	<0.001	<0.001	0.9
Anticoagulant	0 (0%)	2 (5.0%)	3 (10%)	>0.9	0.3	0.6
Statins	6 (33%)	33 (82%)	21 (70%)	<0.001	0.013	0.2
Beta-blocker	1 (5.6%)	8 (20%)	8 (27%)	0.2	0.13	0.5
Angiotensin Converting Enzyme Inhibitors or Angiotensin Receptor Blockers	3 (17%)	18 (45%)	14 (47%)	0.038	0.035	0.9

[1]Mean ± standard deviation; n (%); Median (interquartile range)

[2]Wilcoxon rank sum test; Fisher's exact test; Pearson's Chi-squared test

Figure 9. **Periaortic fat attenuation within 2-mm distance from vessel wall**

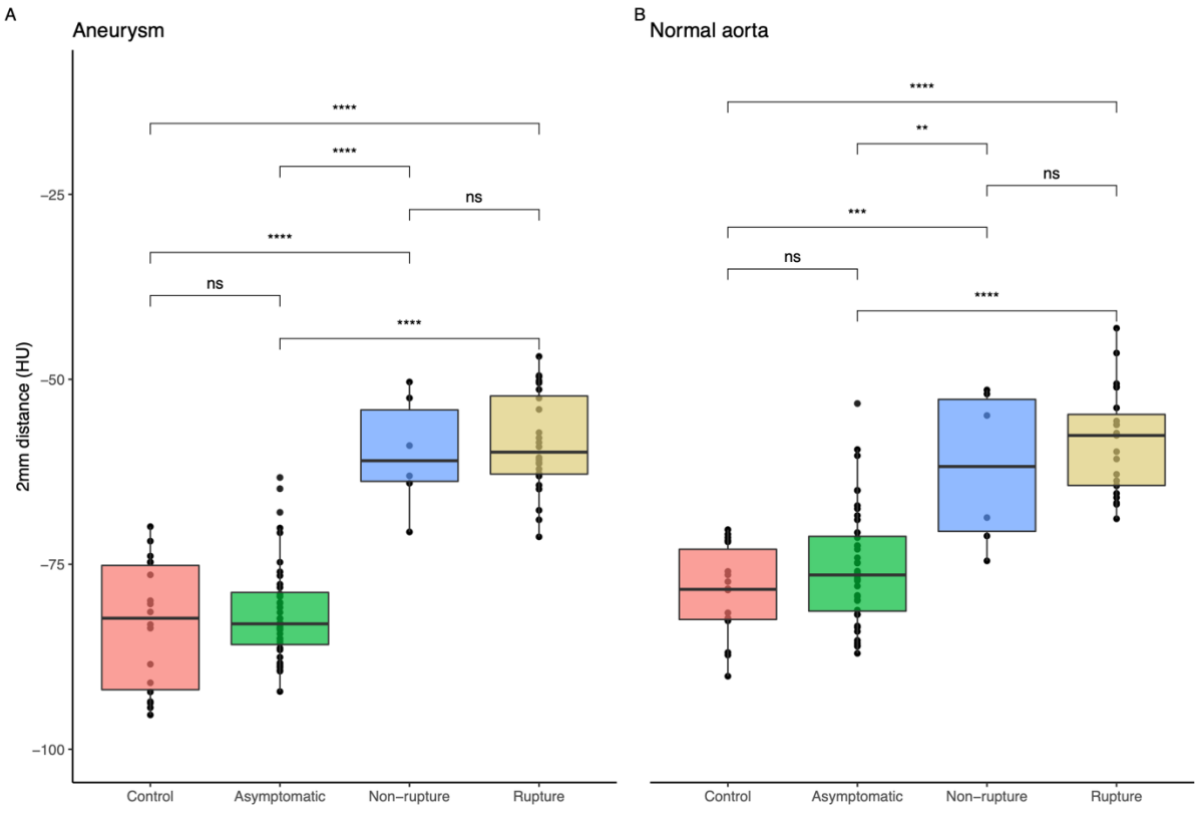

Periaortic fat attenuation in (A) the aneurysmal and (B) non-aneurysmal segments of the abdominal aorta in control subjects†, and patients with asymptomatic and symptomatic aneurysms. Patient groups with symptomatic aneurysms were sub-divided into those with and without rupture.

Each black point represents individual attenuation values. The upper and lower edges of the box represent the interquartile range and the middle horizontal line represents the median value in each group. HU, Hounsfield units; **** = p<0.0001; *** = p<0.001 ns = not significant. †Comparable but non-aneurysmal segments in control subjects were used.

Figure 10. **Periaortic adipose tissue in representative patients**

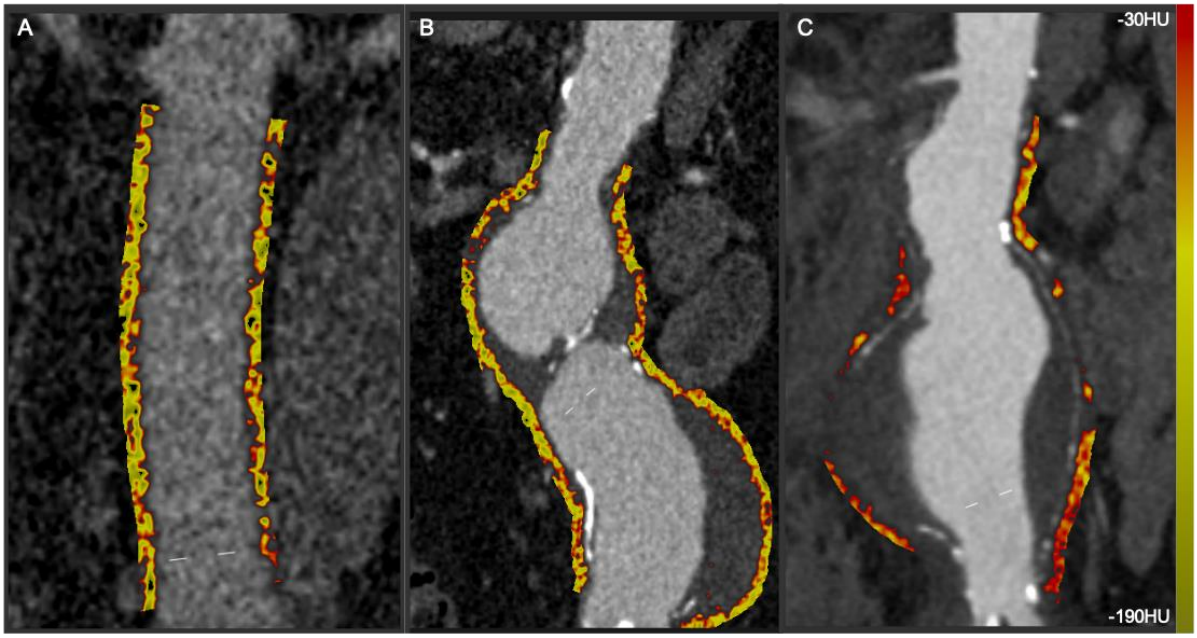

Assessment of periaortic adipose tissue attenuation in sagittal computed tomography images of the aorta in (A) 66-year-old male individual from the control group (mean -93.57±41 HU), (B) a 79-year-old male patient with an asymptomatic aneurysm (mean -89.45±36 HU) and (C) a 71-year-old female patient with aneurysm rupture (mean -59.12±21 HU).

HU, Hounsfield units.

Figure 11. **Visceral and subcutaneous adipose tissue attenuation**

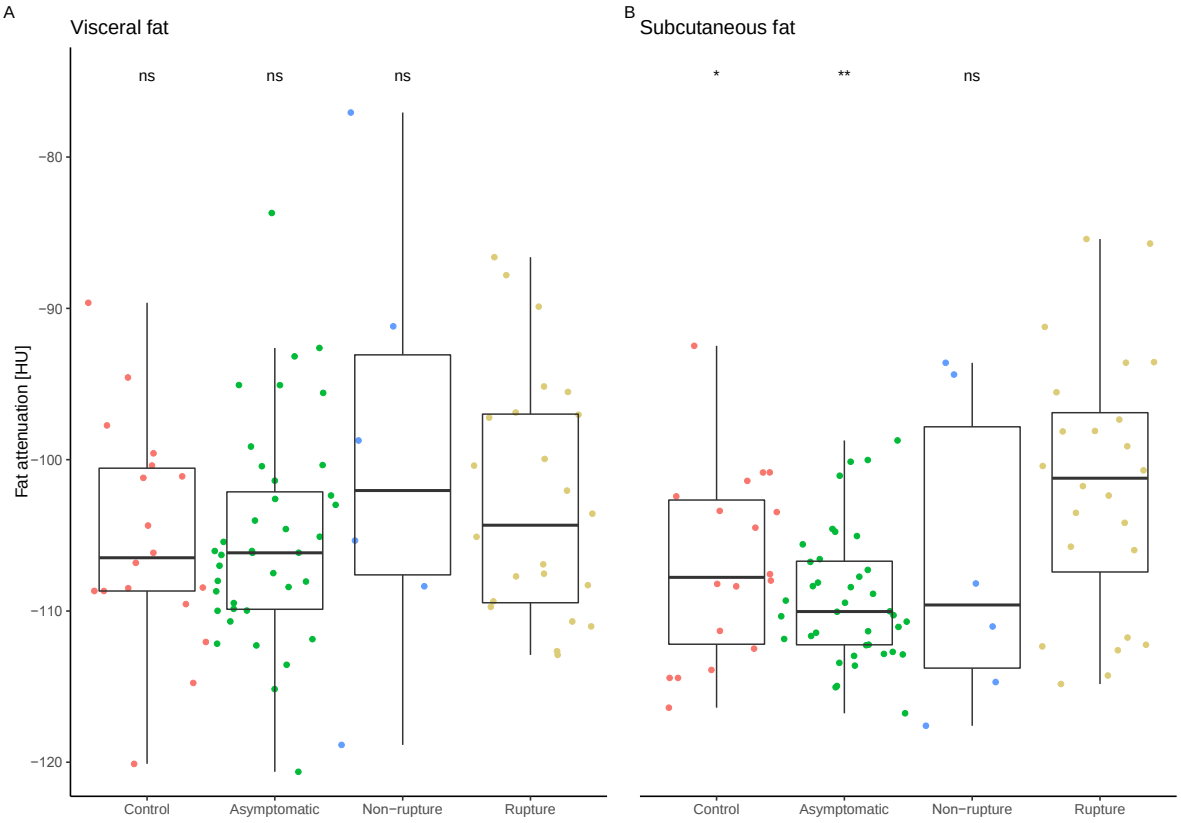

Sub-group analyses of (A) visceral and (B) subcutaneous fat attenuation in control subjects, patients with asymptomatic aneurysms and patients with symptomatic aneurysms sub-divided into those with and without rupture.

Each point represents individual attenuation values displayed at different locations along the x-axis to prevent overplotting. The upper and lower edges of the box represent the interquartile range and the middle horizontal line represents the median value in each group. HU, Hounsfield units; * = p< 0.05; ** = p<0.01; ns = not significant.

aorta. This suggests that increased periaortic adipose tissue attenuation is not a localised feature of active aneurysm disease itself, but a broader generalised aortic response to unstable active disease and acute rupture.

Atherosclerosis is the primary underlying process in the pathogenesis of acute myocardial infarction (Palasubramaniam et al., 2019). The association of all-cause and cardiac mortality with pericoronary adipose tissue attenuation has been most convincingly demonstrated for the right coronary artery where the volume of fat is greatest (Oikonomou et al., 2018; Tzolos et al., 2022). With the abdominal aorta being a much larger vessel and associated with even greater volumes of perivascular fat, we wanted to assess whether periaortic adipose tissue attenuation would associate and correlate with the presence and magnitude of abdominal aortic aneurysm disease. Histological analysis of aneurysm tissue has shown the involvement of various inflammatory cell types, such as macrophages and lymphocytes, and a role of inflammation in the pathogenesis of aneurysm disease has been proposed (Dale et al., 2015; Koch et al., 1990). Furthermore, murine models have shown a link between vascular inflammation and aneurysm formation and perivascular adipose tissue through the angiotensin II type 1a receptor (Sakaue et al., 2017). It is therefore plausible that periaortic adipose tissue attenuation could be linked to, or be a marker of, abdominal aortic aneurysm disease activity. However, we identified no such association in patients with established stable aneurysm disease with periaortic adipose tissue attenuation being similar between not only patients and control subjects, but importantly, also similar between normal

regions of aorta and those affected by aneurysmal disease within the same subject.

In a retrospective study, Dias-Neto and colleagues have previously found that when compared to patients with occlusive aortoiliac disease and without aortic disease, the presence of an abdominal aortic aneurysm was an independent predictor of higher perivascular adipose tissue attenuation around the aneurysm sac and the healthy neck (Dias-Neto et al., 2018). They did however employ a rather different methodology to the pericoronary adipose tissue methodology which we employed here. First, they generated a density value taking the summation of all the attenuation values from a range of -107 to -45 HU and divided them by the area of the region of interest. Second, they included a large 10-mm distance from the outer wall of the aorta which will likely include non-adipose tissue structures. We have here used previously validated semi-automated software (Williams et al., 2020) to obtain mean attenuation values at a 2-mm distance from the aortic wall. We also considered the neck and body of the aorta together and compared a more remote region of healthy aorta away from the aneurysm sac and disease.

In pericoronary adipose tissue, Oikonomou and colleagues used a cut-off of above -70 HU as their at-risk population threshold (Oikonomou et al., 2018). Moreover, the overall differences in pericoronary adipose tissue between those with and without future coronary events were small (~4-6 HU). Here, we have observed very large differences in periaortic adipose tissue attenuation

between those with asymptomatic and symptomatic disease: approximately 25 HU. This dramatic difference is striking and importantly was seen in both the region of the aneurysm as well as the more distant non-aneurysmal unruptured aorta. This suggests that this is not a regional effect at the segment of active disease and rupture but a more global aortic phenomenon. We wondered if this was a systemic effect that would affect all adipose tissue throughout the body and therefore explored adipose tissue attenuation in both subcutaneous and visceral fat. Here, we noted only a slight difference (approximately 8 HU) in the subcutaneous fat tissue of symptomatic ruptured patients. This change may perhaps reflect fluid shifts in the extracellular space consequent to systemic shock or intravenous fluid resuscitation leading to non-specific increases in adipose tissue attenuation. However, this effect was not observed in visceral fat tissue. Whilst extravasation of blood in acute rupture may account for the difference in periaortic adipose tissue attenuation, this was also observed in symptomatic unruptured patients. The differences in subcutaneous tissue attenuation between the groups are however modest, and could plausibly only account for approximately a third of the overall difference. We believe that the observed changes are most likely to represent the consequences of acute rupture rather than a true reflection of adventitial disease activity because of the lack of a regional effect with generalised changes seen in non-aneurysmal as well as aneurysmal segments of the aorta. Speculatively, this could be related to the increased fibrotic changes and presence of increased adipocyte clusters in the adventitia (Doderer et al., 2018), or perhaps to changes in tissue density in response to adventitial

neurovascular reflexes as part of the physiological response to aortic rupture and systemic hypotension (Di Serafino et al., 2021).

Our study has some limitations. First, data for symptomatic patients were collected in a retrospective fashion from image archives and only minimal clinical data could be collected. A future prospective study could perhaps assess the periaortic adipose tissue on CT imaging in relation to histology of intra-operatively obtained adipose tissue during open abdominal aortic aneurysm repair. Second, asymptomatic patients and control subjects were imaged on a research scanner with a dedicated imaging protocol whereas symptomatic patients were scanned on a variety of clinical scanners in different vascular centres around Scotland. Whilst we have corrected the data for tube voltage, imaging protocols were not uniform. Despite this, we have demonstrated that visceral fat attenuation between scans did not vary between the three study groups. Third, whilst the reproducibility for periaortic fat analysis has not been established, quantitative adipose tissue attenuation has previously shown excellent repeatability in much smaller structures, such as the pericoronary adipose tissue (Tzolos, McElhinney, et al., 2021). Fourth, this study provides a single snapshot assessment of periaortic adipose tissue but does not provide an assessment over time and we cannot comment on its association with aneurysm development or progression.

3.6 Clinical Perspectives

Periaortic adipose tissue attenuation assessed on CT is not associated with stable aortic aneurysm disease but is markedly increased in symptomatic abdominal aortic aneurysms including patients with acute rupture. These changes in perivascular adipose tissue attenuation are not generalisable to all vascular beds or cardiovascular diseases. Large systemic changes in attenuation occur in patients with symptomatic abdominal aortic aneurysm disease but are not localised to the diseased or ruptured segment itself. Further larger studies are needed to establish whether periaortic adipose tissue attenuation has any role in the prediction of aneurysm disease progression and its role in acute symptomatic disease. However, further work could explore other analyses of the obtained CT-imaging by extracting different but related quantitative matrices to perivascular adipose tissue through the use of artificial intelligence in radiomics.

Chapter 4: Quantifying sodium [^{18}F]fluoride uptake in abdominal aortic aneurysms

Published by **Debono S**, Nash J, Fletcher AJ, Syed MBJ, Semple SI, van Beek EJR, Fletcher A, Cadet S, Williams MC, Dey D, Slomka PJ, Forsythe RO, Dweck MR, Newby DE. Quantifying sodium [^{18}F]fluoride uptake in abdominal aortic aneurysms. *EJNMMI Res.* 2022 Jun 6;12(1):33. doi: 10.1186/s13550-022-00904-z. PMID: 35666397; PMCID: PMC9170850.

4.1 Abstract

4.1.1 Background

Sodium [^{18}F]fluoride PET-CT uptake in the thoracic aorta has been recently measured as aortic microcalcification activity. The aim of this study was to compare and to modify this method for use within the infrarenal aorta of patients with abdominal aortic aneurysms.

4.1.2 Methods

Twenty-five patients with abdominal aortic aneurysms underwent an sodium [^{18}F]fluoride PET-CT. Maximum and mean tissue to background ratios (TBR) and abdominal aortic microcalcification activity were determined following application of a thresholding and variable radius method to correct for vertebral sodium [^{18}F]fluoride signal spill-over and the non-linear changes in aortic diameter respectively. Agreement between the methods, and the repeatability of these approaches were assessed.

4.1.3 Results

The aortic microcalcification activity method was much quicker to perform than the TBR method (14 versus 40 min, $p<0.001$). There was moderate to good agreement between TBR and aortic microcalcification activity measurements for maximum (intraclass correlation co-efficient, 0.67) and mean (intraclass correlation co-efficient, 0.88) values. These correlations sequentially improved with the application of thresholding (intraclass correlation coefficient 0.93, 95% confidence interval 0.89-0.95) and variable diameter (intraclass correlation

coefficient 0.97, 95% confidence interval 0.94-0.99) techniques. The optimised method had good intra-observer (mean 1.57 ± 0.42, bias 0.08, co-efficient of repeatability 0.36 and limits of agreement -0.43 to 0.43) and inter-observer (mean 1.57 ± 0.42, bias 0.08, co-efficient of repeatability 0.47 and limits of agreement -0.53 to 0.53) repeatability.

4.1.4 Conclusion

Aortic microcalcification activity is a quick and simple method which demonstrates good intra-observer and inter-observer repeatability and provides measures of sodium [^{18}F]fluoride uptake that are comparable to established methods.

4.2 Introduction

As described in Chapters 1 and 2, sodium [^{18}F]fluoride PET-CT is a non-invasive multimodality imaging technique that detects early calcification activity as a marker of vascular injury (Tzolos & Dweck, 2020). Conventional CT imaging can visualise established larger macrocalcified plaques whilst sodium [^{18}F]fluoride binds to microscopic hydroxyapatite and pyrophosphate crystals deposited in the media as part of vascular calcification and aortic degeneration. It is able to identify earlier microcalcification on PET which is beyond the resolution of CT (Aikawa et al., 2007; Ritman, 2007). Sodium [^{18}F]fluoride PET has thus emerged as a promising imaging biomarker for the early detection of vascular injury and calcification activity (M. B. Syed et al., 2019). Previously, binding of sodium [^{18}F]fluoride in explanted aortic aneurysm

tissue has been performed on a single specimen (Forsythe et al., 2018) and further tissue validation is required.

Aortic microcalcification activity (AMA) is a recently described simplified method of measuring aortic sodium [^{18}F]fluoride uptake (Fletcher et al., 2021). It is quick to perform and correlates well with clinical outcomes. However, this technique has only been applied in the thoracic aorta.

This study's aim was to assess the AMA method for quantifying sodium [^{18}F]fluoride uptake within the infrarenal aorta of patients with abdominal aortic aneurysms by comparing it with the established method of tissue to background ratio. Specifically, (i) to investigate the comparability of these measurements, (ii) to assess modifications to account for spill-over of the sodium [^{18}F]fluoride signal from adjacent vertebra and the variable aneurysm diameter, and (iii) to determine the within and between observer repeatability of the optimised analytical approach.

4.3 Methods

Further study methodology is outlined in Chapter 2. In brief however, the study population comprised 25 consecutive patients recruited into the Sodium [^{18}F]Fluoride Imaging in Abdominal Aortic Aneurysms (SoFIA^{3}) study (NCT02229006). Participants were aged over 50 years and under routine clinical surveillance with an asymptomatic abdominal aortic aneurysm defined as ≥40 mm inner-to-inner anteroposterior diameter on ultrasound.

4.3.1 Sodium [^{18}F]fluoride PET-CT

Patients were administered a target dose of 125 MBq of sodium [^{18}F]fluoride intravenously and after 60 min were imaged on a hybrid 128–slice PET-CT scanner (Biograph mCT, Siemens Healthineers, Erlangen, Germany) (Irkle et al., 2015). A low-dose attenuation correction CT scan was performed (120 kV, 50 mAs, 5/3 mm), followed by acquisition of PET data at 10-min intervals in three bed positions to ensure complete coverage of the thoracic and abdominal aorta. Contrast-enhanced CT angiography (120 kV, 145 mAs, 3/3 mm, field of view 400; and 1/1 mm, field of view 300; triggered at 181 Hounsfield units) was performed on the same scanner immediately after PET acquisition. This was centred on the abdominal aortic aneurysm and extended to the aortic bifurcation.

Static PET-CT images were reconstructed with correction applied for attenuation, deadtime, scatter and random coincidences, using an optimised iterative reconstruction algorithm (ultra-High Definition; TrueX + Time-of-Flight, 2 iterations and 21 subsets, matrix 200, zoom 1; Gaussian filter 5 mm).

4.3.2 Image Analysis

All PET analysis was performed on FusionQuant, a custom validated tool (FusionQuant v1.21.0421, Cedars-Sinai Medical Centre, Los Angeles) (Massera et al., 2020) (Figure 8).

4.3.3 Background blood pool

The background blood pool activity was determined by placing two 8-mm radius spheres in the centre of the right and left atria. The cumulative standard uptake values (SUV) within the spheres were then corrected for the spheres' total volume (2.1 cm^3). The mean background pool activity was then used in tissue to background ratio (TBR) and aortic microcalcification activity (AMA) calculations as well as a minimum visualisation threshold.

4.3.4 Volumes of interest within the aorta

On the attenuation correction CT, the thoracic aorta was defined as the region where the first trans-axial slice of the descending aorta starts until the aortic hiatus at the diaphragm (Joshi et al., 2015). Being of normal diameter and non-aneurysmal, the thoracic aorta was considered as a control. Using the CT angiogram, the abdominal aorta was analysed in three separate sections described in Section 2.6.2: the 'suprarenal aorta', the 'neck' and the 'body of the aneurysm' (Figure 7).

4.3.5 Tissue to background ratio

Regions of interest with a thickness of 3-mm were drawn around the aorta in the trans-axial plane along the entire length of the thoracic aorta and each aortic segment in a slice-by-slice fashion (Joshi et al., 2015) (Figure 12). For each region, mean and maximum SUVs (SUV_{mean} and SUV_{max}, respectively) were measured. These values were then divided by the background pool activity to obtain tissue to background ratios (TBR) for both the mean

(TBR_{mean}) and maximum (TBR_{max}) values. Care was taken to exclude regions of overspill from vertebral sodium [^{18}F]fluoride uptake.

4.3.6 Abdominal aortic microcalcification activity

The image analysis programme has a centreline function in a multiplanar reconstruction viewer. This allows the creation of a volume of interest with an adjustable radius and length along a centreline which can be adjusted for the vessel's shape and angulation as necessary. Each volume of interest included the aortic lumen, any thrombus present and the aortic wall. The diameter for each volume of interest matched that of the maximal aortic luminal diameter at that point in the centreline. Four different centrelines were drawn for each aortic segment: thoracic, suprarenal, neck and body of the aneurysm (Figure 12). The cumulative SUV (mean) of each volume of interest created is thus obtained, along with its volume and maximum SUV. As previously described in the AMA method (Fletcher et al., 2021), the cumulative SUV for each of the aortic segments was then divided by the volume and the mean background pool activity to obtain the mean AMA value.

The method was however further enhanced for the abdominal aorta in two ways:

- *Maximum Threshold*: sodium [^{18}F]fluoride is physiologically taken up by the vertebrae. This creates a spill-over effect where there is spill-over of the radiotracer signal into the surrounding tissues including the aneurysm. This leads to higher measures of radiotracer uptake being

Figure 12. **Tissue to background ratio and aortic microcalcification activity regions of interest in the abdominal aorta**

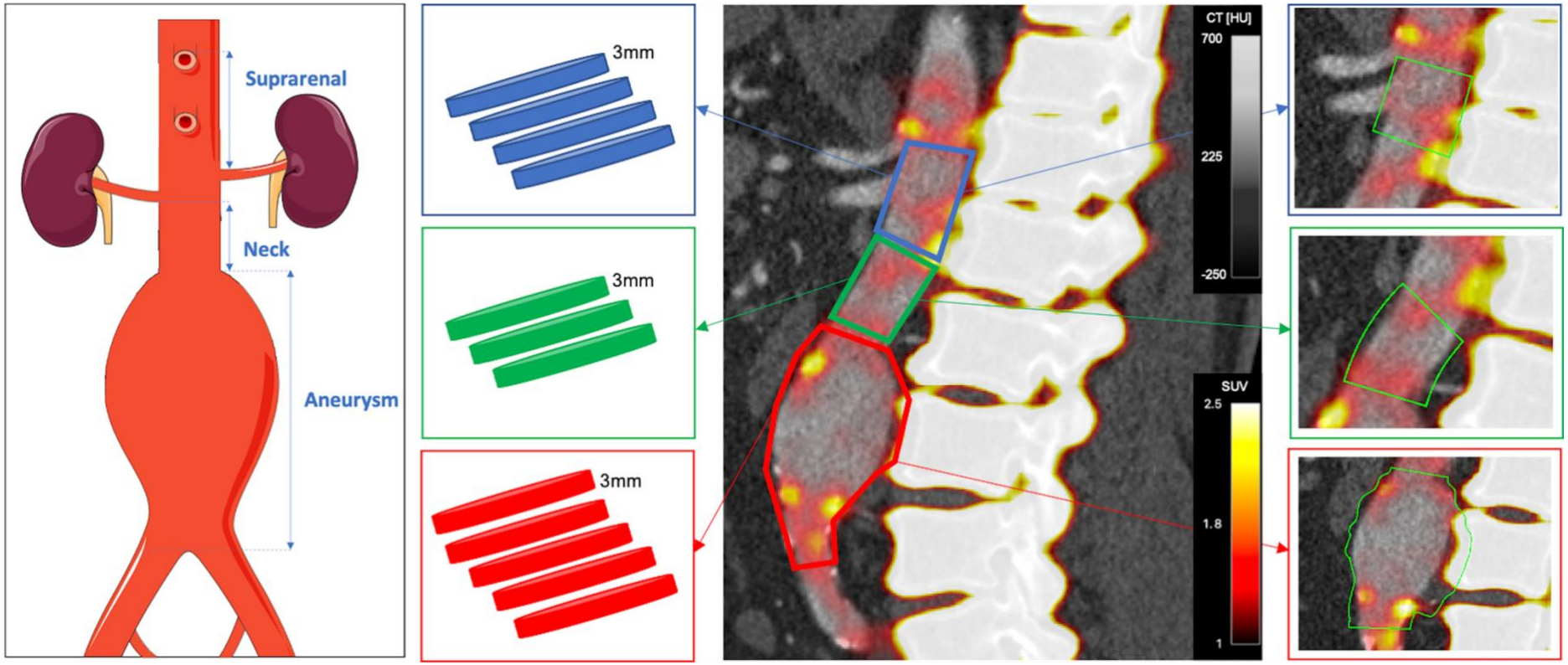

The abdominal aorta was split into three anatomical regions for analysis demonstrated on the panel on the left. Suprarenal – starting from the level of the origin of the coeliac artery till the upper-most renal artery. Neck – starting from the lower-most renal artery until where the aorta becomes aneurysmal. Aneurysm body – starting just after the neck region ends until the aortic

bifurcation. The second panel from the left shows a graphic representation of the slice-by-slice method where sequential 3-mm polygons are taken from the three different aortic regions (suprarenal – blue, neck – green, aneurysm – red). The third panel from the left shows a sagittal view of the abdominal aorta. The right panel shows the volumes of interest drawn on the image analysis programme.

CT [HU], computed tomography grey scale bar in Hounsfield units; SUV, positron emission tomography colour scale bar in standard uptake values.

recorded and is a source of error. For each aortic region, a separate three-dimensional sphere was drawn in the visually highest uptake area, this had to be clearly distinct from the vertebra. The SUV_{max} within this sphere was then applied as an upper voxel intensity threshold for the corresponding region's volume of interest. Any values above this SUV were automatically excluded in the cumulative SUV and volume for that region by the analysis programme. The values for each region were obtained twice, once with the threshold limit applied and once without. This method therefore aims to reduce the magnitude of this radiotracer uptake spill-over by applying a maximum value threshold.

- *Aneurysm variable radius*: Using a uniform centreline function (three-dimensional cylinder) is sufficient if the volume of interest is of the same diameter throughout. Within an abdominal aortic aneurysm, the diameter varies along its length and if the centreline shape is kept uniform, this would lead to inclusion of extra-aortic tissue or exclusion of aneurysm tissue. A varying radius function was therefore introduced to allow the radius of the centreline to be varied across different points of the centreline to capture the aneurysmal volume of interest more accurately. The aneurysm values were obtained twice, with and without a variable radius.

The maximum AMA (AMA_{max}) was also calculated by dividing the SUV_{max} by the background pool activity.

4.3.7 Intra-observer and inter-observer repeatability

The optimised AMA method as described above was repeated for all 25 patients by two trained observers. To minimise recall bias, intra-observer repeatability was assessed by the same trained researcher using repeated assessments performed three months apart and in a random order. Duration of analyses were also recorded for each method of assessment.

4.3.8 Ex vivo tissue

Additionally, aortic aneurysm tissue was obtained from patients who had undergone open aortic surgery at the Edinburgh Vascular Service, Royal Infirmary of Edinburgh. Control aortic tissue specimens were obtained from patients who had died of sudden cardiac death in the community and whose tissue had been donated to the Edinburgh BioBank. Full informed consent was obtained from the patient or their relatives as appropriate, with ethical approval granted by the East of Scotland research ethics committee (15/ES/0094).

Intact aortic tissue underwent micro-positron emission tomography (microPET) with sodium [^{18}F]fluoride. After a 30-min incubation with sodium [^{18}F]fluoride (target concentration 100 kBq/mL), PET data were acquired using a nanoPET/CT scanner (Mediso, Budapest, Hungary) over 30 min, followed by an attenuation correction CT. Image analysis on reconstructed three-dimensional PET data was performed using PMOD 4.2 (PMOD Technologies LLC, Zurich, Switzerland). Whole tissue analysis considered the tissue as one volume of interest, whilst regional analysis involved drawing three equally

sized spherical volumes of interest in the 3 areas of highest and lowest uptake. Average radiotracer uptake values (kBq/cm^3) across each volume of interest were obtained. All values were normalised for the radiotracer incubation concentration by dividing by the corrected radiotracer concentration (kBq/mL) for each study scan.

Guided by areas of high radiotracer uptake, the tissue was then sectioned at 4-µm thickness after being embedded in paraffin blocks. Slides were stained with Haematoxylin and Eosin, von Kossa, Picrosirius Red, elastic Van Giesen's and Alizarin Red S stains, with images captured using Axioscan slide scanner (Zeiss, Jena, Germany).

An experienced pathologist who was blinded to the results of microcalcification imaging and patient status, performed histopathologic severity scoring. The system used was that adapted from that described by Bruijn and colleagues (Bruijn et al., 2021). Samples were scored on the following categories of disease activity: mesenchymal cell loss, intimal or medial fibrosis, elastin degradation, aorta wall thickness, inflammation measured both as transmural lymphoid infiltrates and tertiary lymphoid organs-like structures in the adventitia, neovascularisation, atherosclerotic lesion, microcalcification and adventitial adipocytic degeneration. The final score represents a sum of each category with possible scores ranging from 0 to 30.

Dewaxed and rehydrated slides were incubated at room temperature with 100 kBq/mL of sodium [^{18}F]fluoride in phosphate buffered saline for 60 min and a blocking control (10 µmol/L sodium fluoride). This was followed by two 5-min washes in phosphate buffered saline and a brief dip in deionised water. Autoradiography imaging (Amersham Typhoon IP Biomolecular Imager, Cytiva, Amersham, United Kingdom) was performed after the slides were exposed to a high-resolution autoradiography plate overnight (BAS-IP-SR 2040; Cytiva, Amersham, United Kingdom) (Fletcher, Nash, et al., 2022). FIJI software (v2.0.0, open source) was used to quantify the radiotracer signal by drawing regions of interest around the tissue and the empty glass slide to calculate a tissue to background ratio.

4.3.9 Statistical analysis

Associations between quantification methods were evaluated as a continuous variable (Pearson's correlation coefficient). Quantification methods were compared using intraclass correlation coefficient (consistency and 2-way random effects model) (Koo & Li, 2016) and Bland-Altman plots (Bland & Altman, 1986). Reliability of intraclass correlation coefficient values were described as: poor when less than 0.5; moderate when 0.5 to 0.75; good when 0.75 to 0.9; and excellent when greater than 0.9 (Koo & Li, 2016). Intra- and inter-observer repeatability was similarly assessed using mean bias, 95% limits of agreement and coefficient of repeatability (Vaz et al., 2013). Statistical significance was taken as a two-sided $p<0.05$.

4.4 Results

Patients had a median age of 72 years and were predominantly male (Table 4). Sodium [^{18}F]fluoride uptake was present in the thoracic and abdominal aorta of all 25 patients, although it varied between the thoracic aorta and the three regions of the abdominal aorta for both the TBR and AMA methods (Figure 13 and Figure 14).

The AMA method was quicker to perform, with the TBR method taking approximately 26 minutes longer (14 [13 to 17] versus 40 [34 to 44] min, $p<0.001$) per patient.

4.4.1 Abdominal aortic aneurysm sodium [^{18}F]fluoride uptake

4.4.1.1 Maximum Values

Within the abdominal aorta, TBR_{max} values ranged from 1.41 to 4.69 with a mean of 2.49±0.65, and AMA_{max} values ranged from 0.68 to 2.12 with a mean of 1.2±0.35. While the values were correlated ($r=0.79$, $p<0.001$; Figure 15A), there was evidence of substantial bias and wide limits of agreement when comparing the two approaches (Figure 16). Overall, there was moderate agreement between TBR_{max} and AMA_{max} (intraclass correlation coefficient 0.67, 95% confidence interval 0.52-0.78).

4.4.1.2 Mean Values

TBR_{mean} values ranged from 0.89 to 2.61 with a mean of 1.6±0.42, and AMA_{mean} values ranged from 0.75 to 2.73 with a mean of 1.62±0.44. The

values were highly correlated (r=0.95, p<0.001; Figure 15B) with lower bias and narrower limits of agreement (Figure 17) as well as very good agreement (Table 5).

4.4.2 Enhanced image analysis technique

4.4.2.1 Maximum Threshold

After applying the maximum threshold technique, there was good to excellent agreement between TBR_{mean} and AMA_{mean} (intraclass correlation coefficient 0.93, 95% confidence interval 0.89-0.95). Similarly, there were marked improvements in the mean bias and 95% limits of agreement (Table 5, Figure 17).

4.4.2.2 Aneurysm variable radius

There was good to excellent agreement between TBR_{mean} and AMA_{mean} without the variable radius approach (intraclass correlation coefficient 0.94, 95% confidence interval 0.88-0.98). This was further improved with the application of a variable radius (intraclass correlation coefficient 0.97, 95% confidence interval 0.94-0.99). This approach was also associated with improvements in bias and limits of agreement between the two measures (Table 5, Figure 18). Finally, applying both these techniques resulted in excellent agreement between TBR_{mean} and AMA_{mean} (Table 5, Figure 18).

Table 4. **Patient characteristics**

Characteristics of the twenty-five study patients including their medical history, current medication and aortic features.

Characteristic	**N = 25**
Age (years)	72 [61 to 83]
Male	21 (84%)
Female	4 (16%)
Systolic blood pressure (mmHg)	138 [101 to 180]
Diastolic blood pressure (mmHg)	81 [56 to 112]
Heart rate (beats/min)	72 [58 to 86]
Body Mass Index (kg/m2)	27.0 [20.2 to 36.3]
Medical History	
Current smoker	8 (33%)
Hypertension	18 (72%)
Hypercholesterolaemia	21 (84%)
Diabetes	5 (20%)
Ischaemic heart disease	6 (24%)
Peripheral arterial disease	6 (24%)
Cerebrovascular disease	3 (12%)
Family history of aneurysms	4 (16%)
Medication	
Antiplatelet agents	17 (68%)
Statins	21 (84%)
Anticoagulant agents	2 (8.0%)

Characteristic	**N = 25**
Beta-blockers	7 (28%)
Angiotensin-Converting Enzyme Inhibitors or Angiotensin Receptor Blockers	13 (52%)
Aorta	
Aortic diameter (mm)	46 [40 to 85]
Concurrent iliac aneurysm	6 (24%)
Subsequent aortic repair	5 (20%)

Median [Range]; number (%).

Figure 13. **Mean radiotracer uptake in different regions of the aorta**

Mean tissue to background ratio (red) and aortic microcalcification activity (blue) in the regions of the abdominal aorta and the thoracic aorta.

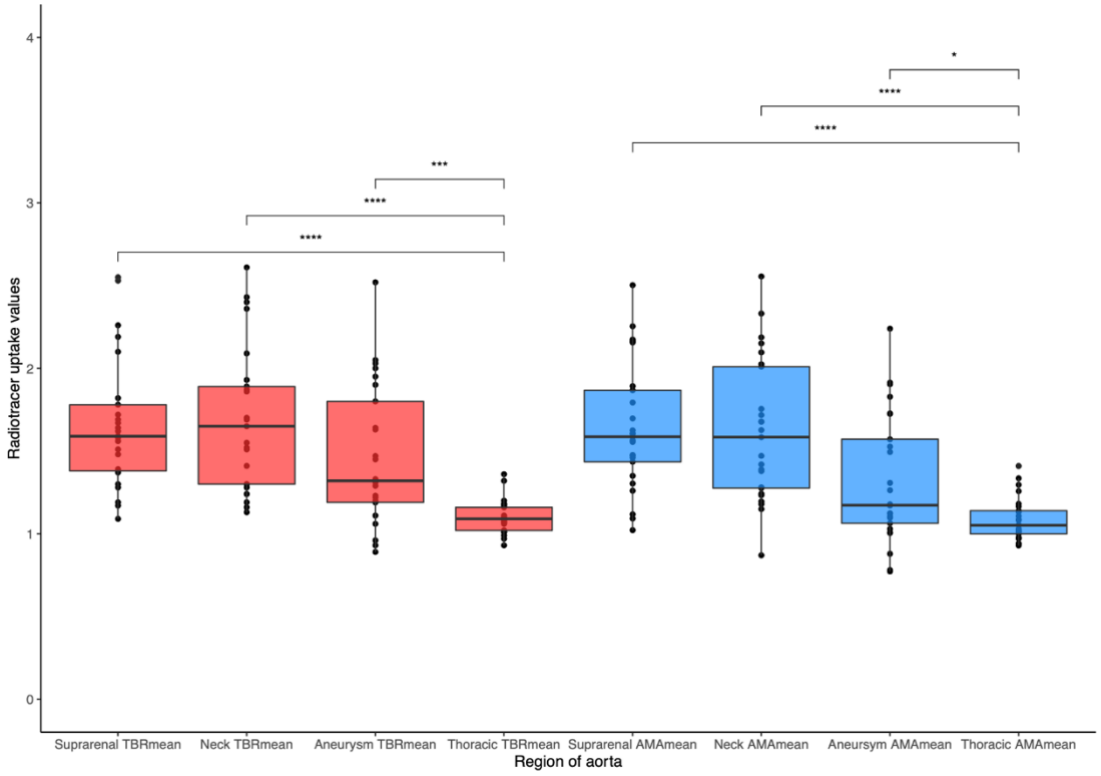

AMA, aortic microcalcification activity; TBR, tissue to background ratio. * = $p < 0.05$, *** = $p < 0.001$, **** = $p < 0.0001$.

Figure 14. **Maximum radiotracer uptake in different regions of the aorta**

Maximum tissue to background ratio (red) and maximum aortic microcalcification activity (blue) in the regions of the abdominal aorta and the thoracic aorta.

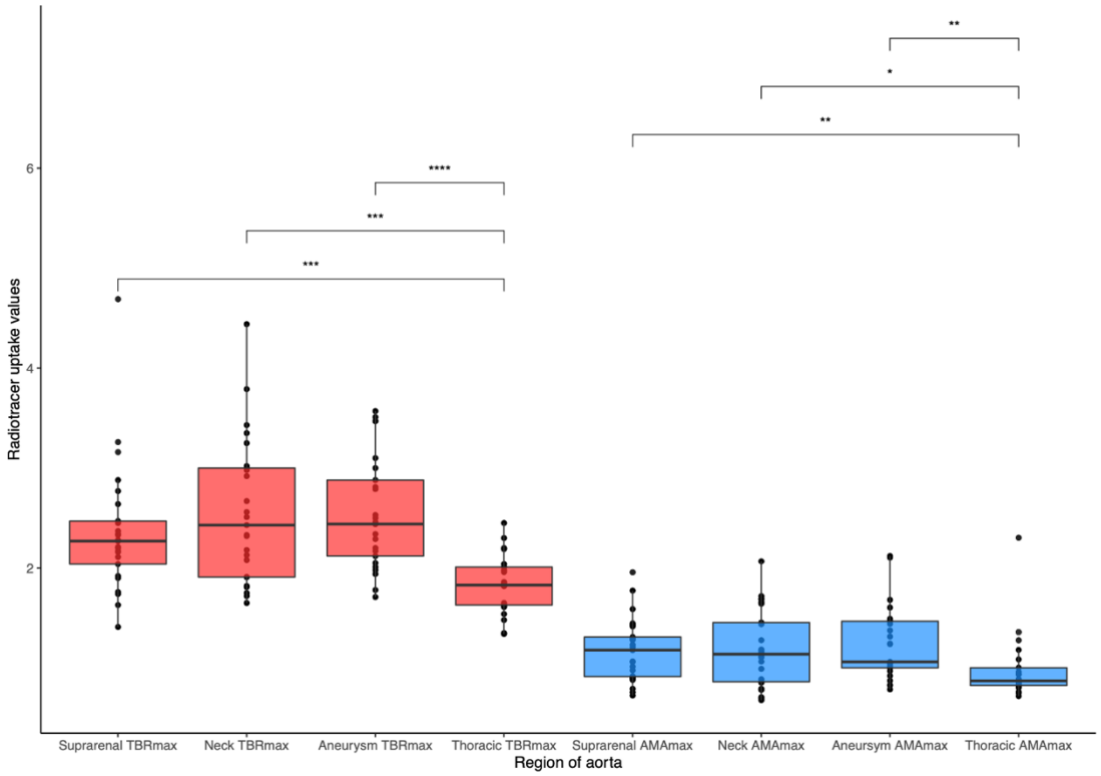

AMA, aortic microcalcification activity; max, maximum; TBR, tissue to background ratio. * = $p < 0.05$, ** = $p < 0.01$, *** = $p < 0.001$, **** = $p < 0.0001$.

Figure 15. **Scatter plots of the different values quantifying sodium [^{18}F]fluoride in the abdominal aorta**

TBR_{max} and AMA_{max} values (a), TBR_{mean} and AMA (b), one observer performing the same AMA method twice (c), two observers performing the same AMA method (d).

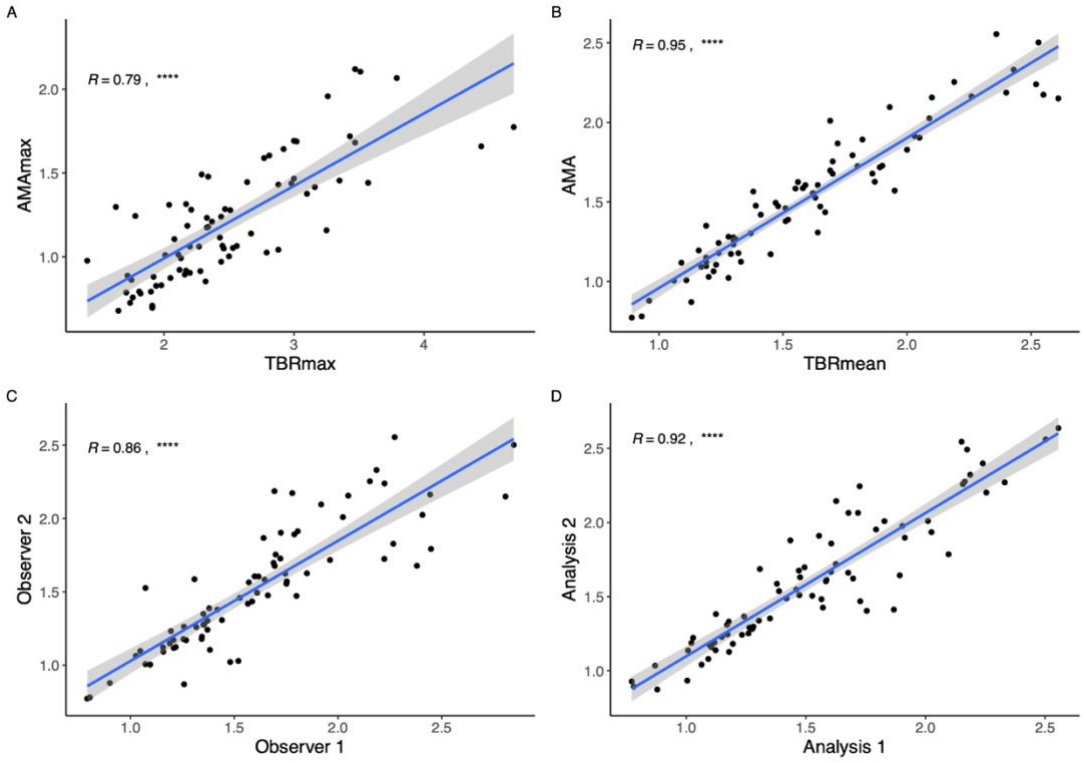

AMA, aortic microcalcification activity; max, maximum; R, Pearson's correlation coefficient; TBR, tissue to background ratio. **** = $p < 0.0001$.

Figure 16. **Maximum tissue to background ratio (TBR_{max}) and maximum abdominal aortic microcalcification activity (AMA_{max})**

Bland-Altmann plots with actual difference (A), and percentage difference (B) with mean bias (blue line) and 95% limits of agreement (red lines) for TBR_{max} and AMA_{max}. Mean bias = -1.3 (70%), 95% limits of agreement = -0.45 to 0.45 (40%).

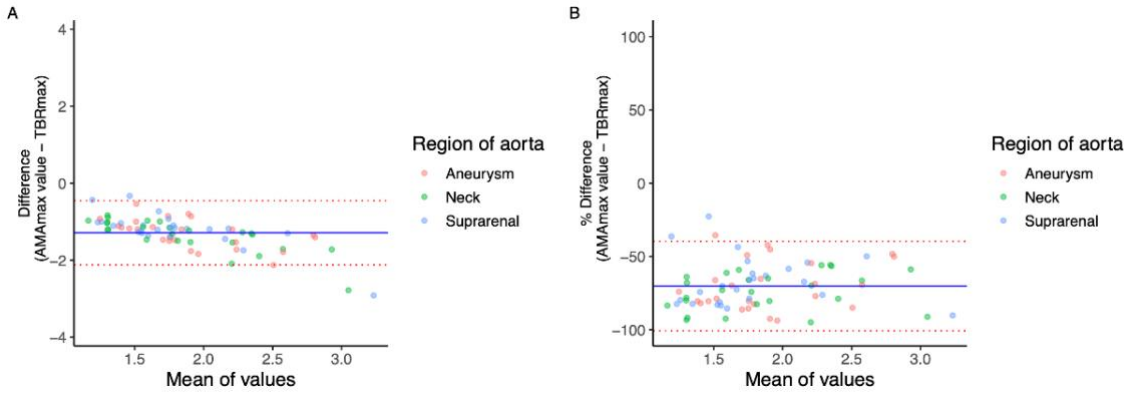

Y-axis limits are set to the mean of the values +2 and -2 and +1% and -1% respectively. AMA, aortic microcalcification activity; max, maximum; TBR, tissue to background ratio.

Figure 17. **Mean tissue to background ratio (TBR_{mean}) and mean abdominal aortic microcalcification activity (AMA)**

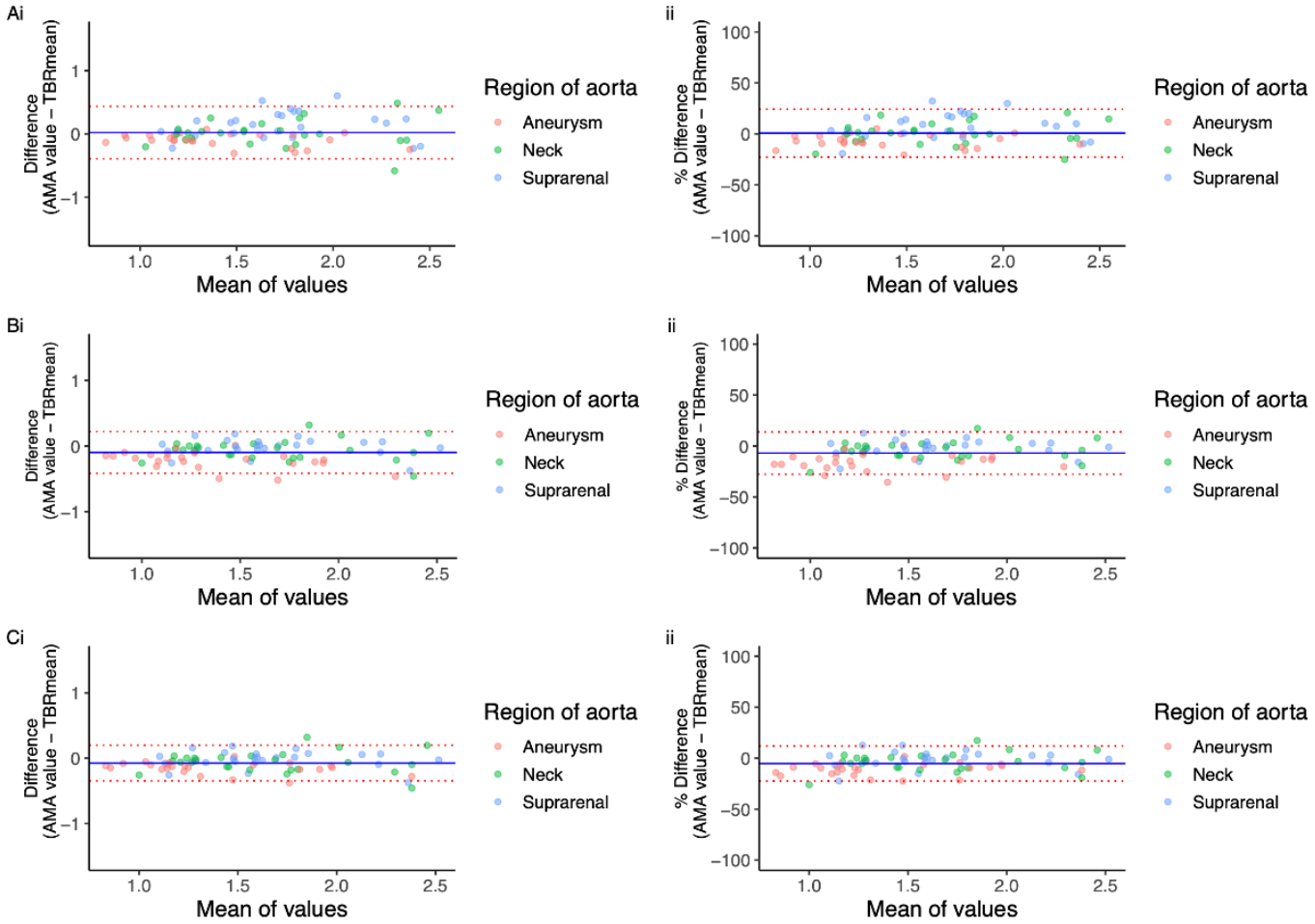

Bland-Altmann plots with actual difference (left, i) and percentage difference (right, ii), mean bias (blue line) and 95% limits of agreement (red lines) for: A. All regions without applying threshold: Intraclass correlation coefficient 0.88, mean bias = 0.02 (0.7%), 95% limits of agreement = -0.44 to 0.44 (24%). B. All regions after applying threshold: Intraclass correlation coefficient 0.93, mean bias = -0.1 (7%), 95% limits of agreement = -0.22 to 0.22 (14%). C. All regions after applying both threshold and variable radius: Intraclass correlation coefficient 0.95, mean bias = -0.08 (5%), 95% limits of agreement = -0.2 to 0.2 (12%).

Y-axis limits in the actual difference plots are set to the mean of the values. AMA, aortic microcalcification activity; TBR, tissue to background ratio.

Table 5. **Comparison of mean aortic microcalcification activity to mean tissue to background ratio**

Comparison of mean aortic microcalcification activity to mean tissue to background ratio detailing the mean bias and intraclass correlation coefficient between the different levels of enhancement.

	Range	**Mean**	**Mean Bias (95% limits of agreement)**	**Intraclass Correlation Coefficient**
AMA without threshold	0.75 to 2.73	1.62 ± 0.44	0.02 (-0.44 to 0.44)	0.88
AMA with threshold	0.74 to 2.56	1.5 ± 0.43	-0.1 (-0.22 to 0.22)	0.93
Aneurysm AMA without variable radius	0.74 to 2.06	1.25 ± 0.36	0.21 (-0.47 to 0.47)	0.94
Aneurysm AMA with variable radius	0.77 to 2.24	1.32 ± 0.39	0.15 (-0.33 to 0.33)	0.97
AMA	0.77 to 2.56	1.53 ± 0.42	-0.08 (-0.19 to 0.19)	0.95

AMA, aortic microcalcification activity; Mean ± standard deviation.

Figure 18. **Aneurysm mean tissue to background ratio (TBR_{mean}) and mean aneurysm aortic microcalcification activity (AMA)**

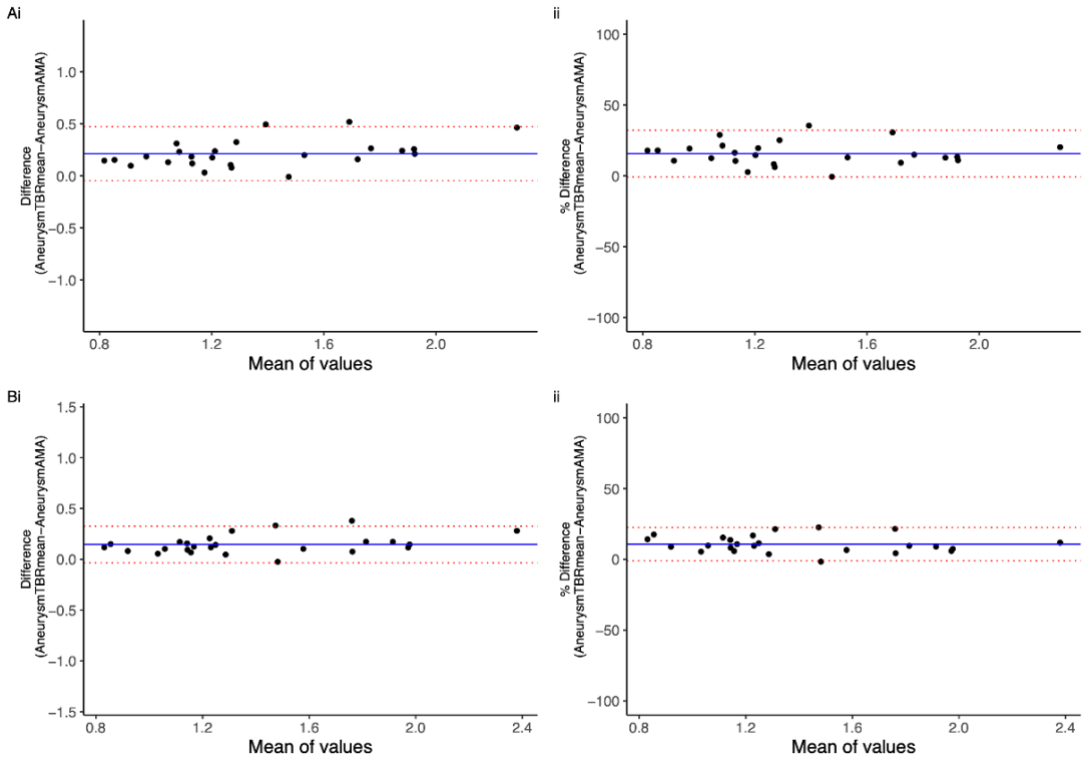

Bland-Altmann plots with actual difference (left, i) and percentage difference (right, ii), mean bias (blue line) and 95% limits of agreement (red lines) for aneurysm region: A. Without variable radius: Intraclass correlation coefficient 0.94, mean bias = 0.21 (16%), 95% limits of agreement = -0.47 to 0.47 (32%). B. With variable radius: Intraclass correlation coefficient 0.97, mean bias = 0.15 (11%), 95% limits of agreement = -0.33 to 0.33 (22%).

Y-axis limits in the actual difference plots are set to the mean of the values. AMA, aortic microcalcification activity; TBR, tissue to background ratio.

4.4.3 Intra-observer and inter-observer repeatability

Intra-observer and inter-observer assessments were highly correlated (Figure 15) and demonstrated good to excellent repeatability (Figure 19).

4.4.4 Ex vivo tissue

Nine aortic aneurysm and 7 control tissue specimens were obtained. Whole tissue analysis demonstrated a higher mean sodium [^{18}F]fluoride uptake in aneurysm specimens (0.07±0.04 versus 0.03±0.01, $p<0.01$) (Figure 20). This was confirmed on regional radiotracer uptake in areas of high uptake (0.83 [0.62 to 1.27] versus 0.33 [0.24 to 0.39], $p<0.0001$), and in areas of low uptake (0.17 [0.10 to 0.27] versus 0.06 [0.05 to 0.11], $p<0.0001$) (Figure 20).

Histological examination of the tissue showed a spectrum of morphological changes including mesenchymal cell loss accompanied by medial fibrosis and marked elastic fibre fragmentation and loss (Figure 21). Microcalcification was present and cholesterol crystals were observed in the interface between intima and media. Extensive adventitial fibrosis and variable transmural lymphocyte infiltration was also present in a proportion of cases.

Aneurysm tissue had higher total aneurysmal histopathological scores (24 [22 to 26]) when compared to non-aneurysmal tissue (12 [9 to 17]; $p<0.05$) (Table 7). Microcalcification was present in 6 out of 7 analysed aneurysm specimens but only in 2 out of 7 non-aneurysmal specimens. Sodium [^{18}F]fluoride uptake on autoradiography strongly corresponded to areas of microcalcification on

Figure 19. **Intra-observer and Inter-observer repeatability**

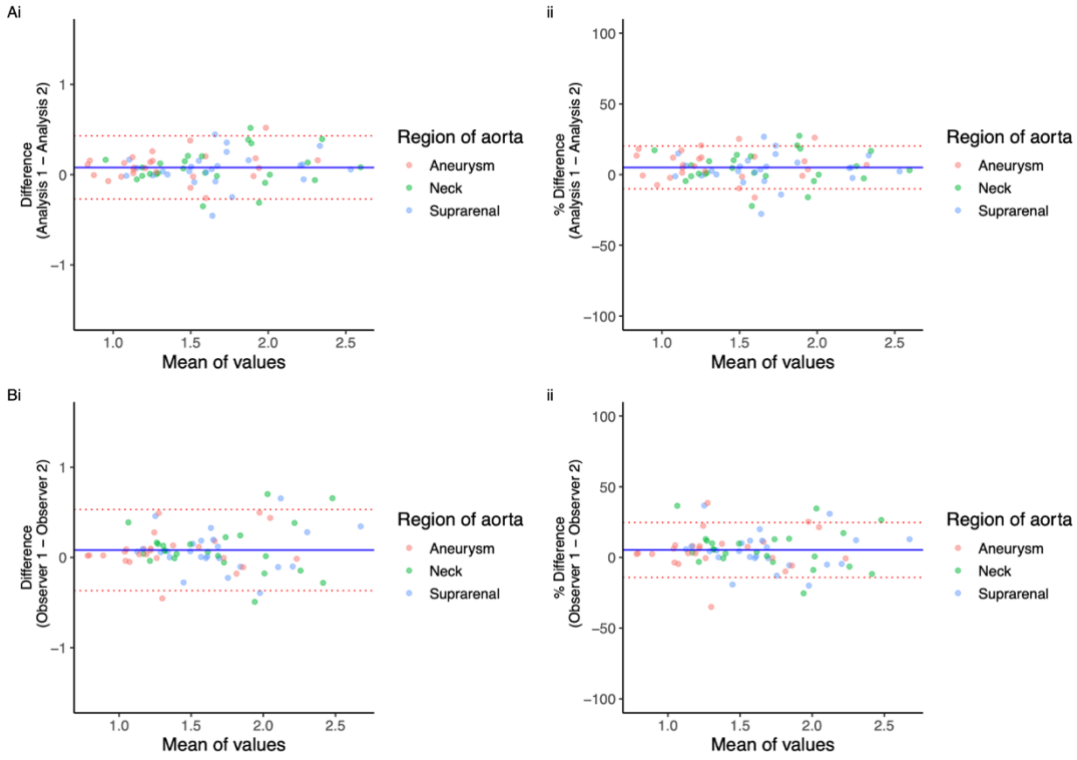

Bland-Altmann plots with actual difference (left, i) and percentage difference (right, i), mean error (blue line) and 95% limits of agreement (red lines) for: A. Intra-observer, coefficient of reproducibility 0.36, intraclass correlation coefficient 0.92, mean error = 0.08 (5%), 95% limits of agreement = -0.43 to 0.43 (26%). B. Inter-observer, coefficient of reproducibility 0.47, intraclass correlation coefficient 0.86, mean error = 0.08 (5%), 95% limits of agreement = -0.53 to 0.53 (25%).

Y-axis limits in the actual difference plots are set to the mean AMA value. AMA, aortic microcalcification activity; TBR, tissue to background ratio.

Table 6. **Intra-observer and inter-observer repeatability**

Mean bias, coefficient of repeatability and intraclass correlation coefficient of intra-observer and inter-observer values.

	Range	**Mean**	**Mean Bias (95% limits of agreement)**	**Coefficient of Repeatability (% of mean)**	**Intraclass Correlation Coefficient**
Intra-observer	0.77 to 2.64	1.57 ± 0.42	0.08 (-0.43 to 0.43)	0.36 (23.0%)	0.92
Inter-observer	0.77 to 2.85	1.57 ± 0.42	0.08 (-0.53 to 0.53)	0.47 (30.0%)	0.86

Mean ± standard deviation.

Figure 20. **Sodium [^{18}F]fluoride uptake in aortic aneurysm tissue and control aortic tissue**

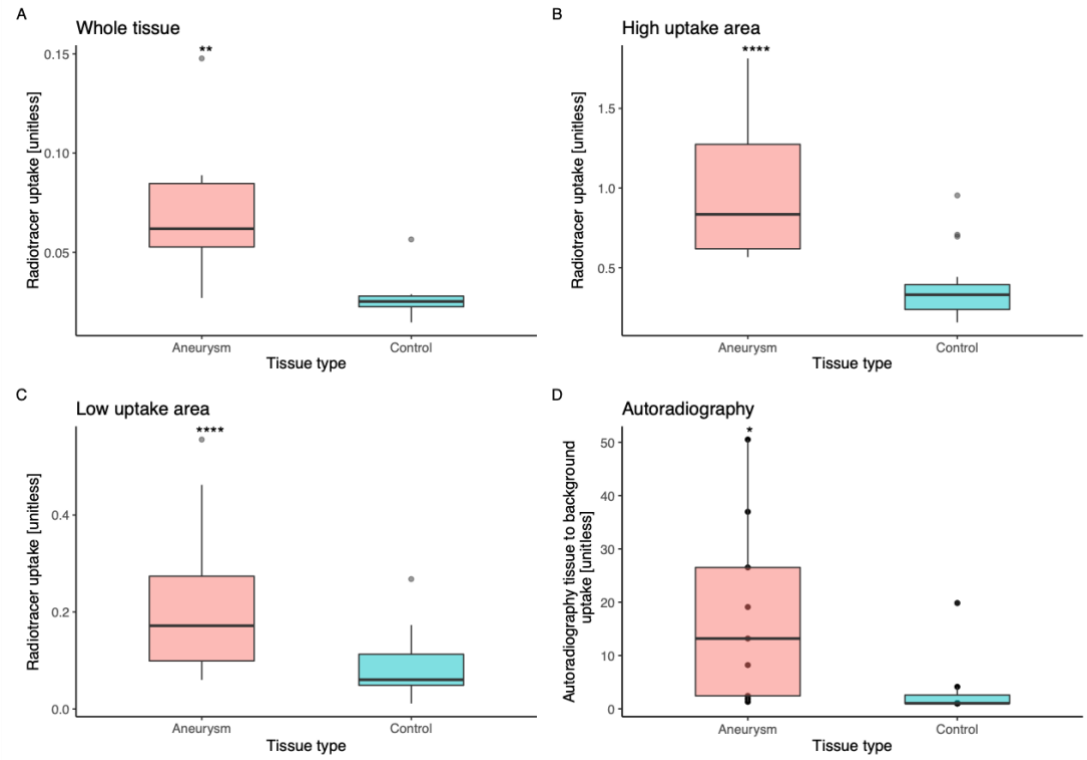

(A) Whole tissue sample, (B) regions of high uptake, and (C) regions of low uptake on micro-positron emission tomography, and (D) mean tissue uptake to background uptake on autoradiography.

* = $p < 0.05$, ** = $p < 0.01$, **** = $p < 0.0001$.

Figure 21. **Aortic tissue histology and autoradiography imaging**

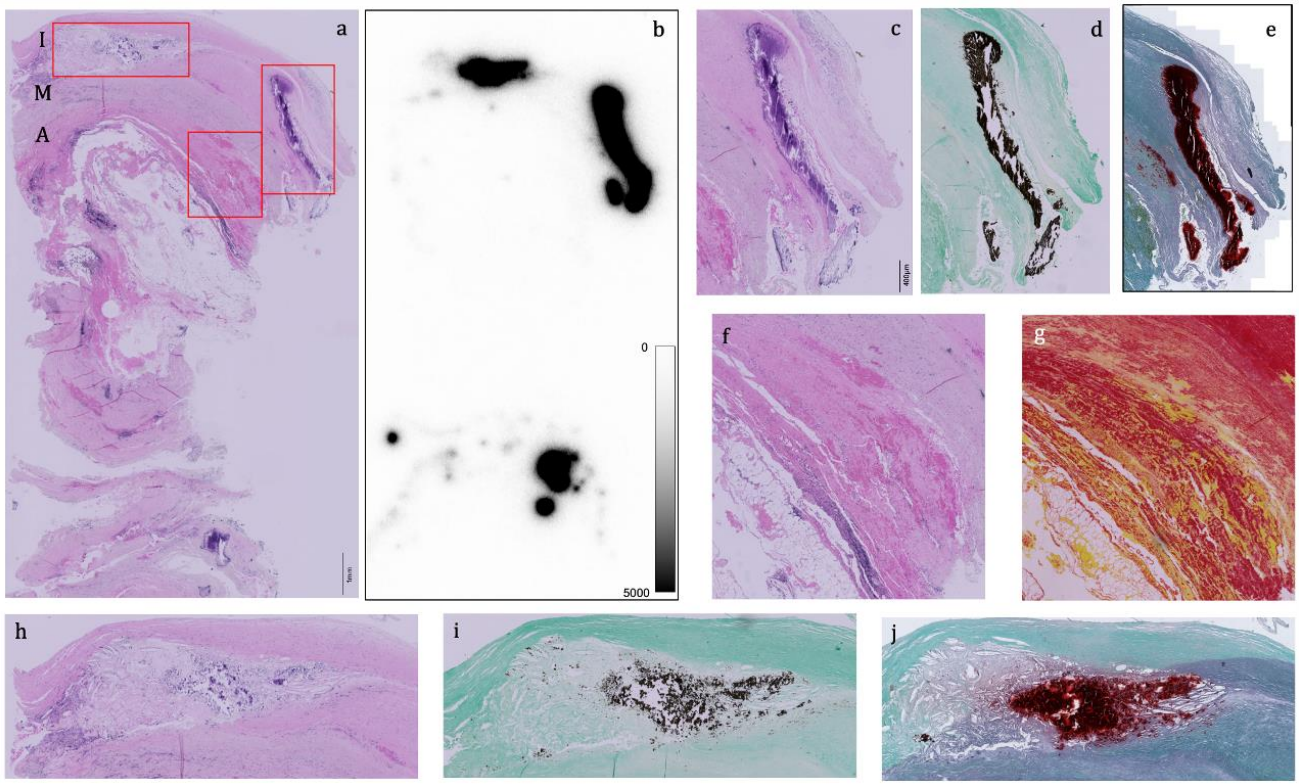

(a) Haematoxylin and Eosin (H&E) stain of a representative section of aneurysm tissue and the corresponding sodium [^{18}F]fluoride autoradiography image (b), H&E demonstrated established dense calcified plaque (c), confirmed by von Kossa stain (black), (d) and Alizarin Red S stain (red) (e) (20x magnification). Similarly medial and adventitial fibrosis (f), was highlighted by

Picrosirius Red stain (g). Cholesterol microcrystals within the atherosclerotic plaque identified on autoradiography were localised on H&E, (h), von Kossa (i) and Alizarin Red S (j).

(a) 4x magnification, (c-j) 20x magnification. Red squares indicate which areas are magnified. Colour scale bar in (b) refers to the adjusted mean grey intensity. I = Intima, M = Media, A = Adventitia.

Table 7. **Tissue aneurysmal histology scores**

Categories 1 to 5

Sample	**Tissue type**	**Mesenchymal cell loss**	**Intimal or medial fibrosis**	**Elastin degradation**	**Aorta wall thickness**	**Transmural lymphoid infiltrates**	**Total score**
Maximum obtainable score		5	5	2	4	2	30
1	Aneurysm	3	4	1	4	1	20
2	Aneurysm	3	5	2	3	1	23
3	Aneurysm	5	5	2	4	2	27
4	Aneurysm	-	-	-	-	-	-
5	Aneurysm	2	2	1	1	0	7
6	Aneurysm	-	-	-	-	-	-
7	Aneurysm	5	5	1	4	2	27
8	Aneurysm	5	5	2	3	0	24
9	Aneurysm	5	5	3	3	2	25
10	Control	1	1	0	1	0	7

11	Control	2	2	1	3	0	13
12	Control	5	5	1	3	0	20
13	Control	1	3	0	2	0	12
14	Control	0	1	0	2	0	3
15	Control	0	0	1	3	0	11
16	Control	5	5	2	2	2	21

Categories 6 to10

Sample	**Tissue type**	**Tertiary lymphoid organs-like structures**	**Neovascularisation**	**Atherosclerotic lesions**	**Microcalcification**	**Adventitial adipocytic degeneration**	**Total score**
Maximum score obtainable		2	3	5	1	1	30
1	Aneurysm	0	2	4	1	0	20
2	Aneurysm	0	3	5	1	0	23
3	Aneurysm	2	3	3	0	1	27
4	Aneurysm	-	-	-	-	-	-

5	Aneurysm	0	0	0	1	0	7
6	Aneurysm	-	-	-	-	-	-
7	Aneurysm	1	3	5	1	0	27
8	Aneurysm	0	3	5	1	0	24
9	Aneurysm	0	2	4	1	0	25
10	Control	0	0	4	0	0	7
11	Control	0	0	5	0	0	13
12	Control	0	0	5	1	0	20
13	Control	0	0	5	1	0	12
14	Control	0	0	0	0	0	3
15	Control	0	2	5	0	0	11
16	Control	0	1	4	0	0	21

Ten categories were assessed in total. Another described category, intra-luminal thrombus organisation was not assessed as there had been no pre-defined sampling protocol and therefore scoring this would have been inaccurate.

Tissue samples 4 and 6 could not be assessed due to technical reasons.

Alizarin Red staining (Figure 21). Autoradiography imaging further confirmed higher sodium [^{18}F]fluoride in aneurysm tissue when compared to control (13.2 [2 to 27] versus 1.02 [1.01 to 1.04], $p<0.05$) (Figure 20).

4.5 Discussion

This is the first description of applying the AMA method to the abdominal aorta. This method has excellent levels of agreement and is substantially quicker than previously described conventional PET quantification methods. Moreover, it performs much better when incorporating modifications that account for the spill-over of sodium [^{18}F]fluoride uptake from the adjacent vertebrae and the variable aortic radius of the aneurysm. This quick and highly repeatable technique will improve the practical application and analysis of sodium [^{18}F]fluoride PET-CT assessments of abdominal aortic aneurysms.

Analysing the entire abdominal aorta as a single region would potentially dilute and obscure differences between aneurysmal and non-aneurysmal regions. We therefore divided the aorta into three anatomically defined regions that are easily identifiable on a CT angiogram and can be easily replicated. We also used the thoracic aorta as a non-aneurysmal control segment of aorta. We appreciate that thoracic aortic disease may have a different pathophysiology to abdominal aortic aneurysm disease, and there may be differences in microcalcification activity and radiotracer uptake. However, since the study question here was the method of PET quantification, we feel that using the thoracic aorta as a control is a valid reference comparison.

We have sought to address the problem of signal spillage from the physiological uptake of sodium [^{18}F]fluoride within vertebrae. Previous methods involved manually excluding obvious areas of activity spill-over from the vertebrae, and we applied this method when calculating the TBR values. Akerele and colleagues have previously described other methods to correct for this problem including iterative reconstructions which incorporate a specific background correction that adjusts for this source of error (Akerele et al., 2019). This is labour-intensive and currently there are no software packages to implement this technique. The PET activity spill-over takes place over a range of continuous values and its complete exclusion is not technically feasible. Our thresholding technique corrects for the abnormally high signal, but higher overall values of AMA_{mean} can still occur due to activity spill-over below the region's set threshold. Despite this, we feel that this remains one of the more effective methods available to correct for the spill-over effect from intense vertebral sodium [^{18}F]fluoride uptake because of its rapidity and simplicity as well as the improvement in comparative values with TBR_{mean}.

The obtained AMA_{mean} value is dependent on a calculation involving the region's cumulative SUV, region volume, region threshold and background SUV. Disparities between different image analysts could potentially have an impact on the measured uptake values. However, both intra-observer and inter-observer repeatability were found to be very good if not excellent, especially after application of techniques to make the assessments more robust. Scan-rescan reproducibility has not been assessed within this method;

however, it has already been shown to be very good in the thoracic aorta (Fletcher et al., 2021). The dependence on the region's volume could result in larger aneurysm diameters reducing the region's AMA value. When developing this method, we considered using the length of the volume of interest rather than its volume, but the values obtained were not comparable to TBR values.

Forsythe and colleagues used the "most diseased segment" TBR_{max} approach to measure sodium [^{18}F]fluoride uptake in abdominal aortic aneurysms (Forsythe et al., 2018). These values demonstrated higher signal for aneurysmal segments compared to non-aneurysmal segments. This is a well-established approach that has previously been used to quantify 2-[^{18}F]fluoro fluoro-2-deoxyglucose uptake in aortic and carotid atheroma and sodium [^{18}F]fluoride uptake in the aortic valve (Fayad et al., 2011; Pawade et al., 2016; Vesey et al., 2017). The AMA_{mean} method described here is similar to the TBR_{mean} value: it calculates the average activity across a region of interest but it does not aim to replicate the "most diseased segment" approach which is dependent on a single voxel value across a region of interest. This explains the lower values in the aneurysmal segments in the present study. AMA_{max} would be more similar to this method, however it compares less well to the TBR_{max} across the region. The "most diseased segment" method is valuable when investigating conditions where regions of intense activity are more important than mean global activity. For example, this has been used as a measure of atherosclerotic disease activity and the risk of plaque rupture in

coronary artery disease (Joshi et al., 2015; Joshi et al., 2014). It is unknown whether aneurysm rupture or expansion are dependent on the most intensely active degenerative region in the aneurysm (which would correspond to the “most diseased segment”) or whether these events may be better reflected through a global average measure of the burden of vascular degeneration within the whole vessel (AMA_{mean}). Mean radiotracer uptake was the method that was optimised here because in the context of endovascular aneurysm repair and progressive aneurysm disease burden and overall activity was felt to be an important marker to consider.

The histopathological results are unsurprising but important. In the present ex vivo study, there is markedly higher sodium [^{18}F]fluoride uptake in aneurysm tissue on both microPET and autoradiography, and this corresponded with higher histopathological scores in aneurysm tissue. Although some individual categories in the scoring system were higher in aneurysm tissue (fibrosis, neovascularisation and microcalcification), microcalcification appeared to be a dominant feature for the majority of the aneurysmal tissue.

It is important to highlight some limitations to our study. Whilst we have introduced enhancements in our technique to deal with the spill-over effect from physiological vertebral uptake, this remains a source of error and it is unclear whether our method adequately corrects for this. Since it is not possible with the current technology to have zero signal spillage with this radiotracer, calculating a true mean error is challenging. Some more

sophisticated spill-over correction methods could be performed in the future, but they may require availability of dynamic imaging. Our study population consisted of patients with abdominal aortic aneurysms and we have not assessed our technique in a truly healthy population or other diseased states. There is also some dependence on the total volume of interest using our method. One potential way to improve direct assessment of the aortic aneurysm would be to have a hollow cylindrical volume of interest and thereby consider only the vessel wall itself. However, this incorporated increased complexity, took greater analysis time and performed poorly between different observers. We have sought to quantify sodium [^{18}F]fluoride uptake in abdominal aortic aneurysms. This radiotracer has not been validated for clinical use and future studies are needed to determine if this AMA method can serve as a biomarker for aortic disease. We recognise that nuclear medicine departments may not routinely perform a contrast-enhanced CT acquisition. Hypothetically, a recent contrast-enhanced CT scan could be co-registered to a PET acquisition scan to allow more accurate determination of the aortic regions, and arterial landmarks.

4.6 Clinical Perspectives

Aortic microcalcification activity can be quantified across the abdominal aorta quickly and accurately and this compares very favourably with standard quantification methods. Comparative measures and repeatability are enhanced by modifications that include minimising the effect of spill-over from vertebral sodium [^{18}F]fluoride uptake and variations in the aneurysm diameter.

Future studies could determine whether this sodium [^{18}F]fluoride quantification method could serve as a biomarker for aortic disease.

Chapter 5: Aortic sodium [^{18}F]fluoride uptake following endovascular aneurysm repair

Published by **Debono S**, Nash J, Fletcher AJ, Syed M, van Beek EJR, Williams MC, Falah O, Tambyraja A, Dweck MR, Newby DE, Forsythe RO. Aortic sodium [^{18}F]fluoride uptake following endovascular aneurysm repair. *Heart.* 2023 Oct 26;109(22):1677-1682. doi: 10.1136/heartjnl-2023-322514. PMID: 37164479; PMCID: PMC10646867.

5.1 Abstract

5.1.1 Background

In patients with abdominal aortic aneurysms, sodium [^{18}F]fluoride positron emission tomography identifies aortic microcalcification and disease activity. Increased uptake is associated with aneurysm expansion and adverse clinical events. The effect of endovascular aneurysm repair (EVAR) on aortic disease activity and sodium [^{18}F]fluoride uptake is unknown. This study aimed to compare aortic sodium [^{18}F]fluoride uptake before and after treatment with EVAR.

5.1.2 Methods

In a preliminary proof-of-concept cohort study, preoperative and post-operative sodium [^{18}F] fluoride PET-CT was performed in patients with an infrarenal abdominal aortic aneurysm undergoing EVAR according to current guideline-directed size treatment thresholds. Regional aortic sodium [^{18}F]fluoride uptake was assessed using aortic microcalcification activity (AMA): a summary measure of mean aortic sodium [^{18}F]fluoride uptake.

5.1.3 Results

Ten participants were recruited (76±6 years) with a mean aortic diameter of 57±2 mm at time of EVAR. Mean time from EVAR to repeat scan was 62±21 months. Prior to EVAR, there was higher abdominal aortic AMA when compared with the thoracic aorta (AMA 1.88 versus 1.2; $p<0.001$). Following EVAR, sodium [^{18}F]fluoride uptake was markedly reduced in the suprarenal

(change in AMA 0.62, p=0.03), neck (change in AMA 0.72, p=0.02) and body of the aneurysm (change in AMA 0.69, p=0.02) while it remained unchanged in the thoracic aorta (change in AMA 0.11, p=0.41).

5.1.4 Conclusion

EVAR is associated with a reduction in AMA within the stented aortic segment. This suggests that EVAR can modify aortic disease activity and aortic sodium [^{18}F]fluoride uptake is a promising non-invasive surrogate measure of aneurysm disease activity.

5.2 Introduction

As discussed in Chapter 1, EVAR has changed the elective treatment of abdominal aortic aneurysms. Compared to open surgical repair, it is a much less invasive procedure and is associated with lower perioperative morbidity and mortality and improved short-term outcomes (Greenhalgh, Brown, Powell, Thompson, Epstein, et al., 2010). The stent graft provides a physical barrier that excludes the aneurysm from the circulation and reduces mortality from aneurysm rupture. EVAR use is limited by its durability, including the formation of endoleaks and stent migration necessitating life-long post-operative surveillance programs (Chaikof et al., 2018). Following EVAR, shrinkage of the aneurysm sac can be observed, and this is taken as a positive morphological sign of procedural success.

Aortic aneurysm formation is characterised by medial wall atrophy and degeneration (Chapter 1) (Ladich et al., 2016). This progressive and degenerative disease processes triggers a vascular calcific response (M. B. J. Syed et al., 2019) which is characterised by deposition of calcium- and phosphate-containing hydroxyapatite crystals and is termed microcalcification (Aikawa et al., 2007). This is distinct from the end-stage macrocalcification which can be readily identified by computed tomography (CT). Sodium [^{18}F]fluoride is a PET radiotracer which binds to the deposited hydroxyapatite crystals and can detect aortic microcalcification (Chapter 2).

In the Sodium [^{18}F]Fluoride Imaging of Abdominal Aortic Aneurysms (SoFIA^{3}) study (NCT02229006), aortic sodium [^{18}F]fluoride uptake specifically localised to abdominal aortic aneurysms and was associated with more rapid aneurysm expansion and a higher chance of rupture or elective repair secondary to aneurysm growth (Forsythe et al., 2018).

The aim of this study was to investigate aortic sodium [^{18}F]fluoride uptake after successful EVAR implantation, hypothesising that this would be reduced. In an exploratory proof-of-concept study, repeated sodium [^{18}F]fluoride PET-CT was performed in participants of the SoFIA^{3} study who had undergone EVAR.

5.3 Methods

The study methods are also discussed in further depth in the relevant section in Chapter 2.

Briefly however, this was a longitudinal observational study (NCT04577716) where study participants were studied at baseline and at a minimum of 1 year following EVAR. The study population consisted of patients originally recruited into the Sodium [^{18}F]Fluoride Imaging in Abdominal Aortic Aneurysms study (NCT02229006) who had undergone successful elective EVAR. These patients were invited for recruitment into the PET-EVAR Study (Predicting Endoleaks Following Endovascular Aortic Aneurysm Repair Using Sodium [^{18}F]Fluoride).

5.3.1 Study assessments

At each of the two study visits, participants underwent a clinical assessment prior to imaging. Patients were then administered a target dose of 125 MBq of sodium [^{18}F]fluoride intravenously, and 60 min later they were imaged on a hybrid 128–slice PET-CT scanner (Biograph mCT, Siemens Healthineers, Erlangen, Germany). A low-dose attenuation correction CT scan was performed (120 kV, 50 mAs, 5/3 mm), followed by acquisition of PET data at 10-min intervals in three or four bed positions to cover the thoracic and abdominal aorta. A contrast-enhanced aortic CT angiogram (120 kV, 145 mAs, 3/3 mm, field of view 400; and 1/1 mm, field of view 300; triggered at 181 Hounsfield units) was performed on the same scanner immediately after PET acquisition. This was preceded by a non-contrast CT aortic calcium score at the second visit. Static PET-CT images were reconstructed with correction applied for attenuation, dead-time, scatter and random coincidences, using an optimised iterative reconstruction algorithm (ultra-High Definition; TrueX +

Time-of-Flight, 2 iterations and 21 subsets, matrix 200, zoom 1; Gaussian filter 5 mm).

5.3.2 Image Analysis

5.3.2.1 Aortic morphology and calcium score

Aneurysm morphology, including pre-operative and post-operative aortic sac size, neck length and length of common iliac arteries, was measured using PACS (Carestream Health). Calcium score was measured using dedicated software (Vitrea Advanced, Toshiba Systems) and quantified as calcium score (AU), calcium volume (mm^3) and calcium mass (mg). The threshold for calcification was set at a computed tomographic density of 130 Hounsfield units having an area $\geq$1 mm^2 (Agatston et al., 1990).

5.3.2.2 Aortic microcalcification activity

Sodium [^{18}F]fluoride uptake was measured in four anatomically distinct regions of interest: the descending thoracic aorta, the suprarenal region, aneurysm neck and body of the aneurysm as described previously (Section 2.6.2.1). The four regions were defined as: (i) the *descending thoracic aorta*; (ii) the *suprarenal* region; (iii) the *neck*; and (iv) the *aneurysm body* (Figure 7).

The aortic microcalcification activity (AMA), a summary measure of mean aortic sodium [^{18}F]fluoride uptake in a three-dimensional volume, was calculated for each region. In brief, AMA is calculated by measuring the mean radiotracer uptake value of each region using a custom validated tool (Fusion

Quant v1.21.0421, Cedars-Sinai Medical Centre, Los Angeles), and then each region is normalised for its volume (cm^3) and for the background blood pool activity of the right and left atria. The AMA analysis method also includes a threshold technique to correct for the spill-over effect created by physiological radiotracer uptake in the vertebrae (Chapter 4).

5.3.3 Statistical Analysis

Apart from the generic statistical analyses as described in Chapter 2, a simple main effect one-way model was used to assess regional difference in the AMA. A Kruskal-Wallis rank sum test was used to assess regional differences in the AMA between the timepoints. Wilcoxon signed-rank test was used to test pre-operative and post-operative calcium scores.

5.4 Results

Twelve of 72 participants of the original study population underwent elective EVAR. One participant was ineligible due to renal failure and one participant declined further participation. Ten patients were successfully recruited (Figure 22).

Recruited patients were predominantly male and had a mean age of 76 ± 6 years (Table 8). The mean interval between the pre-operative and post-operative scans was 78 ± 5 months and the time from EVAR to post-operative scan was 62 ± 21 months.

Figure 22. **Diagrammatical representation of the study population for the aortic sodium [^{18}F]fluoride uptake following EVAR study**

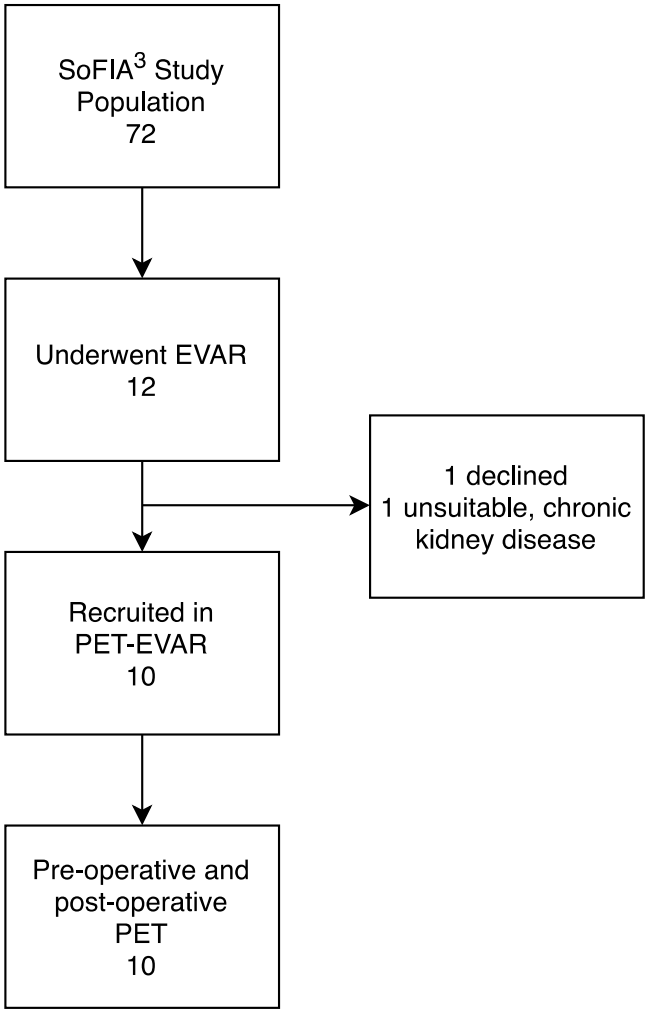

Ten patients were recruited into the Predicting Endoleaks Following Endovascular Aortic Aneurysm Repair Using Sodium [^{18}F]Fluoride (PET-EVAR) study from the 12 patients who underwent EVAR after being recruited into the Sodium [^{18}F]Fluoride Imaging in Abdominal Aortic Aneurysms (SoFIA^{3}) study and having a pre-operative positron emission tomography (PET) scan.

5.4.1 Aortic morphology

All treated aneurysms were infrarenal and had a mean aortic diameter of 57 ± 2 mm at time of EVAR. Six patients had a concurrent iliac aneurysm. All stent grafts were inserted according to manufacturers' instructions for use (Table 9).

In eight patients (80%), there was no change, or there was a reduction in the aneurysm sac size following EVAR (mean change -6 ± 12 mm). In the remaining two patients, there was an increase in sac size at follow up. In one patient, there was a 14-mm increase due to a type II endoleak. This was being actively managed and there had been multiple endovascular attempts to treat it (by embolisation and by CT-guided Onyx infiltration to the sac). In the second patient, there was a 6-mm increase. This patient had the shortest follow-up period of the cohort (13 months) and had previously demonstrated a type II endoleak at 8 months after EVAR.

The median post-operative thoracic calcium score was increased in all three measures when compared to the pre-operative score (1924 versus 686 AU, p=0.02), but there were no differences in the suprarenal aorta (525 versus 232 AU, p=0.32) (Table 10).

5.4.2 Aortic microcalcification activity

The AMA at baseline was twice as high in all three abdominal aortic regions when compared with the thoracic aorta. Following EVAR, AMA was reduced

Table 8. **Patient characteristics at post-operative scan**

Characteristic	**N = 10**
Age (years)	76 ± 6
Male	9 (90%)
Female	1 (10%)
Systolic blood pressure (mmHg)	156 ± 15
Diastolic blood pressure (mmHg)	83 ± 8
Heart rate (beats/min)	68 ± 15
Body mass index (kg/m^2)	27.1 ± 3.2
Medical History	
Current or ex-smoker	10 (100%)
Hypertension	8 (80%)
Hypercholesterolemia	9 (90%)
Diabetes	2 (20%)
Ischemic heart disease	4 (40%)
Peripheral arterial disease	2 (20%)
Cerebrovascular accident	3 (30%)
Chronic obstructive pulmonary disease	3 (30%)
No family history of aneurysm disease	10 (100%)
Medications	
Antiplatelet agents	7 (70%)
Anticoagulant agents	2 (20%)
Statins	9 (90%)
Beta-blockers	5 (50%)

Characteristic	N = 10
Angiotensin-converting enzyme or angiotensin receptor blockers	4 (40%)
Calcium channel antagonist	3 (30%)

Mean ± standard deviation; number (%)

Table 9. **Aortic morphology and stent graft details**

	N = 10
Pre-operative aortic size (mm)	57 ± 2
Post-operative aortic size (mm)	51 ± 12
Concurrent iliac aneurysm	6 (60%)
Iliac aneurysm size (mm)	21 ± 3
Morphology	
Length of neck (mm)	16 (15 to 26)
Neck angulation (°)	31 (29 to 44)
Left iliac length (mm)	54 ± 24
Right iliac length (mm)	55 ± 23
Stent graft repair type	
Cook	3 (30%)
Gore C3 Excluder	3 (30%)
Medtronic Endurant	4 (40%)

Mean ± standard deviation; Median (interquartile range); number (%).

Table 10. **Pre-operative and post-operative aortic calcium scores**

	Pre-operative	**Post-operative**	**p value**
Thoracic Agatston score, AU	686 (35 to 1528)	1924 (557 to 4698)	0.002
Thoracic calcium volume, mm^3	718 (28 to 1323)	1638 (550 to 3838)	0.002
Thoracic calcium mass, mg	165 (8 to 383)	489 (132 to 1260)	0.002
Suprarenal Agatston score, AU	232 (58 to 797)	524 (170 to 1138)	0.32
Suprarenal calcium volume, mm^3	220 (58 to 764)	510 (211 to 926)	0.43
Suprarenal calcium mass, mg	58 (14 to 197)	129 (42 to 275)	0.19

Median (interquartile range). AU, Agatston units

in all abdominal aortic regions but not in the thoracic aorta (Figure 23). The change in AMA was present in the suprarenal (0.62, p=0.03), neck (0.72, p=0.02) and aneurysm body (0.69, p=0.02) but not in the thoracic aorta (0.11, p=0.41; Figure 24, Table 11).

A positive correlation was observed between the change in thoracic calcium score and the pre-operative AMA (R=0.33, p=0.04). However, no relationships were observed between the pre-operative, post-operative and change in AMA, and the aortic sac size or the change in aortic sac size.

The patient with an active endoleak during the post-operative visit had the highest AMA in the suprarenal and neck regions and the second highest AMA in the thoracic and aneurysm region on the pre-operative PET-CT. Despite also demonstrating a reduction, this patient's post-operative AMA was the highest of the cohort in all four aortic regions.

5.5 Discussion

EVAR is associated with shrinkage of the abdominal aortic aneurysm sac: a key morphological indicator of procedural success (Wanhainen et al., 2019). For the first time, we have shown that EVAR is also associated with a reduction in sodium [^{18}F]fluoride uptake within the abdominal aorta. This reduction was prominent in the regions of the abdominal aorta covered by the stent graft and

Figure 23. **Representative patient with a pre-operative and a post-operative sodium [^{18}F]fluoride positron emission tomography and computed tomography angiogram**

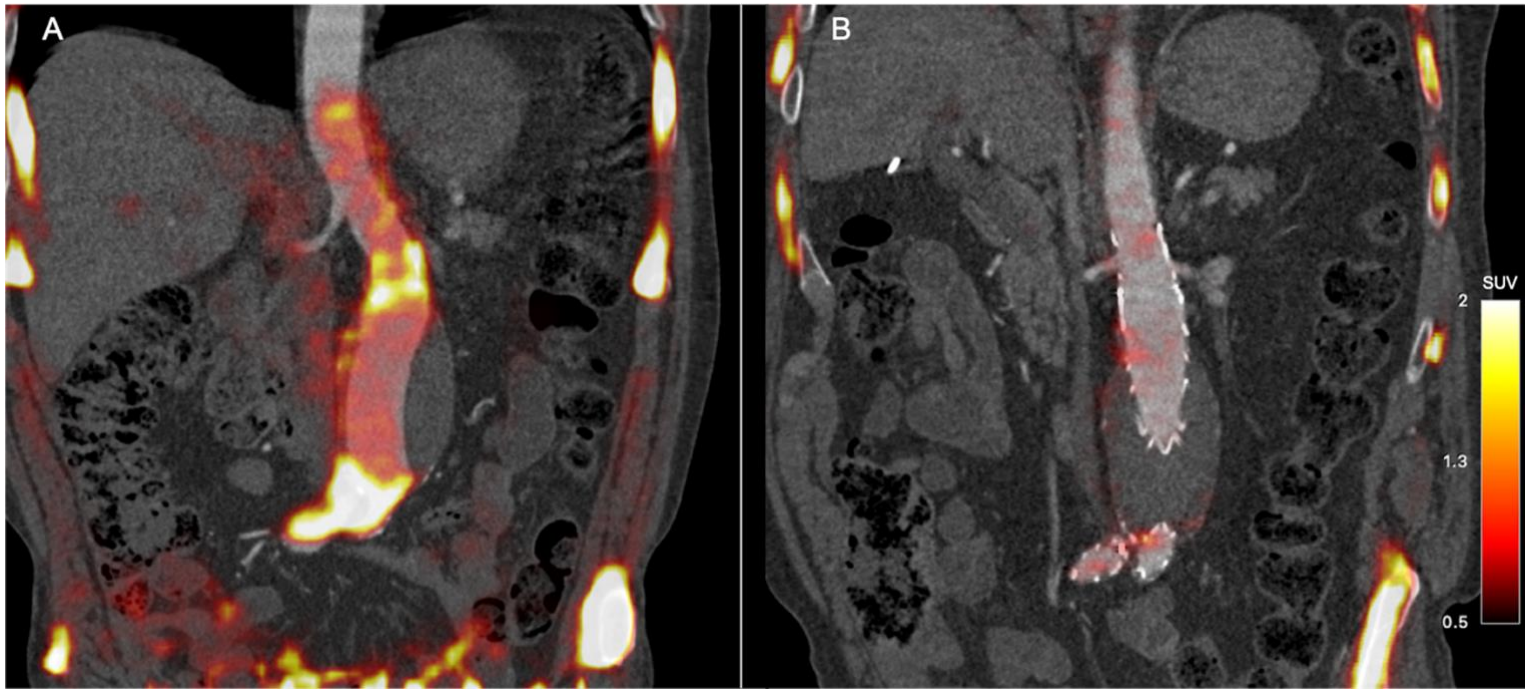

The computed tomography (CT) angiogram is performed immediately after acquisition of positron emission tomography (PET) data. A visual reduction in sodium [^{18}F]fluoride uptake can be observed when comparing (A) the pre-operative PET-CT and (B) the post-operative PET-CT in the same patient.

Standard uptake values (SUV) represented in the colour scale bar.

Figure 24. **Regional aortic sodium [^{18}F]fluoride uptake and aortic microcalcification activity in positron emission tomography and computed tomography**

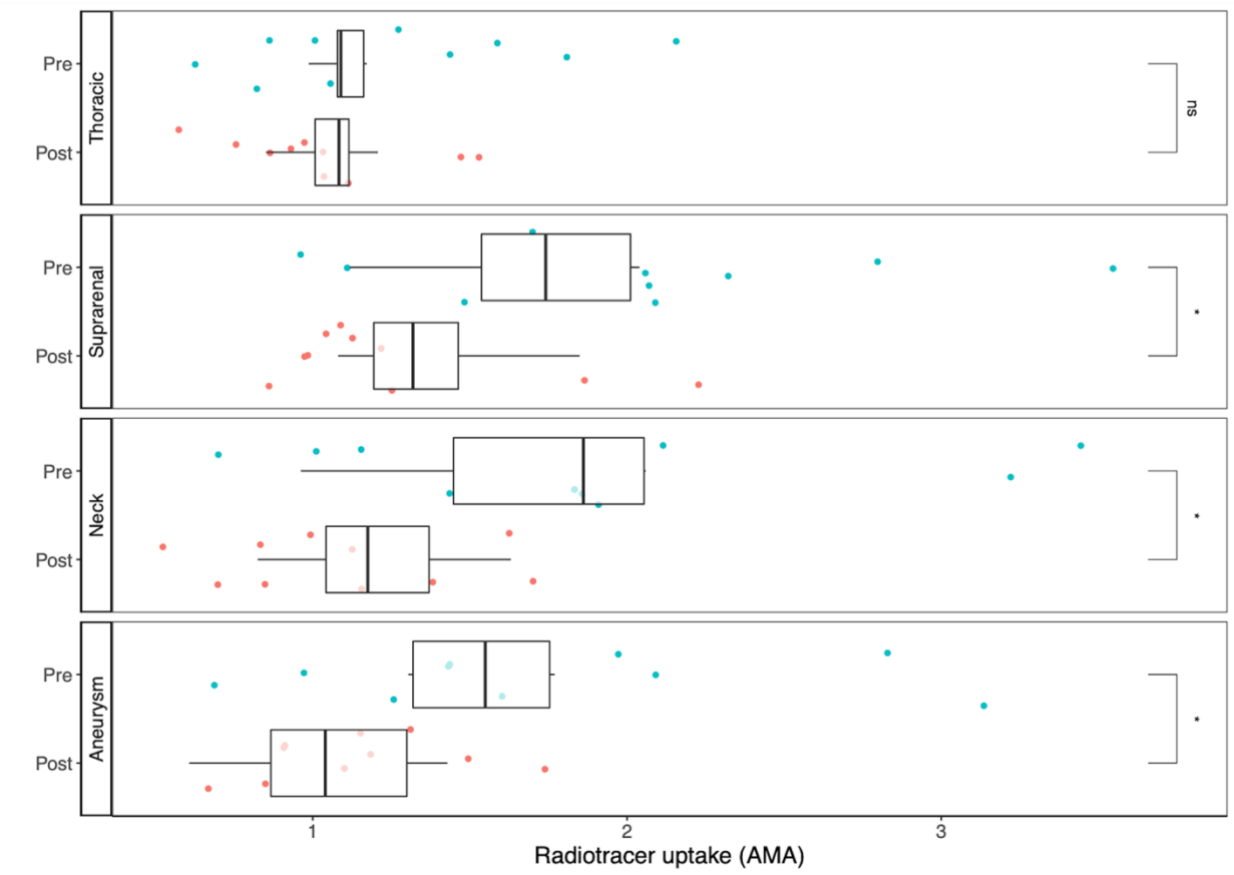

Radiotracer uptake in the four aortic regions (descending thoracic, suprarenal, neck and aneurysm body) before (pre) after (post) endovascular aneurysm repair.

AMA, aortic microcalcification activity. * = $p < 0.05$; ns = not significant.

Table 11. **Pre-operative and post-operative aortic microcalcification activity**

Mean aortic microcalcification activity (AMA) values across each aortic region, and change in AMA following endovascular aneurysm repair (EVAR).

Aortic region	Pre-operative mean (min - max)	Post-operative mean (min - max)	Change in AMA	P value
Thoracic	1.20 (0.99 - 1.69)	1.09 (0.85 - 1.47)	-0.11	0.41
Suprarenal	1.98 (1.12 - 3.6)	1.36 (1.08 - 1.85)	-0.62	0.03
Neck	1.93 (0.96 - 3.54)	1.21 (0.82 - 1.63)	-0.72	0.02
Aneurysm body	1.74 (0.6 - 3.24)	1.05 (0.61 - 1.43)	-0.69	0.02

was not apparent in the thoracic aorta. This suggests that EVAR protects the aortic aneurysm from rupture not only by providing a physical barrier but also by reducing aortic aneurysm disease activity within the wall itself.

Calcification is a marker of disease burden and disease progression in coronary artery disease. Coronary sodium [^{18}F]fluoride uptake correlates with progression of coronary calcification (Doris et al., 2020; Youn et al., 2020) and is a marker of coronary atherosclerotic disease activity (Creager et al., 2019; Moss et al., 2020; Wen et al., 2022). It is also associated with ischaemic stroke (Fletcher, Tew, et al., 2022; Irkle et al., 2015) and the future risk of myocardial infarction (Kwiecinski et al., 2020). The significance of aortic macrocalcification and the associated aortic Agatston calcium score is not well documented for aortic aneurysm disease. In a retrospective study of patients undergoing CT angiography as part of elective treatment work-up of abdominal aortic aneurysm disease, Chowdhury and colleagues observed that higher aortic calcium scores are associated with poorer outcomes (Chowdhury et al., 2018). Conversely, in sub-threshold abdominal aortic aneurysms, Klopf and colleagues observed an inverse relationship between increased abdominal aortic calcification and aneurysm disease progression over a six-month period (Klopf et al., 2022). Here, we observed an association between the change in thoracic calcium score and the pre-operative AMA suggesting that a generally higher aortic disease activity correlates with increasing macrocalcification within the aorta. This could underline the relationship between vascular sodium [^{18}F]fluoride uptake and aneurysm disease activity. Alternatively, the change

in calcium score could merely reflect the processes of calcification as a result of ageing. One way of testing this would be to further perform PET-CT on the SoFIA^{3} patients who had open repair as controls and to assess whether such a relationship also exists.

An increase in aneurysm diameter and a change in radiotracer uptake over time has previously been observed using 2-[^{18}F]fluoro-2-deoxyglucose ([^{18}F]FDG), where patients whose aneurysm diameter increased, had demonstrated lower radiotracer uptake on baseline PET-CT 9 months previously (Morel et al., 2015). This observation was attributed to cyclical periods of inflammation within the aneurysm wall and periods of aneurysm expansion. Rather than inflammation, sodium [^{18}F]fluoride, detects microcalcification, which is increasingly becoming a specific and reliable marker of disease activity within the aorta. Sodium [^{18}F]fluoride uptake quantifies microcalcification within the aortic media of patients with thoracic aortopathy (Fletcher, Nash, et al., 2022) and is associated with greater aortic growth after acute aortic syndrome (Syed et al., 2022). In the present study, AMA was highest in the baseline PET-CT of the abdominal aorta where there is active abdominal aortic aneurysm disease. It is also noteworthy that one of the highest sodium [^{18}F]fluoride uptakes in the cohort occurred in a patient with a type II endoleak and sac enlargement. Although the small cohort size is insufficient to draw definitive conclusions, it does provide promising preliminary data to suggest that high aortic sodium [^{18}F]fluoride uptake may reflect disease activity. As an indicator of reduced aneurysm metabolic activity, suppression

of uptake could confirm or predict treatment efficacy of EVAR, and may have a role in a select group of patients who demonstrate sac expansion on routine screening.

The reduction in AMA we observed following EVAR suggests that insertion of the stent graft can decrease aneurysm disease activity or that it somehow alters the aneurysm biology. The mechanism of such reduced disease activity has not been addressed by our study, but this could plausibly include reducing biomechanical stress within the aortic wall, preventing the build-up of further luminal thrombus or inflammatory mediators, or providing a physical barrier to luminal blood pressure which could otherwise exacerbate aneurysmal dilatation. In turn, these processes could lead to a reduction or cessation in further degeneration in the aortic media which leads to reduced deposition of hydroxyapatite crystals and a reduction in surface area for sodium [^{18}F]fluoride binding. Irrespective of the mechanism, our findings highlight the potential of positron emission tomography to provide an imaging biomarker of treatment efficacy in abdominal aortic aneurysm disease, especially for EVAR but potentially also for other future treatment interventions. Conversely, failure to suppress aortic sodium [^{18}F]fluoride uptake may herald the development of complications and endoleaks not yet visible on CT. Speculatively, it could guide baseline patient selection for EVAR if intense uptake at baseline heralds likely future treatment failure.

Although not the specific aim of this study, in a prospective fashion, EVAR treatment with stent insertion should result in a reduction in aneurysm activity. This would then be observed as a rapid reduction in microcalcification activity following EVAR on serial PET-CT imaging.

This is a small single centre proof-of-concept study, with the small sample size a result of recruitment of only those patients from the original SoFIA[3] study who underwent EVAR. As such, our findings are preliminary and require further external validation. We should also acknowledge several other limitations of this pilot study. First, scan analysis was performed without blinding to the timing of the scans and clearly the aortic stent graft is readily visible on the attenuation correction CT. Second, although the AMA method used to quantify sodium [^{18}F]fluoride uptake has shown excellent levels of agreement with conventional PET quantification methods as demonstrated in Chapter 4, it has not been externally validated. Third, survival bias may play a role, although the majority (83%) of patients who underwent an EVAR operation from the original cohort were recruited into the study. Fourth, since the patients recruited in the study underwent their baseline scan at different timepoints in the natural history of their disease, their baseline radiotracer uptake, time to EVAR and follow up time differed across the cohort. However, this does not preclude a comparison of uptake before and after EVAR. Fifth, the PET reconstruction algorithm uses the attenuation correction CT which is not specifically designed to account for the presence of a stent graft. However, in coronary studies, the presence of a stent usually results in overestimation

of the PET signal rather than a reduction in signal (Cheng et al., 2012). Finally, it was not possible to calculate the calcium score for all abdominal aortic regions due to the presence of the stent graft.

5.6 Clinical Perspectives

This study demonstrates that EVAR leads to a reduction in microcalcification activity in the abdominal aorta, detected as a reduction in aortic sodium [^{18}F]fluoride uptake on PET-CT. This suggests that apart from the commonly observed change in aneurysm sac size, EVAR is also associated with a biological change within the aorta. This technique holds promise as a non-invasive marker of aneurysm disease activity and treatment efficacy following EVAR treatment.

Chapter 6: Aortic disease activity in patients with endoleak after endovascular aneurysm repair

6.1 Abstract

6.1.1 Background

Aortic aneurysm disease activity can be assessed using sodium [^{18}F]fluoride positron emission tomography and increased aortic sodium [^{18}F]fluoride uptake is associated with higher rates of abdominal aortic aneurysm expansion and adverse clinical events. The study objective was to establish whether increased aortic disease activity is associated with patients who have developed an endoleak after endovascular aneurysm repair (EVAR).

6.1.2 Methods

Patients whose abdominal aortic aneurysm had been treated with EVAR underwent sodium [^{18}F]fluoride positron emission tomography and computed tomography angiography. Regional aortic radiotracer uptake was assessed by measuring the aortic microcalcification activity (AMA): a summary measure of mean sodium [^{18}F]fluoride uptake.

6.1.3 Results

Thirty-seven, predominantly male (97%) patients, with a mean age of 76±6 years were recruited (15 with an endoleak and 22 without an endoleak). Median aortic diameter at treatment was 58 [interquartile range 56 to 63] mm. There was no difference in the mean interval from EVAR to imaging between the groups (49±24 versus 50±19 months respectively, p=0.9). When compared to those without an endoleak, patients with an endoleak had higher AMA in the thoracic (1.22±0.2 versus 1.07±0.2, p<0.01), suprarenal (1.58±0.3 versus

1.36±0.2, p<0.01) and neck (1.40±0.3 versus 1.14±0.3, p<0.05) regions of the aorta but not within the aneurysm body (0.94±0.3 versus 1.08±0.3, p=0.10).

6.1.4 Conclusion

Active endoleaks after EVAR are associated with higher aortic microcalcification activity in aortic regions outwith the aneurysm. This suggests that EVAR protects against further aortic degeneration in the aneurysm body, but ongoing aortic degeneration continues beyond the aneurysm and is associated with the presence of endoleaks.

6.2 Introduction

Chapter 1 discussed that the initial mortality benefit for endovascular aneurysm repair (EVAR) when compared to open surgical repair is diminished when longer-term complications such as endoleaks occur. Since endoleaks can occur in up to a third of EVAR cases, and result in higher re-intervention rates, they mandate the use of post-operative surveillance programmes. A shrunken aneurysm sac over time is considered a sign of successful EVAR with a lower risk of late post-operative complications. Conversely, endoleaks are associated with reduced sac shrinkage and worse outcomes (Bastos Gonçalves et al., 2014; Lal et al., 2015).

Implantation of the stent graft causes an alteration in the biomechanical characteristics of the abdominal aortic aneurysm wall (Georgakarakos et al., 2012). Positron emission tomography combined with computed tomography

(PET-CT) angiography is a potential method of tracking this aortic aneurysm disease activity. The sodium [^{18}F]fluoride PET radiotracer can quantify aortic microcalcification activity as an indirect measure of aortic aneurysm disease activity by binding to hydroxyapatite crystals in the aortic media. The proof-of-concept study in Chapter 5 shows a reduction of aortic sodium [^{18}F]fluoride uptake following EVAR. This reduction was particularly striking in regions of the abdominal aorta covered by the EVAR stent graft.

In this case-control study, sodium [^{18}F]fluoride PET-CT was used to quantify radiotracer uptake in patients with or without an active endoleak. We hypothesised that patients with an endoleak will have higher sodium [^{18}F]fluoride uptake as a result of unsuccessful suppression of aortic aneurysm disease activity.

6.3 Methods

The study methods are also discussed in further depth in the relevant section in Chapter 2.

This was a case-control observational study, conducted with the written informed consent of all subjects, in accordance with the declaration of Helsinki, with approval by the South-East Scotland Research Ethics Committee (20/SS/0119), and registered with National Institutes of Health ClinicalTrial.gov (NCT04577716). All study visits were conducted at the Centre for

Cardiovascular Science and the Queen's Medical Research Institute, University of Edinburgh, United Kingdom.

6.3.1 Study population

Study participants with an endoleak were identified by clinicians through outcomes obtained at multidisciplinary vascular team meetings within four Scottish regional health boards: National Health Service (NHS) Lothian, NHS Greater Glasgow & Clyde, NHS Lanarkshire and NHS Tayside health boards. Separately, EVAR implant databases kept by the health boards were screened to identify control patients. The main inclusion criteria were age of 50 years or above, no contraindications to performing PET-CT scans, previous EVAR performed within manufacturers' instructions for use and the presence of any active type of endoleak (as defined by European Society for Vascular Surgery guidelines) (Wanhainen et al., 2019). Patients were excluded if they had known severe chronic kidney disease (defined as estimated glomerular filtration rate of ≤ 30 mL/min/1.73 m^2), major or untreated cancer reducing life expectancy to below 2 years and a known history of connective tissue disease. Control subjects were selected using the same criteria except that they had no known current endoleaks.

6.3.2 Positron emission tomography and computed tomography

Study imaging was performed on a hybrid 128–slice PET-CT scanner (Biograph mCT, Siemens Healthineers, Erlangen, Germany). Patients were administered a target dose of 125 MBq of sodium [^{18}F]fluoride intravenously

and imaged after 60 min of uptake time. A low-dose attenuation correction CT scan was performed (120 kV, 50 mAs, 5-mm thickness, 3-mm increments), followed by acquisition of PET data at 10-min intervals in four bed positions to cover the thoracic and abdominal aorta. Static PET-CT images were reconstructed as described in Section 2.6. Immediately after PET acquisition, an arterial and delayed-phase contrast-enhanced aortic CT angiogram (120 kV, 145 mAs, 3-mm thickness, 3-mm increments, field of view 400; and 1/1 mm, field of view 300; triggered at 181 Hounsfield units) was performed.

6.3.3 Image analysis

Sodium [^{18}F]fluoride uptake was quantified using a custom validated tool (FusionQuant v1.21.0421, Cedars-Sinai Medical Centre, Los Angeles, USA) by measuring the aortic microcalcification activity (AMA), a summary measure of mean aortic sodium [^{18}F]fluoride uptake in a three-dimensional volume as described in Chapters 2 and 4. Uptake was measured in the four previously described anatomically distinct regions of interest: the descending thoracic aorta, the suprarenal region, the aneurysm neck and the body of the aneurysm.

Pre-operative CT angiograms were accessed through a national Picture Archiving and Communications System (PACS, Carestream Health, Rochester, USA). This allowed pre-operative measurements of aneurysm morphology, aortic sac size, neck length and length of common iliac arteries. CT angiograms performed at the study visit confirmed the presence of an

active endoleak and sac diameter through an independent vascular multidisciplinary team meeting process.

6.3.4 Statistical analysis

Apart from the generic statistical analyses as described in Chapter 2, radiotracer uptake was expressed as aortic microcalcification activity (AMA) (unitless) for each region and as a ratio of aneurysm AMA. A two-way repeated measures ANOVA was used to assess regional differences in the AMA between the two groups. P-values were adjusted using the Bonferroni multiple testing correction method. Change in aneurysm sac size was corrected for the interval distance between the pre-operative and post-operative scan (mm/year). Pearson's correlation coefficient was used to assess the association between change in aneurysm sac size and AMA ratio.

6.4 Results

From 491 screened patients, 63 patients with no endoleak met the inclusion criteria and 22 consented to participate. Separately, 46 patients with an endoleak were referred. Of these, 28 patients were suitable and 15 agreed to participate. Patients had a mean age of 76±6 years and were predominantly male (97%) (Table 12). All abdominal aortic aneurysms were infrarenal and all stent grafts were inserted according to the manufacturers' instructions for use (Table 13).

Table 12. **Patient characteristics**

Characteristic	**Overall**	**Endoleak**	**No endoleak**	**p-value**[2]
	N = 37[1]	N = 15[1]	N = 22[1]	
Age (years)	76 ± 6	77 ± 7	75 ± 6	0.4
Male	36 (97%)	15 (100%)	21 (95%)	>0.9
Systolic blood pressure (mmHg)	150 ± 20	148 ± 24	151 ± 17	0.5
Diastolic blood pressure (mmHg)	81 ± 9	82 ± 11	81 ± 7	0.4
Heart rate (beats/min)	71 ± 16	75 ± 16	68 ± 15	0.095
Body mass index (kg/m2)	29.9 ± 5.1	29.1 ± 5.8	30.4 ± 4.7	0.3
Medical History				
Current or ex-smoker	28 (76%)	8 (53%)	20 (91%)	0.017
Hypertension	27 (73%)	12 (80%)	15 (68%)	0.5
Hypercholesterolemia	33 (89%)	12 (80%)	21 (95%)	0.3
Diabetes	5 (14%)	2 (13%)	3 (14%)	>0.9
Ischaemic heart disease	13 (35%)	4 (27%)	9 (41%)	0.4
Peripheral arterial disease	5 (14%)	1 (6.7%)	4 (18%)	0.6
Cerebrovascular disease	6 (16%)	3 (20%)	3 (14%)	0.7
Chronic obstructive pulmonary disease	5 (14%)	1 (6.7%)	4 (18%)	0.6
Positive aneurysm family	4 (11%)	1 (6.7%)	3 (14%)	0.6

Characteristic	Overall	Endoleak	No endoleak	p-value[2]
	N = 37[1]	N = 15[1]	N = 22[1]	
history				
Medication				
Antiplatelet agents	23 (62%)	10 (67%)	13 (59%)	0.6
Anticoagulant agents	9 (24%)	2 (13%)	7 (32%)	0.3
Statins	32 (86%)	11 (73%)	21 (95%)	0.14
Beta-blocker	15 (41%)	7 (47%)	8 (36%)	0.5
Angiotensin-converting enzyme inhibitors or angiotensin receptor blockers	16 (43%)	8 (53%)	8 (36%)	0.3
Calcium channel antagonist	12 (32%)	6 (40%)	6 (27%)	0.5
Diuretic	3 (8.1%)	1 (6.7%)	2 (9.1%)	>0.9
Nitrate	1 (2.7%)	0 (0%)	1 (4.5%)	>0.9
Aorta				
Time from EVAR to PET (months)	50 ± 21	49 ± 24	50 ± 19	>0.9
Aortic diameter at treatment, mm	58 [56 to 63]	60 [58 to 65]	57 [56 to 61]	0.10
Concurrent iliac aneurysm	14 (38%)	4 (27%)	10 (45%)	0.2

[1]Mean ± standard deviation; n (%); Median [25% to 75%]

[2]Wilcoxon rank sum test; Fisher's exact test; Wilcoxon rank sum exact test; Pearson's Chi-squared test

EVAR, endovascular aneurysm repair; PET, positron emission tomography.

Table 13. **Aortic morphology and stent graft details**

Characteristic	Overall	Endoleak	No endoleak	p-value[2]
	N = 37[1]	N = 15[1]	N = 22[1]	
Pre-operative aortic diameter (mm)	58 [56 to 63]	60 [58 to 65]	57 [56 to 61]	0.10
Aortic diameter at follow-up (mm)	57 ± 17	74 ± 8	45 ± 11	<0.001
Concurrent iliac aneurysm	14 (38%)	4 (27%)	10 (45%)	0.2
Iliac aneurysm diameter (mm)	21 [20 to 25]	20 [20 to 26]	22 [20 to 25]	0.7
Morphology				
Length of healthy neck (mm)	23 [16 to 29]	24 [22 to 27]	20 [16 to 30]	0.4
Neck angulation (°)	29 [15 to 40]	25 [15 to 42]	30 [20 to 33]	0.7
Left iliac length (mm)	56 ± 18	55 ± 20	57 ± 16	0.8
Right iliac length (mm)	55 ± 17	53 ± 14	58 ± 19	0.5

[1]Median [25% to 75%]; Mean ± standard deviation; n (%)

[2]Wilcoxon rank sum test; Pearson's Chi-squared test; Fisher's exact test

Most endoleaks were type II endoleaks (11 (73%)). One was diagnosed as type I at explant, one was diagnosed as type III following treatment of a type II, one had stent graft migration and the remaining patient had no visible endoleak but significant sac expansion (Table 14). The majority of patients in the endoleak group demonstrated sac expansion (14 (93%)), one had shown no sign of sac regression after EVAR treatment (Table 14). As expected, patients in the endoleak group had a mean increase in aortic diameter of 12±7 mm (Table 13).

6.4.1 Aortic microcalcification activity

The region with the highest mean aortic sodium [^{18}F]fluoride uptake (AMA) was the suprarenal aorta, and the lowest was the body of the aortic aneurysm: Thoracic 1.13±0.16 ($p=0.021$), suprarenal 1.45±0.24 ($p<0.0001$), neck 1.25±0.31 ($p=0.003$) and aneurysm 1.02±0.27 (P-values refer to comparison with the aneurysm AMA).

Compared to those without an endoleak, patients with an endoleak had higher AMA in the thoracic, suprarenal and neck regions (Figure 25), but there were no differences in AMA within the body of the aneurysm itself (Table 15, Figure 26). A moderate correlation was observed between the change in aneurysm sac size and AMA ratios ($R=0.42$, $p<0.0001$).

Table 14. **Individual endoleak and aneurysm sac size changes**

	Type	**Diagnosis**	**Treatment**	**Pre-operative sac size (mm)**	**Post-operative sac size (mm)**	**Sac expansion**
1	Type II. Changed to Type IA at explant	Lumbar type II and sac expansion on CT	Lumbar embolisation and Onyx injection to sac. Explant performed	61	88	Yes
2	Type II	Lumbar type II on CT	Surveillance only	58	60	Yes, had reduced to 54 mm post-operatively
3	Type II	Lumbar type II on CT	Surveillance only	65	70	Yes
4	Type II	Sac expansion, iliolumbar type II on CT & DSA	Failed embolisation, open artery ligation performed	67	77	Yes
5	Type II	Lumbar type II (present since insertion) and sac expansion	Embolisation but persistent on CT, further embolisation performed	60	73	Yes

6	Type II	Sac expansion on USS, lumbar type II on CT	Failed embolisation attempt, Onyx infiltration performed	58	72	Yes
7	Type II	Sac expansion on USS, lumbar type II on CT	Failed embolisation attempt, Onyx infiltration performed	55	65	Yes
8	Unknown	Sac expansion on USS, no endoleak on multiple CTs but stent graft migration noted	Conservative, patient unfit for explant. Aortic cuff with EndoAnchors performed	65	78	Yes
9	Type II	Mesenteric & lumbar on post-operative CT	Surveillance only	69	69	No, but demonstrated no sac size reduction in 14 months
10	Type II (treated), type III	Sac expansion on USS, mesenteric type II on CT	IMA embolisation but had continued sac expansion and further CT showed type III from right limb	55	70	Yes

11	Type II	Sac expansion on USS, iliolumbar type II on CT	Previous IMA embolisation. Had continued sac expansion, unsuccessful attempts at iliolumbar embolisation. Surveillance stopped due to patient frailty	58	76	Yes
12	Unknown	Sac expansion on USS, no endoleak on CT	Negative DSA. Patient unfit for explant, surveillance only	77	88	Yes
13	Type II	Sac expansion on CT and iliolumbar endoleak, expansion weakened top seal and right limb seal	Aortic cuff and EndoAnchors and right limb extension	63	73	Yes
14	Type II	Sac expansion on CT, IMA and iliolumbar endoleak. Impending type IB due to sac expansion	Direct Onyx injection to lumbar vessel, persistent IMA endoleak. Ongoing sac expansion and confirmation of lumbar endoleak on DSA. Onyx sac injection but continued sac expansion. Patient declined laparoscopic IMA ligation and bilateral limb extensions	57	78	Yes

15	Type II	Sac expansion on CT and type II endoleak	Embolisation to iliolumbar but still present therefore planned for direct sac embolisation with IIA embolisation and right limb extension	60	74	Yes

Where patients had definitive endoleak treatment, the majority had their positron emission tomography scan performed before treatment. In patients 6 and 10, this was performed after, but within 1 month from endoleak treatment.

CT, computed tomography; USS, ultrasound scan; DSA, digital subtraction angiography; IMA, inferior mesenteric artery; IIA, internal iliac artery.

Figure 25. **Sagittal images of positron emission tomography and computed tomography angiogram of three representative cases**

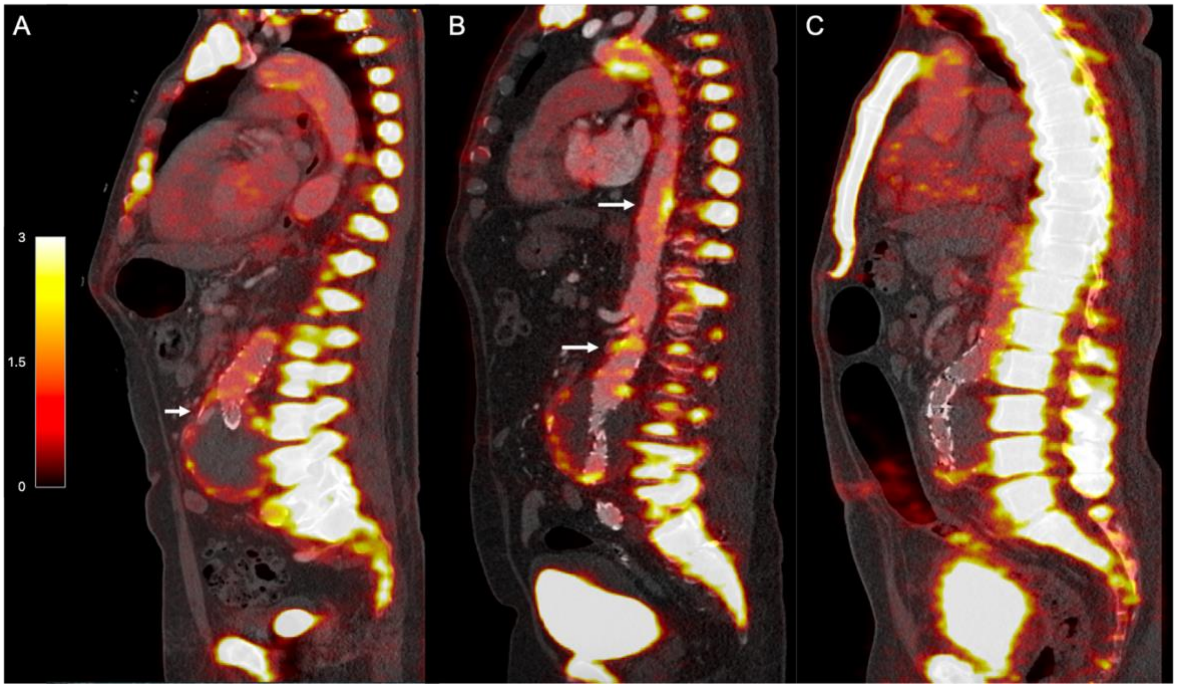

Sagittal images of positron emission tomography and computed tomography angiogram of three representative cases.

A. Radiotracer uptake around the aneurysm sac with a visible endoleak (short white arrow); thoracic AMA 1.06, suprarenal AMA 1.27.
B. Patient with an endoleak (not visible here) with areas of high uptake visible mid-way along the thoracic aorta and just inferior to the superior mesenteric artery (long white arrows); thoracic AMA 1.25, suprarenal AMA 1.69.
C. Minimal areas of radiotracer uptake visible in a patient without an endoleak and a visible stent graft; thoracic AMA 1.03, suprarenal AMA 1.08.

Standard uptake values (SUV) represented in the colour scale bar; AMA, aortic microcalcification activity.

Table 15. **Mean aortic microcalcification activity in the four analysed regions of the aorta**

Region	Endoleak	No endoleak	Difference	P-value	Adjusted p-value
Thoracic	1.22±0.15	1.07±0.15	0.15	0.006	0.02
Thoracic ratio	1.25 [1 to 1.7]	1.08 [0.8 to 1.2]	0.17	0.015	0.02
Suprarenal	1.58±0.25	1.36±0.19	0.22	0.005	0.02
Suprarenal ratio	1.72 [1.5 to 2.2]	1.24 [1.1 to 1.6]	0.48	0.001	0.003
Neck	1.40±0.32	1.14±0.27	0.26	0.012	0.048
Neck ratio	1.53 [1.3 to 1.8]	1.03 [0.9 to 1.2]	0.50	<0.001	0.001
Aneurysm	0.94±0.29	1.08±0.25	-0.14	0.119	0.48

The microcalcification activity in the thoracic, suprarenal and neck regions was also expressed as a ratio of the aneurysm aortic microcalcification activity.

Mean ± standard deviation; Median [25% to 75%]

P-values were adjusted using the Bonferroni multiple testing correction method.

Figure 26. **Sodium [^{18}F]fluoride uptake in endoleak and no endoleak patients**

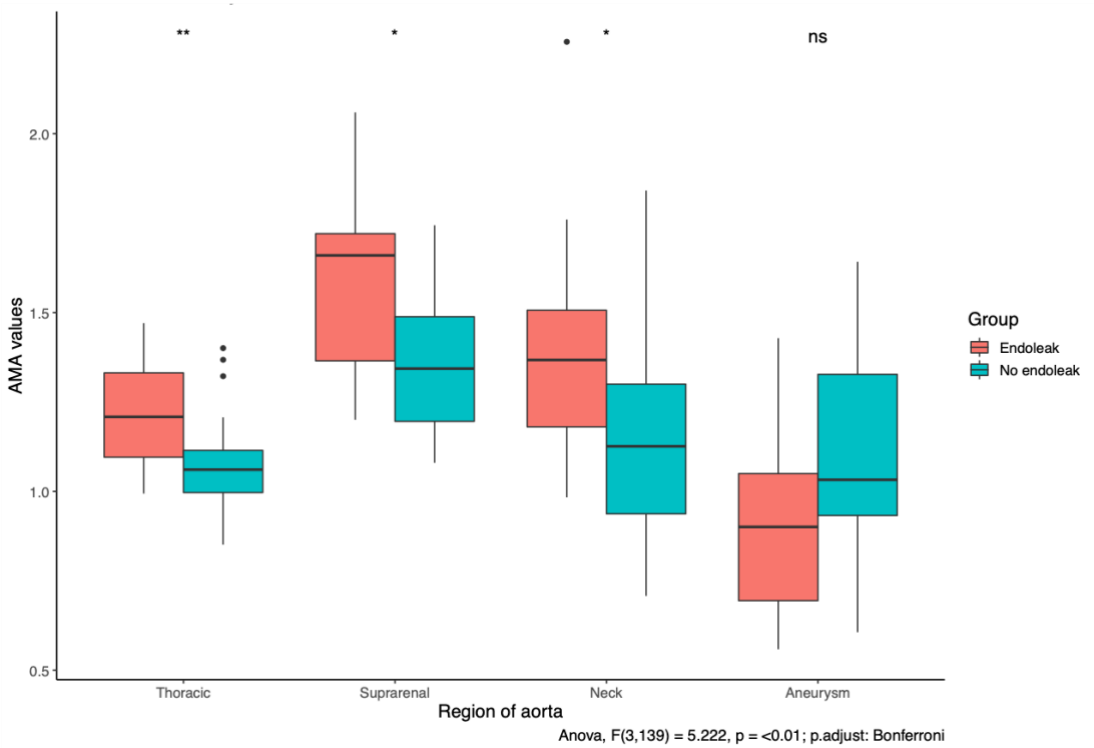

Sodium [^{18}F]fluoride uptake (expressed as aortic microcalcification activity (AMA)) in the four analysed aortic regions (descending thoracic, suprarenal, neck and aneurysm body) in patients with or without an endoleak.

A two-way repeated measures ANOVA was performed to evaluate the effect of being in the endoleak group on regional AMA. Three degrees of freedom were present in the numerator and 139 in the denominator. F refers to the obtained F-statistic value. P-values were adjusted using the Bonferroni multiple testing correction method.

AMA, aortic microcalcification activity. ANOVA, analysis of variance. * = $p < 0.05$, ** = $p < 0.01$, *** = $p < 0.001$, ns = not significant.

6.5 Discussion

This is the first prospective case-control study of patients with abdominal aortic aneurysms which has explored the influence of EVAR and endoleaks on aortic sodium [^{18}F]fluoride uptake. This study has shown that patients with an active endoleak after EVAR have higher AMA suggesting ongoing aneurysm disease activity which may be driving the development of endoleaks. These findings also confirm some of the findings in Chapter 5, a reduction in AMA in the treated aneurysm segment of patients who undergo EVAR, suggesting a reduction in aneurysm disease activity. In contrast to the study hypothesis however, the increased disease activity, was predominantly seen in non-stented regions of the aorta, away from the aneurysm itself, suggesting that the development of endoleaks reflects generalised aortic disease activity rather than local focal areas of disease activity.

In all patients within this study, the aneurysmal segment of the aorta had lower sodium [^{18}F]fluoride uptake when compared to the rest of the aorta. In the serial study described in Chapter 5, there was a marked reduction in AMA of the abdominal aorta following EVAR stent implantation. This appears to be consistent with the findings in this study, and although PET imaging prior to EVAR implantation was not available, the stented segment had a lower and a suppressed AMA compared to the non-stented regions of the abdominal aorta. This indicates that EVAR implantation protects the aortic wall from further disease progression, and perhaps provides some explanation for the mechanism of benefit of this therapeutic intervention.

The study hypothesis centred around persistent AMA within the aneurysm being correlated to, or predicting the development of endoleaks. However, this study did not show this. The AMA within the stented segment was similar in both study groups and was low irrespective of the development of an endoleak. This suggests that the development of an endoleak is not caused by persistent microcalcification activity within this segment of the aorta and that EVAR has resulted in suppressed aneurysm activity. Alternatively, the reduced AMA in the stented segment could reflect end-stage disease. In thoracic aortopathy, a progressive increase in sodium [^{18}F]fluoride uptake with disease severity was observed except in those with the most advanced disease, where sodium [^{18}F]fluoride uptake suddenly and rapidly declined (Fletcher, Nash, et al., 2022). In this context, the loss of sodium [^{18}F]fluoride uptake appeared to be linked to the loss of aortic elastin content since sodium [^{18}F]fluoride uptake requires the presence of microcalcific nodules that bind to fragmented elastin fibres. In the absence of elastin, no binding occurred. In our histology of excised abdominal aortic aneurysm tissue (Chapter 4), we observed depletion of elastin fibres suggesting again, that sodium [^{18}F]fluoride uptake may be lost in end-stage disease.

Perhaps unexpectedly, patients with an endoleak had higher AMA values within the untreated aortic segments. These differences were most marked in the adjacent neck and the suprarenal segments of the abdominal aorta but were also present in the thoracic aorta. This suggests that aortic regions adjacent to the aneurysm play a bigger role in the presence of endoleaks or

their formation, and that this ongoing disease activity in the aorta can lead to endoleak development and EVAR failure. Intuitively, one would have anticipated the development of type I endoleaks if the neck regions continued to expand and caused a loss of proximal EVAR seal. However, whilst some patients did experience a type I endoleak, the majority were type II endoleaks with sac expansion.

It is not entirely clear if higher radiotracer uptake in the context of an endoleak means that they have active aneurysm disease. However, a globally higher AMA in the aorta could suggest that aortic degeneration continues to progress despite treating the aneurysm segment with EVAR. This degeneration leaves an aneurysm sac that is more vulnerable to expansion even if this is through low-pressure retrograde blood flow such as in a type II endoleak. This “global” radiotracer uptake phenomenon resonates with the findings that overall sodium [^{18}F]fluoride uptake in the coronary arteries and the thoracic aorta are associated with an increased risk of future myocardial infarction and ischaemic stroke respectively (Fletcher, Tew, et al., 2022; Kwiecinski et al., 2020). Perhaps assessing radiotracer uptake in other visceral branches such as the renal arteries may help explain this association. Alternatively, a re-pressurised aneurysm sac secondary to endoleak could re-activate the aneurysm disease process and lead to an increase in distant AMA activity. Whatever the cause or mechanism, sac expansion would then lead to loss of EVAR seal resulting in a pressurised sac and potentially aortic rupture. Testing these differing hypotheses would require further studies with repeated serial PET imaging.

It is important to recognise some limitations of this study. The image analysis method, whose development has been described in Chapter 4 has not been externally validated. However, as discussed in Chapter 4 it has shown good intra- and inter-observer repeatability and provides comparable measures of sodium [^{18}F]fluoride uptake with established measures, such as tissue-to-background ratio, while also correcting for radiotracer overspill from the vertebrae. Just over a third of study patients also had iliac aneurysms but radiotracer uptake could not be easily quantified here and we are unable to comment on whether concurrent iliac aneurysm disease has an effect on abdominal aortic aneurysm disease. Attempts at minimising case selection bias sought to approach patients from different vascular centres around Scotland, and only included patients who had standard EVAR treatment inserted within manufacturers' instructions for use. However, enrolled patients had undergone EVAR on average 4 years previously. There is therefore the potential for both survival and case-selection bias, where patients who had immediate endoleaks which required treatment, those who ruptured as a result of leak formation, and those who were too frail, could not be recruited. It is therefore possible that patients with rapidly progressive disease after EVAR did not have higher AMA values within the stented segment. Finally, whilst the analytical approach was robust and repeatable, a degree of observer bias cannot be excluded since a large aneurysm sac size and endoleaks are visible on the CT angiogram performed as part of the PET-CT examination.

6.6 Clinical Perspectives

This study suggests that the development of endoleaks could be related to more than just failure of the EVAR stent graft, but appears to be related to the extent of generalised and active aortic degeneration. Ensuring optimal aortic morphology and the appropriate stent graft to achieve an adequate seal may not be the only technical considerations in the endovascular treatment of abdominal aortic aneurysms.

Sodium [^{18}F]fluoride PET-CT is a promising imaging biomarker that can track abdominal aortic aneurysm disease activity and could be used to better understand the presence of endoleaks after EVAR which can in turn improve patient outcomes.

Chapter 7: Conclusions and Future Directions

7.1 Main findings

This thesis considered two non-invasive imaging methods to follow abdominal aortic aneurysm disease activity and to contextualise these findings to endovascular repair of an abdominal aortic aneurysm.

CT imaging was first used to assess the periaortic adipose tissue attenuation in different abdominal aortic aneurysm disease states. Three disease states were considered: symptomatic abdominal aortic aneurysm disease which included rupture, asymptomatic disease and control subjects (absence of aneurysm). The perivascular adipose tissue attenuation was assessed in both aneurysmal and non-aneurysmal segments.

Sodium [^{18}F]fluoride PET-CT, as a molecular imaging modality, was then used to assess radiotracer uptake as a measure of aortic aneurysm disease activity in patients treated with EVAR. We first developed an analysis method, adapted from colleagues' previous work in quantifying microcalcification activity in the ascending aorta, to assess the sodium [^{18}F]fluoride uptake in the aneurysmal abdominal aorta. This included obtaining a cumulative standard uptake value (SUV) in three-dimensional segments of the aorta and then correcting the measures obtained for the segment's volume and the blood pool. The analysis was specifically adapted to the aneurysmal aorta and to the use of sodium [^{18}F]fluoride radiotracer.

We also wanted to correlate sodium [^{18}F]fluoride uptake with tissue characteristics as defined by histology. We therefore compared the sodium [^{18}F]fluoride uptake in ex vivo tissue using microPET and autoradiography in advanced aneurysm tissue obtained during open abdominal aortic aneurysm repair and non-aneurysmal tissue from controls.

Following this, we looked at an initial cohort of patients who had previously had sodium [^{18}F]fluoride PET-CT imaging of their aneurysmal aorta. We followed up patients who had undergone EVAR as part of routine treatment and obtained post-operative PET-CT imaging. This allowed us to compare the radiotracer uptake in each individual patient's two disease states – untreated and treated abdominal aortic aneurysm.

Endoleak development diminishes the benefits of EVAR, so we also wanted to investigate this diseased state. In a cross-sectional case control fashion, we therefore examined patients with an endoleak after EVAR and patients without an endoleak. Due to the unclear significance of certain types of endoleak, we restricted recruitment to patients with an endoleak who also demonstrated aneurysm sac expansion. We then compared the sodium [^{18}F]fluoride uptake on PET-CT between these two groups.

7.1.1 Periaortic adipose tissue

In Chapter 3, the periaortic adipose tissue attenuation of patients with an asymptomatic abdominal aortic aneurysm did not differ from that of control

patients without an abdominal aortic aneurysm. On the other hand, patients with a symptomatic abdominal aortic aneurysm demonstrated an increase in the periaortic adipose tissue attenuation from these other two groups of patients. This difference was not just localised to the abdominal aortic aneurysm but also to the non-aneurysmal aorta. This suggests that the change in periaortic adipose tissue attenuation is likely to be driven by an acute but non-specific systemic effect of abdominal aortic aneurysm disease or aneurysm rupture.

Periaortic adipose tissue attenuation is ideally placed as a biomarker or risk stratification tool for the prediction of disease progression because as demonstrated in this study it can be obtained from routinely acquired CT imaging. However, it appears to be of limited clinical value in abdominal aortic aneurysm disease. The changes in perivascular adipose tissue attenuation, as observed in pericoronary adipose tissue (Oikonomou et al., 2018; Tzolos et al., 2022), do not appear to be generalisable to all vascular beds or cardiovascular diseases. Large systemic differences in attenuation have been observed in patients with symptomatic abdominal aortic aneurysm disease when compared to asymptomatic patients and control subjects, but these are not localised to the diseased or ruptured segment itself.

7.1.2 Sodium [^{18}F]fluoride PET-CT

Chapter 4 was focused on developing a method of quantifying sodium [^{18}F]fluoride uptake on PET-CT. This was termed aortic microcalcification

activity (AMA). This method was then used for the analysis in Chapters 5 and 6. AMA is quicker and less-labour intensive whilst being simpler to apply and demonstrated good intra-observer and inter-observer repeatability. More importantly, it showed that the measures of radiotracer uptake provided were comparable to the more established measures of SUV in a slice-by-slice method. The method was further enhanced by modifications that include minimising the effect of spill-over from vertebral sodium [^{18}F]fluoride uptake and variations in the aneurysm diameter along its length.

The ex vivo tissue analysis confirmed that advanced aneurysm disease has higher sodium [^{18}F]fluoride uptake than non-aneurysmal control tissue. Radiotracer uptake on autoradiography also highly corresponded to areas of established aneurysm disease activity within the aortic media on histology.

Chapter 5 demonstrated the proof-of-concept that the change in aneurysm disease activity following EVAR can be followed by exploring the aortic microcalcification activity within the aorta. EVAR was associated with a reduction in aortic sodium [^{18}F]fluoride uptake on PET-CT. This reduction was most prominent in the stented regions of the aorta. Apart from the commonly observed change in aneurysm sac size (which can be noted on routine imaging), EVAR is also associated with a biological change within the aorta and this can be detected as a change in microcalcification activity. Furthermore, we observed an association between the change in the thoracic calcium score and the preoperative AMA, suggesting that generally higher

aortic disease activity correlated with increasing macrocalcification within the aorta. This underlines the relationship between sodium [^{18}F]fluoride uptake in the aorta and aneurysm disease activity.

The cross-sectional case control study in Chapter 6 showed increased AMA in patients with an endoleak after EVAR when compared to control patients. Higher AMA was observed in aortic regions away from the aneurysm but not in the body of the aneurysm itself. This region had the lowest uptake from the aortic regions. This suggests that whilst EVAR protects against further aortic degeneration in the aneurysm body, ongoing aortic degeneration can continue beyond the aneurysm and this may potentially contribute to the formation of endoleaks. The study also suggests that sodium [^{18}F]fluoride can describe aneurysm disease activity because it can distinguish between patients who have failure of their EVAR (i.e., an active endoleak with sac expansion).

Sodium [^{18}F]fluoride PET-CT is a promising imaging biomarker in treated abdominal aortic aneurysm disease. This technique holds promise as a non-invasive marker of aortic aneurysm disease activity and treatment efficacy following EVAR treatment.

7.2 Future directions

This thesis has explored the use of two potential imaging biomarkers for abdominal aortic aneurysm disease, periaortic adipose tissue and PET-CT with sodium [^{18}F]fluoride. It is important to appreciate this work did not occur

in isolation but that it has continued to build on previous research and it has provided a basis for further future research.

7.2.1 Perivascular adipose tissue in patients with peripheral arterial disease

We had attempted to emulate the success observed in assessment of perivascular adipose tissue in atherosclerotic disease such as the coronary circulation. However, these findings do not appear to be generalisable to abdominal aortic aneurysm disease, which is perhaps unsurprising since whilst overlapping, atherosclerosis is a different disease process to aneurysm disease.

In the peripheral circulation, atherosclerotic disease drives peripheral arterial disease. To address whether our findings reflect the differing disease processes of atheroma and aneurysm, a further proof-of-concept study is required and we are currently exploring CT angiography in patients with peripheral arterial disease. Along with perivascular adipose tissue attenuation, it will analyse arterial plaque features such as composition, volume, burden and calcification of this peripheral plaque. These data will then be correlated to adverse clinical outcomes such as mortality and major adverse limb events. This has the potential of informing a larger prospective study in patients with peripheral arterial disease.

7.2.2 Aortic radiotracer quantification

The image analysis methodology in Chapter 4 was an essential component of this thesis by demonstrating that sodium [^{18}F]fluoride uptake can be quantified in the descending thoracic and abdominal aorta in a repeatable fashion.

Since the quantification method has yielded important results (as demonstrated in Chapters 5 and 6), it would perhaps be prudent to apply this analysis method to previously obtained PET imaging in patients under surveillance with an abdominal aortic aneurysm (The SoFIA^3 Study). This could result in more exciting findings in relation to abdominal aortic aneurysm disease expansion. Similarly, technological improvements such as artificial intelligence and the use of radiomics could see the research data obtained as part of this thesis further re-analysed to provide different insights and perhaps discover new patterns of radiotracer uptake quantification and how these relate to aneurysm disease.

Along with previous methodology developed by colleagues in the ascending thoracic aorta and aortic arch (Fletcher et al., 2021), this method has been further taken forward in a collaborative manner. We are working with colleagues at the Department of Imaging and Division of Cardiology, Massachusetts General Hospital and Harvard Medical School, Boston, Massachusetts in the United States to expand this technique for use in [^{18}F]FDG PET imaging.

Our simple and rapid AMA technique will be validated alongside clinical outcomes in a cohort of around 500 patients. Using routinely-performed [^{18}F]FDG PET, the collaboration will assess whether uptake would allow the prediction of the risk of future cardiovascular risk as had been previously performed in this same cohort using the substantially slower, more subjective and expert-driven SUV techniques of quantification (Figueroa et al., 2013).

Should these efforts prove fruitful, the AMA technique would be taken forward from a software-design perspective. It can be added as an adjunctive tool to clinical PET viewers. With the use of artificial-intelligence, the software adjunct tool would be able to quantify radiotracer uptake in the aorta at the click of a button and alert clinicians to commence risk-factor modifying medication in patients deemed to be at higher risks of future cardiovascular events.

7.2.3 Predicting endoleaks following EVAR using sodium [^{18}F]fluoride

The findings in Chapter 5 and 6 are very promising. They demonstrated that quantifying sodium [^{18}F]fluoride uptake on PET-CT in patients before and after EVAR can serve as an imaging biomarker of abdominal aortic aneurysm disease activity.

The next research step is a prospective clinical outcome study. A prospective longitudinal observational cohort study was set up along with the work as described in this thesis. The aim of this study is to determine whether sodium [^{18}F]fluoride uptake, as a measure of aortic degeneration, can predict the

development of endoleaks post-operatively. The study hypothesis will test whether individuals who develop an endoleak after EVAR have higher sodium [^{18}F]fluoride uptake on their pre-operative PET-CT. Sixty-five patients undergoing endovascular treatment of their abdominal aortic aneurysm have been recruited. These patients attended for a pre-operative PET-CT scan and will undergo CT angiography at twelve months from their treatment and will complete a total of two years of clinical follow up (Figure 27).

It will be important to determine whether this prospective longitudinal cohort study confirms our preliminary cross-sectional case-control study. In addition, we will need to establish whether, and where, the AMA can predict endoleak development as this will be critical for determining its clinical utility. Although we await the results of this study, if positive, they could lead to a clinical trial of sodium [^{18}F]fluoride PET-CT as a pre-operative clinical tool to predict EVAR stent graft failure, to provide a means of personalising EVAR surveillance, or even to select patients who will benefit most from EVAR. In a clinical pathway, if we could predict stent graft failure pre-operatively using PET-CT, then these patients would perhaps undergo an open surgical repair rather than EVAR. On the other hand, if we could identify patients with lower risk of endoleak development by performing a post-operative PET-CT, then perhaps these patients need not to be enrolled into frequent post-operative EVAR surveillance with ultrasound.

Figure 27. **Study flow chart for the predicting endoleaks following EVAR using sodium [^{18}F]fluoride study**

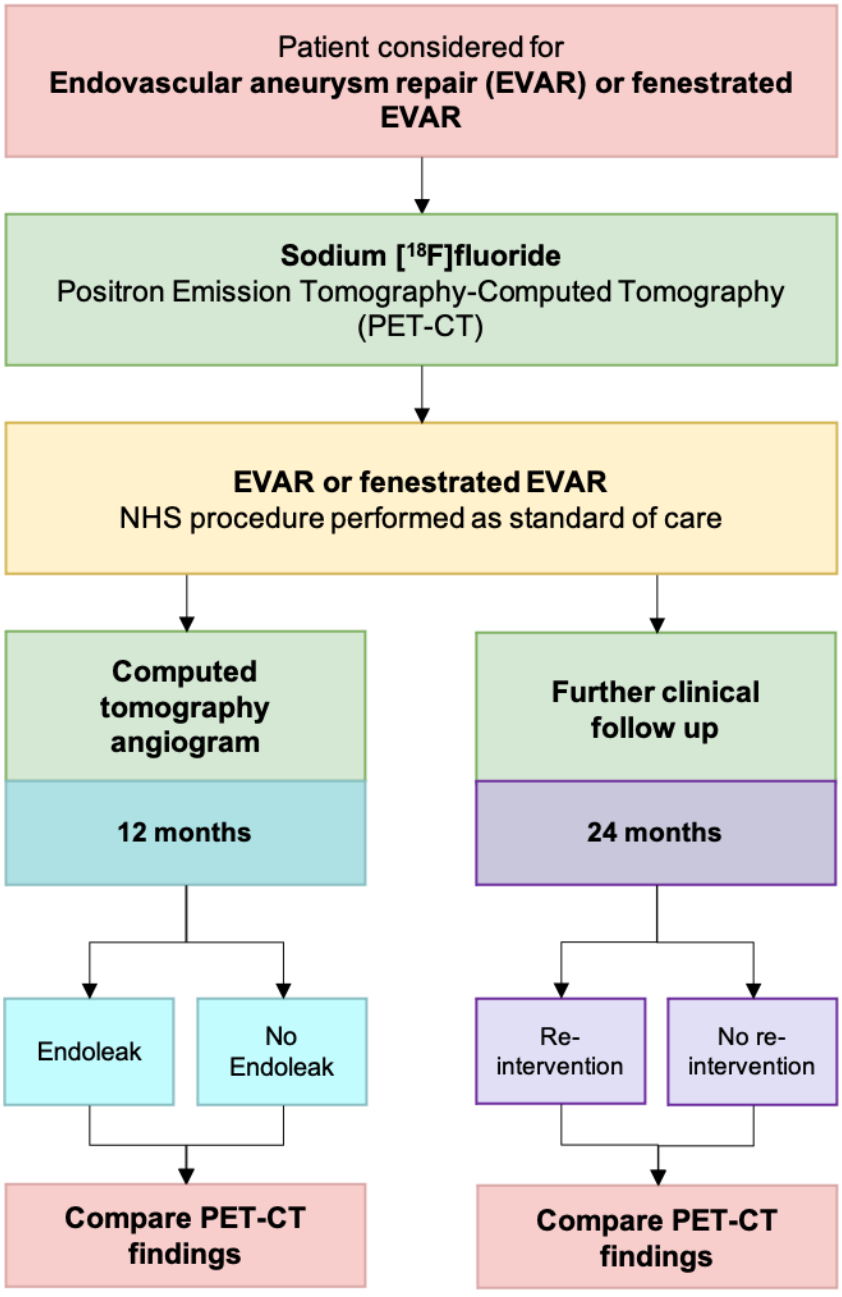

This study recruited patients being considered for standard endovascular aneurysm repair (EVAR) or fenestrated endovascular aneurysm repair who underwent a sodium [^{18}F]fluoride positron emission tomography-computed tomography (PET-CT) pre-operatively. Patients then went on to have their

procedure as planned by their clinical teams. Follow up at 12 months from the procedure using computed tomography in arterial and delayed phases will identify patients with an endoleak (primary outcome) and will be able to record patient's post-operative aneurysm sac size (secondary outcome). Further follow up at 24 months will interrogate the patient's electronic health records to see which patients required re-intervention (secondary outcome) as part of their follow up. Changes in health circumstances will also be confirmed with patients by phone call. The findings on the pre-operative PET-CT will be compared between the outcome groups.

Chapter 1 (Section 1.5) has alluded to the importance of a way of measuring aneurysm disease activity and the lack of medical treatment available. This has been hindered by the lack of a biomarker to measure aneurysm disease activity. The establishment of PET-CT as a measure of aneurysm disease activity could also serve this purpose. It could be used as an imaging biomarker in future research work in aneurysm development including drug development. Here, a reduction in radiotracer uptake could serve as a study endpoint which could be used to quantify and measure a change brought about by the investigational medicinal product.

7.2.4 Other radiotracers

The majority of the work performed in this thesis focused on the utility of molecular PET imaging. The successes of the studies support the use of further PET imaging within vascular surgery. In particular, future PET studies will be needed to investigate other cardiovascular disease processes, and this will increase our understanding of novel biological pathways that are critically involved in the aetiology and pathogenesis of a range of vascular diseases.

One such pathway is tissue fibrosis. Novel radiotracers which can target the fibroblast activation protein and provide a measure of fibrosis occurring in vascular tissue is emerging. These can be labelled with either Fluorine-18 or Gallium-68 (Barton et al., 2023). Several PET studies using these radiotracers are now running in the department. The current studies are investigating myocardial and endocardial injury states including acute infarction, chronic

and delayed valvular disease (particularly aortic valve stenosis), chemotherapy-induced cardiotoxicity and carcinoid heart disease. Tracking of the fibrotic disease process would be useful in other cardiovascular diseases such as in renal artery stenosis and central venous stenosis as they could increase our understanding of these poorly understood diseases. When renal artery stenosis is caused by fibromuscular dysplasia, recognition of the pathology is only possible when this manifests as uncontrolled hypertension. Here, the process of loss of nephrons and kidney atrophy has already started. Earlier recognition could identify treatment strategies which can alter the course of the disease. In dialysis-dependent patients who have previously had central venous canulation, central venous stenosis could result in early failure of access for future dialysis. Understanding the disease process could allow development of therapeutic strategies to treat or reduce the process of central venous stenosis.

A further pathway of interest is the detection of activated platelets as a method of detecting thrombus formation. When elarofiban, which specifically binds to the glycoprotein IIb/IIIa receptors on activated platelets, is bound to Fluorine-18 as [^{18}F]GP1, it provides a highly sensitive marker for thrombus formation. This radiotracer is able to detect thrombus in the coronary vessels in patients with acute myocardial infarction (Tzolos et al., 2023; Tzolos, Bing, et al., 2021) and on bioprosthetic aortic valves which regresses with anticoagulation (Bing et al., 2022). In carotid artery disease, using this radiotracer in patients who have had a thrombo-embolic stroke can help confirm if the carotid plaque is

the culprit-plaque by demonstrating uptake within the plaque (Whittington et al., 2023). Carotid endarterectomy for symptomatic carotid artery disease is a recognised surgical treatment which reduces the long-term risk of future stroke. Plaque rupture with thrombus formation and embolisation can lead to a cerebrovascular event in the form of stroke or a transient ischaemic attack. Cross-sectional imaging (e.g., CT angiography) and dynamic imaging (duplex ultrasound) can grade the level of carotid artery stenosis but cannot always comment on the acuteness of the event. Being able to detect radiotracer uptake both within the carotid plaque and the cerebral circulation would reduce this diagnostic uncertainty and avoid exposing patients with non-culprit plaque but significant carotid stenosis to the unnecessary risk of carotid endarterectomy.

[^{18}F]GP1 could have a role in mesenteric atherosclerotic disease. Atherosclerosis in the mesenteric circulation can result in acute or chronic mesenteric ischaemia, which are sometimes challenging to diagnose. Macrocalcification within the vessels may lead to even more diagnostic uncertainty as contrast-enhanced CT angiography of the mesenteric vessels cannot easily differentiate between an acute thrombotic occlusion and long-standing occlusive disease. [^{18}F]GP1 could identify thrombus within the small mesenteric vessels and be used as an adjunctive tool in clinical management. A further pathway being studied is macrophage-driven inflammation through the 18-kDa translocator protein which is highly expressed on mitochondrial outer membrane of macrophages. The pathway has until recently been

hampered by genetic polymorphisms present in up to 60% of human populations. A new ligand, termed LW223 (and also bound to Fluorine-18), appears to have overcome this challenge (MacAskill et al., 2021). It has shown promise in rat myocardial infarction models and will now be taken forward in human research and will be used in healthy volunteers and patients who have had a myocardial infarction. In the future, this radiotracer could be used in cardiovascular inflammatory conditions such as inflammatory aortitis or giant cell arteritis. Here, such a specific radiotracer could have use in tracking the disease process and the response to anti-inflammatory treatments.

7.3 Conclusion

Across the United Kingdom, around 8 patients undergo treatment for their abdominal aortic aneurysms every day (Waton et al., 2022). Treatment with open surgical repair is associated with a 3% post-operative mortality, whilst EVAR mandates enrolment in a resource-heavy post-operative surveillance programme.

The use of molecular imaging can help bridge the gaps in our knowledge of aneurysm disease and provide us with the tools to personalise abdominal aortic aneurysm treatment and post-operative EVAR surveillance. This thesis has further advanced the use of sodium [^{18}F]fluoride PET-CT as one of the tools which can lead this progress, by showing an association between higher aortic microcalcification activity and failing EVAR treatment.

Journal Publications and Prizes

Debono S, Nash J, Tambyraja AL, Newby DE, Forsythe RO. Endovascular repair for abdominal aortic aneurysms. *Heart*. 2021 Nov;107(22):1783-1789. doi: 10.1136/heartjnl-2020-318288. Epub 2021 Mar 4. PMID: 33674354.

Debono S, Nash J, Fletcher AJ, Syed MBJ, Semple SI, van Beek EJR, Fletcher A, Cadet S, Williams MC, Dey D, Slomka PJ, Forsythe RO, Dweck MR, Newby DE. Quantifying sodium [^{18}F]fluoride uptake in abdominal aortic aneurysms. EJNMMI Res*. 2022 Jun 6;12(1):33. doi: 10.1186/s13550-022-00904-z. PMID: 35666397; PMCID: PMC9170850.*

Debono S, Nash J, Fletcher AJ, Syed M, van Beek EJR, Williams MC, Falah O, Tambyraja A, Dweck MR, Newby DE, Forsythe RO. Aortic sodium [^{18}F]fluoride uptake following endovascular aneurysm repair. *Heart.* 2023 Oct 26;109(22):1677-1682. doi: 10.1136/heartjnl-2023-322514. PMID: 37164479; PMCID: PMC10646867.

Debono S, Tzolos E, Syed MBJ, Nash J, Fletcher AJ, Dweck MR, Newby DE, Dey D, Forsythe RO, Williams MC. CT Attenuation of Periaortic Adipose Tissue in Abdominal Aortic Aneurysms. *Radiol Cardiothorac Imaging*. 2024 Feb;6(1):e230250. doi: 10.1148/ryct.230250. PMID: 38329405.

Second place in best e-Poster Presentation. European Society for Vascular Surgery (ESVS) 37th Annual Meeting, Belfast, Northern Ireland. Title: Sodium [^{18}F]fluoride uptake in patients with endoleak after endovascular aneurysm repair.

References

Agatston, A. S., Janowitz, W. R., Hildner, F. J., Zusmer, N. R., Viamonte, M., Jr., & Detrano, R. (1990, Mar 15). Quantification of coronary artery calcium using ultrafast computed tomography. *J Am Coll Cardiol, 15*(4), 827-832. https://doi.org/10.1016/0735-1097(90)90282-t

Aggarwal, S., Qamar, A., Sharma, V., & Sharma, A. (2011, Spring). Abdominal aortic aneurysm: A comprehensive review. *Exp Clin Cardiol, 16*(1), 11-15.

Ahuja, K., Sotoudeh, H., Galgano, S. J., Singh, R., Gupta, N., Gaddamanugu, S., & Choudhary, G. (2020, Mar). (18)F-Sodium Fluoride PET: History, Technical Feasibility, Mechanism of Action, Normal Biodistribution, and Diagnostic Performance in Bone Metastasis Detection Compared with Other Imaging Modalities. *J Nucl Med Technol, 48*(1), 9-16. https://doi.org/10.2967/jnmt.119.234336

Aikawa, E., Nahrendorf, M., Sosnovik, D., Lok, V. M., Jaffer, F. A., Aikawa, M., & Weissleder, R. (2007, Jan 23). Multimodality molecular imaging identifies proteolytic and osteogenic activities in early aortic valve disease. *Circulation, 115*(3), 377-386. https://doi.org/10.1161/circulationaha.106.654913

Akerele, M. I., Karakatsanis, N. A., Forsythe, R. O., Dweck, M. R., Syed, M., Aykroyd, R. G., Sourbron, S., Newby, D. E., & Tsoumpas, C. (2019, Nov 11).

Iterative reconstruction incorporating background correction improves quantification of [(18)F]-NaF PET/CT images of patients with abdominal aortic aneurysm. *J Nucl Cardiol*. https://doi.org/10.1007/s12350-019-01940-4

Antoniou, G. A., Antoniou, S. A., & Torella, F. (2020, Mar). Editor's Choice - Endovascular vs. Open Repair for Abdominal Aortic Aneurysm: Systematic Review and Meta-analysis of Updated Peri-operative and Long Term Data of Randomised Controlled Trials. *Eur J Vasc Endovasc Surg, 59*(3), 385-397. https://doi.org/10.1016/j.ejvs.2019.11.030

Antonopoulos, A. S., Sanna, F., Sabharwal, N., Thomas, S., Oikonomou, E. K., Herdman, L., Margaritis, M., Shirodaria, C., Kampoli, A. M., Akoumianakis, I., Petrou, M., Sayeed, R., Krasopoulos, G., Psarros, C., Ciccone, P., Brophy, C. M., Digby, J., Kelion, A., Uberoi, R., Anthony, S., Alexopoulos, N., Tousoulis, D., Achenbach, S., Neubauer, S., Channon, K. M., & Antoniades, C. (2017, Jul 12). Detecting human coronary inflammation by imaging perivascular fat. *Sci Transl Med, 9*(398). https://doi.org/10.1126/scitranslmed.aal2658

Bahia, S. S., Vidal-Diez, A., Seshasai, S. R., Shpitser, I., Brownrigg, J. R., Patterson, B. O., Ray, K. K., Holt, P. J., Thompson, M. M., & Karthikesalingam, A. (2016, Nov). Cardiovascular risk prevention and all-cause mortality in primary care patients with an abdominal aortic aneurysm. *Br J Surg, 103*(12), 1626-1633. https://doi.org/10.1002/bjs.10269

Barton, A. K., Tzolos, E., Bing, R., Singh, T., Weber, W., Schwaiger, M., Varasteh, Z., Slart, R., Newby, D. E., & Dweck, M. R. (2023, Feb 17). Emerging molecular imaging targets and tools for myocardial fibrosis detection. *Eur Heart J Cardiovasc Imaging, 24*(3), 261-275. https://doi.org/10.1093/ehjci/jeac242

Bastos Gonçalves, F., Baderkhan, H., Verhagen, H. J., Wanhainen, A., Björck, M., Stolker, R. J., Hoeks, S. E., & Mani, K. (2014, Jun). Early sac shrinkage predicts a low risk of late complications after endovascular aortic aneurysm repair. *Br J Surg, 101*(7), 802-810. https://doi.org/10.1002/bjs.9516

Baxter, B. T., Matsumura, J., Curci, J. A., McBride, R., Larson, L., Blackwelder, W., Lam, D., Wijesinha, M., & Terrin, M. (2020, May 26). Effect of Doxycycline on Aneurysm Growth Among Patients With Small Infrarenal Abdominal Aortic Aneurysms: A Randomized Clinical Trial. *Jama, 323*(20), 2029-2038. https://doi.org/10.1001/jama.2020.5230

Becquemin, J. P., Pillet, J. C., Lescalie, F., Sapoval, M., Goueffic, Y., Lermusiaux, P., Steinmetz, E., & Marzelle, J. (2011, May). A randomized controlled trial of endovascular aneurysm repair versus open surgery for abdominal aortic aneurysms in low- to moderate-risk patients. *J Vasc Surg, 53*(5), 1167-1173.e1161. https://doi.org/10.1016/j.jvs.2010.10.124

Bergström, M., Awad, R., Estrada, S., Mälman, J., Lu, L., Lendvai, G., Bergström-Pettermann, E., & Långström, B. (2003, Nov-Dec). Autoradiography with positron emitting isotopes in positron emission tomography tracer discovery. *Mol Imaging Biol, 5*(6), 390-396. https://doi.org/10.1016/j.mibio.2003.09.004

Bersi, M. R., Khosravi, R., Wujciak, A. J., Harrison, D. G., & Humphrey, J. D. (2017, Nov). Differential cell-matrix mechanoadaptations and inflammation drive regional propensities to aortic fibrosis, aneurysm or dissection in hypertension. *J R Soc Interface, 14*(136). https://doi.org/10.1098/rsif.2017.0327

Bing, R., Deutsch, M. A., Sellers, S. L., Corral, C. A., Andrews, J. P. M., van Beek, E. J. R., Bleiziffer, S., Burchert, W., Clark, T., Dey, D., Friedrichs, K., Gummert, J. F., Koglin, N., Leipsic, J. A., Lindner, O., MacAskill, M. G., Milting, H., Pessotto, R., Preuss, R., Raftis, J. B., Rudolph, T. K., Rudolph, V., Slomka, P., Stephens, A. W., Tavares, A., Tzolos, E., Weir, N., White, A. C., Williams, M. C., Zabel, R., Dweck, M. R., Hugenberg, V., & Newby, D. E. (2022, Jun). 18F-GP1 Positron Emission Tomography and Bioprosthetic Aortic Valve Thrombus. *JACC Cardiovasc Imaging, 15*(6), 1107-1120. https://doi.org/10.1016/j.jcmg.2021.11.015

Bland, J. M., & Altman, D. G. (1986, Feb 8). Statistical methods for assessing agreement between two methods of clinical measurement. *Lancet, 1*(8476), 307-310.

Boron, W. F., & Boulpaep, E. L. (2005). *Medical Physiology*. Elsevier.

Britton, K. A., & Fox, C. S. (2011, Feb). Perivascular adipose tissue and vascular disease. *Clin Lipidol, 6*(1), 79-91. https://doi.org/10.2217/clp.10.89

Bruijn, L. E., van Stroe Gómez, C. G., Curci, J. A., Golledge, J., Hamming, J. F., Jones, G. T., Lee, R., Matic, L., van Rhijn, C., Vriens, P. W., Wågsäter, D., Xu, B., Yamanouchi, D., & Lindeman, J. H. (2021). A histopathological classification scheme for abdominal aortic aneurysm disease. *JVS Vasc Sci, 2*, 260-273. https://doi.org/10.1016/j.jvssci.2021.09.001

Carmo, M., Colombo, L., Bruno, A., Corsi, F. R., Roncoroni, L., Cuttin, M. S., Radice, F., Mussini, E., & Settembrini, P. G. (2002, Jun). Alteration of elastin, collagen and their cross-links in abdominal aortic aneurysms. *Eur J Vasc Endovasc Surg, 23*(6), 543-549. https://doi.org/10.1053/ejvs.2002.1620

Chaikof, E. L., Blankensteijn, J. D., Harris, P. L., White, G. H., Zarins, C. K., Bernhard, V. M., Matsumura, J. S., May, J., Veith, F. J., Fillinger, M. F., Rutherford, R. B., & Kent, K. C. (2002, May). Reporting standards for

endovascular aortic aneurysm repair. *J Vasc Surg, 35*(5), 1048-1060. https://doi.org/10.1067/mva.2002.123763

Chaikof, E. L., Dalman, R. L., Eskandari, M. K., Jackson, B. M., Lee, W. A., Mansour, M. A., Mastracci, T. M., Mell, M., Murad, M. H., Nguyen, L. L., Oderich, G. S., Patel, M. S., Schermerhorn, M. L., & Starnes, B. W. (2018, Jan). The Society for Vascular Surgery practice guidelines on the care of patients with an abdominal aortic aneurysm. *J Vasc Surg, 67*(1), 2-77.e72. https://doi.org/10.1016/j.jvs.2017.10.044

Chaikof, E. L., Fillinger, M. F., Matsumura, J. S., Rutherford, R. B., White, G. H., Blankensteijn, J. D., Bernhard, V. M., Harris, P. L., Kent, K. C., May, J., Veith, F. J., & Zarins, C. K. (2002, May). Identifying and grading factors that modify the outcome of endovascular aortic aneurysm repair. *J Vasc Surg, 35*(5), 1061-1066. https://doi.org/10.1067/mva.2002.123991

Charlton-Ouw, K. M., Sandhu, H. K., Huang, G., Leake, S. S., Miller, C. C., 3rd, Estrera, A. L., Azizzadeh, A., & Safi, H. J. (2014, Mar). Reinfection after resection and revascularization of infected infrarenal abdominal aortic grafts. *J Vasc Surg, 59*(3), 684-692. https://doi.org/10.1016/j.jvs.2013.09.030

Cheng, V. Y., Slomka, P. J., Le Meunier, L., Tamarappoo, B. K., Nakazato, R., Dey, D., & Berman, D. S. (2012, Apr). Coronary arterial 18F-FDG uptake by fusion of PET and coronary CT angiography at sites of percutaneous stenting

for acute myocardial infarction and stable coronary artery disease. *J Nucl Med, 53*(4), 575-583. https://doi.org/10.2967/jnumed.111.097550

Chew, D. K., Dong, S., Schroeder, A. C., Hsu, H. W., & Franko, J. (2019, Nov). The role of the inferior mesenteric artery in predicting secondary intervention for type II endoleak following endovascular aneurysm repair. *J Vasc Surg, 70*(5), 1463-1468. https://doi.org/10.1016/j.jvs.2019.01.090

Chowdhury, M. M., Zieliński, L. P., Sun, J. J., Lambracos, S., Boyle, J. R., Harrison, S. C., Rudd, J. H. F., & Coughlin, P. A. (2018, Jan). Editor's Choice - Calcification of Thoracic and Abdominal Aneurysms is Associated with Mortality and Morbidity. *Eur J Vasc Endovasc Surg, 55*(1), 101-108. https://doi.org/10.1016/j.ejvs.2017.11.007

Conway, A. M., Modarai, B., Taylor, P. R., Carrell, T. W., Waltham, M., Salter, R., & Bell, R. E. (2012, Feb). Stent-graft limb deployment in the external iliac artery increases the risk of limb occlusion following endovascular AAA repair. *J Endovasc Ther, 19*(1), 79-85. https://doi.org/10.1583/11-3550.1

Courtois, A., Makrygiannis, G., El Hachemi, M., Hultgren, R., Allaire, E., Namur, G., Hustinx, R., Defraigne, J. O., & Sakalihasan, N. (2019, Aug). Positron Emission Tomography/Computed Tomography Predicts and Detects Complications After Endovascular Repair of Abdominal Aortic Aneurysms. *J Endovasc Ther, 26*(4), 520-528. https://doi.org/10.1177/1526602819849088

Creager, M. D., Hohl, T., Hutcheson, J. D., Moss, A. J., Schlotter, F., Blaser, M. C., Park, M. A., Lee, L. H., Singh, S. A., Alcaide-Corral, C. J., Tavares, A. A. S., Newby, D. E., Kijewski, M. F., Aikawa, M., Di Carli, M., Dweck, M. R., & Aikawa, E. (2019, Jan). (18)F-Fluoride Signal Amplification Identifies Microcalcifications Associated With Atherosclerotic Plaque Instability in Positron Emission Tomography/Computed Tomography Images. *Circ Cardiovasc Imaging, 12*(1), e007835. https://doi.org/10.1161/circimaging.118.007835

Dale, M. A., Ruhlman, M. K., & Baxter, B. T. (2015, Aug). Inflammatory cell phenotypes in AAAs: their role and potential as targets for therapy. *Arterioscler Thromb Vasc Biol, 35*(8), 1746-1755. https://doi.org/10.1161/atvbaha.115.305269

Derstine, B. A., Holcombe, S. A., Ross, B. E., Wang, N. C., Wang, S. C., & Su, G. L. (2022, Feb 11). Healthy US population reference values for CT visceral fat measurements and the impact of IV contrast, HU range, and spinal levels. *Sci Rep, 12*(1), 2374. https://doi.org/10.1038/s41598-022-06232-5

Dey, D., Cheng, V. Y., Slomka, P. J., Nakazato, R., Ramesh, A., Gurudevan, S., Germano, G., & Berman, D. S. (2009, Nov-Dec). Automated 3-dimensional quantification of noncalcified and calcified coronary plaque from coronary CT

angiography. *J Cardiovasc Comput Tomogr, 3*(6), 372-382. https://doi.org/10.1016/j.jcct.2009.09.004

Dey, D., Schepis, T., Marwan, M., Slomka, P. J., Berman, D. S., & Achenbach, S. (2010, Nov). Automated three-dimensional quantification of noncalcified coronary plaque from coronary CT angiography: comparison with intravascular US. *Radiology, 257*(2), 516-522. https://doi.org/10.1148/radiol.10100681

Di Serafino, M., Viscardi, D., Iacobellis, F., Giugliano, L., Barbuto, L., Oliva, G., Ronza, R., Borzelli, A., Raucci, A., Pezzullo, F., De Cristofaro, M. G., & Romano, L. (2021, Jun 5). Computed tomography imaging of septic shock. Beyond the cause: the "CT hypoperfusion complex". A pictorial essay. *Insights Imaging, 12*(1), 70. https://doi.org/10.1186/s13244-021-01006-5

Dias-Neto, M., Meekel, J. P., van Schaik, T. G., Hoozemans, J., Sousa-Nunes, F., Henriques-Coelho, T., Lely, R. J., Wisselink, W., Blankensteijn, J. D., & Yeung, K. K. (2018, Nov). High Density of Periaortic Adipose Tissue in Abdominal Aortic Aneurysm. *Eur J Vasc Endovasc Surg, 56*(5), 663-671. https://doi.org/10.1016/j.ejvs.2018.07.008

Doderer, S. A., Gäbel, G., Kokje, V. B. C., Northoff, B. H., Holdt, L. M., Hamming, J. F., & Lindeman, J. H. N. (2018, Jun). Adventitial adipogenic degeneration is an unidentified contributor to aortic wall weakening in the

abdominal aortic aneurysm. *J Vasc Surg, 67*(6), 1891-1900.e1894. https://doi.org/10.1016/j.jvs.2017.05.088

Doris, M. K., Meah, M. N., Moss, A. J., Andrews, J. P. M., Bing, R., Gillen, R., Weir, N., Syed, M., Daghem, M., Shah, A., Williams, M. C., van Beek, E. J. R., Forsyth, L., Dey, D., Slomka, P. J., Dweck, M. R., Newby, D. E., & Adamson, P. D. (2020, Dec). Coronary (18)F-Fluoride Uptake and Progression of Coronary Artery Calcification. *Circ Cardiovasc Imaging, 13*(12), e011438. https://doi.org/10.1161/circimaging.120.011438

Drake, R. L., Vogl, W., & Mitchell, A. W. M. (2005). *Gray's Anatomy for Students*. Elsevier/Churchill Livingstone.

Dweck, M. R., Chow, M. W., Joshi, N. V., Williams, M. C., Jones, C., Fletcher, A. M., Richardson, H., White, A., McKillop, G., van Beek, E. J., Boon, N. A., Rudd, J. H., & Newby, D. E. (2012, Apr 24). Coronary arterial 18F-sodium fluoride uptake: a novel marker of plaque biology. *J Am Coll Cardiol, 59*(17), 1539-1548. https://doi.org/10.1016/j.jacc.2011.12.037

Etter, D., Warnock, G., Koszarski, F., Niemann, T., Mikail, N., Bengs, S., Buechel, R. R., Kaufmann, P., Gebhard, C., & Rossi, A. (2023, Apr). Towards universal comparability of pericoronary adipose tissue attenuation: a coronary computed tomography angiography phantom study. *Eur Radiol, 33*(4), 2324-2330. https://doi.org/10.1007/s00330-022-09274-5

Faure, E. M., Becquemin, J. P., & Cochennec, F. (2015, May). Predictive factors for limb occlusions after endovascular aneurysm repair. *J Vasc Surg, 61*(5), 1138-1145.e1132. https://doi.org/10.1016/j.jvs.2014.11.084

Fayad, Z. A., Mani, V., Woodward, M., Kallend, D., Abt, M., Burgess, T., Fuster, V., Ballantyne, C. M., Stein, E. A., Tardif, J. C., Rudd, J. H., Farkouh, M. E., & Tawakol, A. (2011, Oct 29). Safety and efficacy of dalcetrapib on atherosclerotic disease using novel non-invasive multimodality imaging (dal-PLAQUE): a randomised clinical trial. *Lancet, 378*(9802), 1547-1559. https://doi.org/10.1016/s0140-6736(11)61383-4

Figueroa, A. L., Abdelbaky, A., Truong, Q. A., Corsini, E., MacNabb, M. H., Lavender, Z. R., Lawler, M. A., Grinspoon, S. K., Brady, T. J., Nasir, K., Hoffmann, U., & Tawakol, A. (2013, Dec). Measurement of arterial activity on routine FDG PET/CT images improves prediction of risk of future CV events. *JACC Cardiovasc Imaging, 6*(12), 1250-1259. https://doi.org/10.1016/j.jcmg.2013.08.006

Fletcher, A. J., Lembo, M., Kwiecinski, J., Syed, M. B. J., Nash, J., Tzolos, E., Bing, R., Cadet, S., MacNaught, G., van Beek, E. J. R., Moss, A. J., Doris, M. K., Walker, N. L., Dey, D., Adamson, P. D., Newby, D. E., Slomka, P. J., & Dweck, M. R. (2021, Jan 20). Quantifying microcalcification activity in the thoracic aorta. *J Nucl Cardiol*. https://doi.org/10.1007/s12350-020-02458-w

Fletcher, A. J., Nash, J., Syed, M. B. J., Macaskill, M. G., Tavares, A. A. S., Walker, N., Salcudean, H., Leipsic, J. A., Lim, K. H. H., Madine, J., Wallace, W., Field, M., Newby, D. E., Bouchareb, R., Seidman, M. A., Akhtar, R., & Sellers, S. L. (2022, Aug). Microcalcification and Thoracic Aortopathy: A Window Into Disease Severity. *Arterioscler Thromb Vasc Biol, 42*(8), 1048-1059. https://doi.org/10.1161/atvbaha.122.317111

Fletcher, A. J., Tew, Y. Y., Tzolos, E., Joshi, S. S., Kaczynski, J., Nash, J., Debono, S., Lembo, M., Kwiecinski, J., Bing, R., Syed, M. B. J., Doris, M. K., van Beek, E. J. R., Moss, A. J., Jenkins, W. S., Walker, N. L., Joshi, N. V., Pawade, T. A., Adamson, P. D., Whiteley, W. N., Wardlaw, J. M., Slomka, P. J., Williams, M. C., Newby, D. E., & Dweck, M. R. (2022, Jul). Thoracic Aortic (18)F-Sodium Fluoride Activity and Ischemic Stroke in Patients With Established Cardiovascular Disease. *JACC Cardiovasc Imaging, 15*(7), 1274-1288. https://doi.org/10.1016/j.jcmg.2021.12.013

Forsythe, R. O., Dweck, M. R., McBride, O. M. B., Vesey, A. T., Semple, S. I., Shah, A. S. V., Adamson, P. D., Wallace, W. A., Kaczynski, J., Ho, W., van Beek, E. J. R., Gray, C. D., Fletcher, A., Lucatelli, C., Marin, A., Burns, P., Tambyraja, A., Chalmers, R. T. A., Weir, G., Mitchard, N., Tavares, A., Robson, J. M. J., & Newby, D. E. (2018, Feb 6). (18)F-Sodium Fluoride Uptake in Abdominal Aortic Aneurysms: The SoFIA(3) Study. *J Am Coll Cardiol, 71*(5), 513-523. https://doi.org/10.1016/j.jacc.2017.11.053

Fransen, G. A., Vallabhaneni, S. R., Sr., van Marrewijk, C. J., Laheij, R. J., Harris, P. L., & Buth, J. (2003, Nov). Rupture of infra-renal aortic aneurysm after endovascular repair: a series from EUROSTAR registry. *Eur J Vasc Endovasc Surg, 26*(5), 487-493. https://doi.org/10.1016/s1078-5884(03)00350-2

Fuery, M. A., Liang, L., Kaplan, F. S., & Mohler, E. R., 3rd. (2018, Apr). Vascular ossification: Pathology, mechanisms, and clinical implications. *Bone, 109*, 28-34. https://doi.org/10.1016/j.bone.2017.07.006

Fujii, T., Banno, H., Kodama, A., Sugimoto, M., Akita, N., Tsuruoka, T., Sakakibara, M., & Komori, K. (2020, Jul). Aneurysm Sac Thrombus Volume Predicts Aneurysm Expansion with Type II Endoleak After Endovascular Aneurysm Repair. *Ann Vasc Surg, 66*, 85-94.e81. https://doi.org/10.1016/j.avsg.2019.11.045

Gandhi, R., Bell, M., Bailey, M., & Tsoumpas, C. (2021, Oct). Prospect of positron emission tomography for abdominal aortic aneurysm risk stratification. *J Nucl Cardiol, 28*(5), 2272-2282. https://doi.org/10.1007/s12350-021-02616-8

Gaudino, M., Hameed, I., Farkouh, M. E., Rahouma, M., Naik, A., Robinson, N. B., Ruan, Y., Demetres, M., Biondi-Zoccai, G., Angiolillo, D. J., Bagiella, E.,

Charlson, M. E., Benedetto, U., Ruel, M., Taggart, D. P., Girardi, L. N., Bhatt, D. L., & Fremes, S. E. (2020, Oct 12). Overall and Cause-Specific Mortality in Randomized Clinical Trials Comparing Percutaneous Interventions With Coronary Bypass Surgery: A Meta-analysis. *JAMA Intern Med*. https://doi.org/10.1001/jamainternmed.2020.4748

Georgakarakos, E., Georgiadis, G. S., Ioannou, C. V., Kapoulas, K. C., Trellopoulos, G., & Lazarides, M. (2012, Jun). Aneurysm sac shrinkage after endovascular treatment of the aorta: beyond sac pressure and endoleaks. *Vasc Med, 17*(3), 168-173. https://doi.org/10.1177/1358863x11431293

Gleinert-Rożek, M., Kosiński, A., Kaczyńska, A., Zajączkowski, M., Kuta, W., Kamiński, R., & Piwko, G. (2020). Metric analysis of the lumbar region of human vertebral column. *Folia Morphol (Warsz), 79*(4), 655-661. https://doi.org/10.5603/FM.a2020.0008

Goeller, M., Tamarappoo, B. K., Kwan, A. C., Cadet, S., Commandeur, F., Razipour, A., Slomka, P. J., Gransar, H., Chen, X., Otaki, Y., Friedman, J. D., Cao, J. J., Albrecht, M. H., Bittner, D. O., Marwan, M., Achenbach, S., Berman, D. S., & Dey, D. (2019, Jun 1). Relationship between changes in pericoronary adipose tissue attenuation and coronary plaque burden quantified from coronary computed tomography angiography. *Eur Heart J Cardiovasc Imaging, 20*(6), 636-643. https://doi.org/10.1093/ehjci/jez013

Golledge, J., Morris, D. R., Pinchbeck, J., Rowbotham, S., Jenkins, J., Bourke, M., Bourke, B., Norman, P. E., Jones, R., & Moxon, J. V. (2019, Jan). Editor's Choice - Metformin Prescription is Associated with a Reduction in the Combined Incidence of Surgical Repair and Rupture Related Mortality in Patients with Abdominal Aortic Aneurysm. *Eur J Vasc Endovasc Surg, 57*(1), 94-101. https://doi.org/10.1016/j.ejvs.2018.07.035

Golledge, J., Pinchbeck, J., Tomee, S. M., Rowbotham, S. E., Singh, T. P., Moxon, J. V., Jenkins, J. S., Lindeman, J. H., Dalman, R. L., McDonnell, L., Fitridge, R., & Morris, D. R. (2020, Aug 26). Efficacy of Telmisartan to Slow Growth of Small Abdominal Aortic Aneurysms: A Randomized Clinical Trial. *JAMA Cardiol, 5*(12), 1-9. https://doi.org/10.1001/jamacardio.2020.3524

Greenhalgh, R. M., Brown, L. C., Powell, J. T., Thompson, S. G., & Epstein, D. (2010, May 20). Endovascular repair of aortic aneurysm in patients physically ineligible for open repair. *N Engl J Med, 362*(20), 1872-1880. https://doi.org/10.1056/NEJMoa0911056

Greenhalgh, R. M., Brown, L. C., Powell, J. T., Thompson, S. G., Epstein, D., & Sculpher, M. J. (2010, May 20). Endovascular versus open repair of abdominal aortic aneurysm. *N Engl J Med, 362*(20), 1863-1871. https://doi.org/10.1056/NEJMoa0909305

Hajibandeh, S., Hajibandeh, S., Antoniou, S. A., Child, E., Torella, F., & Antoniou, G. A. (2016, Dec). Percutaneous access for endovascular aortic aneurysm repair: A systematic review and meta-analysis. *Vascular, 24*(6), 638-648. https://doi.org/10.1177/1708538116639201

Hellenthal, F. A., Buurman, W. A., Wodzig, W. K., & Schurink, G. W. (2009, Aug). Biomarkers of abdominal aortic aneurysm progression. Part 2: inflammation. *Nat Rev Cardiol, 6*(8), 543-552. https://doi.org/10.1038/nrcardio.2009.102

Holt, P. J., Poloniecki, J. D., Gerrard, D., Loftus, I. M., & Thompson, M. M. (2007, Apr). Meta-analysis and systematic review of the relationship between volume and outcome in abdominal aortic aneurysm surgery. *Br J Surg, 94*(4), 395-403. https://doi.org/10.1002/bjs.5710

ICRP. (2007). The 2007 Recommendations of the International Commission on Radiological Protection. ICRP publication 103. *Ann ICRP, 37*(2-4), 1-332. https://doi.org/10.1016/j.icrp.2007.10.003

IMPROVE Trial Investigators. (2015, Aug 14). IMPROVE Trial Investigators. Endovascular strategy or open repair for ruptured abdominal aortic aneurysm: one-year outcomes from the IMPROVE randomized trial. *Eur Heart J, 36*(31), 2061-2069. https://doi.org/10.1093/eurheartj/ehv125

IMPROVE Trial Investigators. (2017, Nov 14). Comparative clinical effectiveness and cost effectiveness of endovascular strategy v open repair for ruptured abdominal aortic aneurysm: three year results of the IMPROVE randomised trial. *Bmj, 359*, j4859. https://doi.org/10.1136/bmj.j4859

Irkle, A., Vesey, A. T., Lewis, D. Y., Skepper, J. N., Bird, J. L., Dweck, M. R., Joshi, F. R., Gallagher, F. A., Warburton, E. A., Bennett, M. R., Brindle, K. M., Newby, D. E., Rudd, J. H., & Davenport, A. P. (2015, Jul 7). Identifying active vascular microcalcification by (18)F-sodium fluoride positron emission tomography. *Nat Commun, 6*, 7495. https://doi.org/10.1038/ncomms8495

Ishizaka, N., Sohmiya, K., Miyamura, M., Umeda, T., Tsuji, M., Katsumata, T., & Miyata, T. (2012, Mar). Infected aortic aneurysm and inflammatory aortic aneurysm--in search of an optimal differential diagnosis. *J Cardiol, 59*(2), 123-131. https://doi.org/10.1016/j.jjcc.2011.10.006

Jacomelli, J., Summers, L., Stevenson, A., Lees, T., & Earnshaw, J. J. (2016, Aug). Impact of the first 5 years of a national abdominal aortic aneurysm screening programme. *Br J Surg, 103*(9), 1125-1131. https://doi.org/10.1002/bjs.10173

Jahangir, E., Lipworth, L., Edwards, T. L., Kabagambe, E. K., Mumma, M. T., Mensah, G. A., Fazio, S., Blot, W. J., & Sampson, U. K. (2015, May). Smoking, sex, risk factors and abdominal aortic aneurysms: a prospective study of 18

782 persons aged above 65 years in the Southern Community Cohort Study. *J Epidemiol Community Health, 69*(5), 481-488. https://doi.org/10.1136/jech-2014-204920

Johansson, M., & Harris, R. P. (2017, Jun 24). Thresholds in women with abdominal aortic aneurysm. *Lancet, 389*(10088), 2446-2448. https://doi.org/10.1016/s0140-6736(17)31110-8

Jordan, W. D., Jr., Mehta, M., Ouriel, K., Arko, F. R., Varnagy, D., Joye, J., Moore, W. M., Jr., & de Vries, J. P. (2016, Apr). One-year results of the ANCHOR trial of EndoAnchors for the prevention and treatment of aortic neck complications after endovascular aneurysm repair. *Vascular, 24*(2), 177-186. https://doi.org/10.1177/1708538115590727

Joshi, N. V., Toor, I., Shah, A. S., Carruthers, K., Vesey, A. T., Alam, S. R., Sills, A., Hoo, T. Y., Melville, A. J., Langlands, S. P., Jenkins, W. S., Uren, N. G., Mills, N. L., Fletcher, A. M., van Beek, E. J., Rudd, J. H., Fox, K. A., Dweck, M. R., & Newby, D. E. (2015, Aug 27). Systemic Atherosclerotic Inflammation Following Acute Myocardial Infarction: Myocardial Infarction Begets Myocardial Infarction. *J Am Heart Assoc, 4*(9), e001956. https://doi.org/10.1161/jaha.115.001956

Joshi, N. V., Vesey, A. T., Williams, M. C., Shah, A. S., Calvert, P. A., Craighead, F. H., Yeoh, S. E., Wallace, W., Salter, D., Fletcher, A. M., van

Beek, E. J., Flapan, A. D., Uren, N. G., Behan, M. W., Cruden, N. L., Mills, N. L., Fox, K. A., Rudd, J. H., Dweck, M. R., & Newby, D. E. (2014, Feb 22). 18F-fluoride positron emission tomography for identification of ruptured and high-risk coronary atherosclerotic plaques: a prospective clinical trial. *Lancet, 383*(9918), 705-713. https://doi.org/10.1016/s0140-6736(13)61754-7

Kent, K. C., Zwolak, R. M., Egorova, N. N., Riles, T. S., Manganaro, A., Moskowitz, A. J., Gelijns, A. C., & Greco, G. (2010, Sep). Analysis of risk factors for abdominal aortic aneurysm in a cohort of more than 3 million individuals. *J Vasc Surg, 52*(3), 539-548. https://doi.org/10.1016/j.jvs.2010.05.090

Klopf, J., Fuchs, L., Schernthaner, R., Domenig, C. M., Gollackner, B., Brostjan, C., Neumayer, C., & Eilenberg, W. (2022, Jun). The prognostic impact of vascular calcification on abdominal aortic aneurysm progression. *J Vasc Surg, 75*(6), 1926-1934. https://doi.org/10.1016/j.jvs.2021.11.062

Koch, A. E., Haines, G. K., Rizzo, R. J., Radosevich, J. A., Pope, R. M., Robinson, P. G., & Pearce, W. H. (1990, Nov). Human abdominal aortic aneurysms. Immunophenotypic analysis suggesting an immune-mediated response. *Am J Pathol, 137*(5), 1199-1213.

Koch, K. M., Hargreaves, B. A., Pauly, K. B., Chen, W., Gold, G. E., & King, K. F. (2010, Oct). Magnetic resonance imaging near metal implants. *J Magn Reson Imaging, 32*(4), 773-787. https://doi.org/10.1002/jmri.22313

Koo, T. K., & Li, M. Y. (2016, Jun). A Guideline of Selecting and Reporting Intraclass Correlation Coefficients for Reliability Research. *J Chiropr Med, 15*(2), 155-163. https://doi.org/10.1016/j.jcm.2016.02.012

Kotze, C. W., Groves, A. M., Menezes, L. J., Harvey, R., Endozo, R., Kayani, I. A., Ell, P. J., & Yusuf, S. W. (2011, Aug). What is the relationship between ^{18}F-FDG aortic aneurysm uptake on PET/CT and future growth rate? *Eur J Nucl Med Mol Imaging, 38*(8), 1493-1499. https://doi.org/10.1007/s00259-011-1799-8

Koukourakis, G., Maravelis, G., Koukouraki, S., Padelakos, P., & Kouloulias, V. (2009, Oct-Dec). Overview of positron emission tomography chemistry: clinical and technical considerations and combination with computed tomography. *J buon, 14*(4), 575-580.

Kwiecinski, J., Tzolos, E., Adamson, P. D., Cadet, S., Moss, A. J., Joshi, N., Williams, M. C., van Beek, E. J. R., Dey, D., Berman, D. S., Newby, D. E., Slomka, P. J., & Dweck, M. R. (2020, Jun 23). Coronary (18)F-Sodium Fluoride Uptake Predicts Outcomes in Patients With Coronary Artery Disease. *J Am Coll Cardiol, 75*(24), 3061-3074. https://doi.org/10.1016/j.jacc.2020.04.046

Ladich, E., Yahagi, K., Romero, M. E., & Virmani, R. (2016, Sep-Oct). Vascular diseases: aortitis, aortic aneurysms, and vascular calcification. *Cardiovasc Pathol, 25*(5), 432-441. https://doi.org/10.1016/j.carpath.2016.07.002

Lal, B. K., Zhou, W., Li, Z., Kyriakides, T., Matsumura, J., Lederle, F. A., & Freischlag, J. (2015, Dec). Predictors and outcomes of endoleaks in the Veterans Affairs Open Versus Endovascular Repair (OVER) Trial of Abdominal Aortic Aneurysms. *J Vasc Surg, 62*(6), 1394-1404. https://doi.org/10.1016/j.jvs.2015.02.003

Lameka, K., Farwell, M. D., & Ichise, M. (2016). Positron Emission Tomography. *Handb Clin Neurol, 135*, 209-227. https://doi.org/10.1016/b978-0-444-53485-9.00011-8

Lederle, F. A., Johnson, G. R., Wilson, S. E., Chute, E. P., Hye, R. J., Makaroun, M. S., Barone, G. W., Bandyk, D., Moneta, G. L., & Makhoul, R. G. (2000, May 22). The aneurysm detection and management study screening program: validation cohort and final results. Aneurysm Detection and Management Veterans Affairs Cooperative Study Investigators. *Arch Intern Med, 160*(10), 1425-1430. https://doi.org/10.1001/archinte.160.10.1425

Lederle, F. A., Kyriakides, T. C., Stroupe, K. T., Freischlag, J. A., Padberg, F. T., Jr., Matsumura, J. S., Huo, Z., & Johnson, G. R. (2019, May 30). Open

versus Endovascular Repair of Abdominal Aortic Aneurysm. *N Engl J Med, 380*(22), 2126-2135. https://doi.org/10.1056/NEJMoa1715955

Lilja, F., Mani, K., & Wanhainen, A. (2017, Jun). Editor's Choice - Trend-break in Abdominal Aortic Aneurysm Repair With Decreasing Surgical Workload. *Eur J Vasc Endovasc Surg, 53*(6), 811-819. https://doi.org/10.1016/j.ejvs.2017.02.031

López-Candales, A., Holmes, D. R., Liao, S., Scott, M. J., Wickline, S. A., & Thompson, R. W. (1997, Mar). Decreased vascular smooth muscle cell density in medial degeneration of human abdominal aortic aneurysms. *Am J Pathol, 150*(3), 993-1007.

Ma, R., Ties, D., van Assen, M., Pelgrim, G. J., Sidorenkov, G., van Ooijen, P. M. A., van der Harst, P., van Dijk, R., & Vliegenthart, R. (2020, Dec). Towards reference values of pericoronary adipose tissue attenuation: impact of coronary artery and tube voltage in coronary computed tomography angiography. *Eur Radiol, 30*(12), 6838-6846. https://doi.org/10.1007/s00330-020-07069-0

MacAskill, M. G., Stadulyte, A., Williams, L., Morgan, T. E. F., Sloan, N. L., Alcaide-Corral, C. J., Walton, T., Wimberley, C., McKenzie, C. A., Spath, N., Mungall, W., BouHaidar, R., Dweck, M. R., Gray, G. A., Newby, D. E., Lucatelli, C., Sutherland, A., Pimlott, S. L., & Tavares, A. A. S. (2021, Apr). Quantification

of Macrophage-Driven Inflammation During Myocardial Infarction with (18)F-LW223, a Novel TSPO Radiotracer with Binding Independent of the rs6971 Human Polymorphism. *J Nucl Med, 62*(4), 536-544. https://doi.org/10.2967/jnumed.120.243600

Mancio, J., Oikonomou, E. K., & Antoniades, C. (2018, Oct). Perivascular adipose tissue and coronary atherosclerosis. *Heart, 104*(20), 1654-1662. https://doi.org/10.1136/heartjnl-2017-312324

Marie, P. Y., Plissonnier, D., Bravetti, S., Coscas, R., Rouer, M., Haulon, S., Mandry, D., Alsac, J. M., Malikov, S., Settembre, N., Gouëffic, Y., Morel, O., Roch, V., Micard, E., Lamiral, Z., Michel, J. B., & Rossignol, P. (2018, Apr). Low baseline and subsequent higher aortic abdominal aneurysm FDG uptake are associated with poor sac shrinkage post endovascular repair. *Eur J Nucl Med Mol Imaging, 45*(4), 549-557. https://doi.org/10.1007/s00259-017-3883-1

Marini, C., Morbelli, S., Armonino, R., Spinella, G., Riondato, M., Massollo, M., Sarocchi, F., Pane, B., Augeri, C., Abete, L., Ghigliotti, G., Palmieri, D., Fiz, F., Cittadini, G., Fulcheri, E., Palombo, D., & Sambuceti, G. (2012, Jan). Direct relationship between cell density and FDG uptake in asymptomatic aortic aneurysm close to surgical threshold: an in vivo and in vitro study. *Eur J Nucl Med Mol Imaging, 39*(1), 91-101. https://doi.org/10.1007/s00259-011-1955-1

Markar, S. R., Vidal-Diez, A., Sounderajah, V., Mackenzie, H., Hanna, G. B., Thompson, M., Holt, P., Lagergren, J., & Karthikesalingam, A. (2019, Jun). A population-based cohort study examining the risk of abdominal cancer after endovascular abdominal aortic aneurysm repair. *J Vasc Surg, 69*(6), 1776-1785.e1772. https://doi.org/10.1016/j.jvs.2018.09.058

Massera, D., Doris, M. K., Cadet, S., Kwiecinski, J., Pawade, T. A., Peeters, F., Dey, D., Newby, D. E., Dweck, M. R., & Slomka, P. J. (2020, Jun). Analytical quantification of aortic valve 18F-sodium fluoride PET uptake. *J Nucl Cardiol, 27*(3), 962-972. https://doi.org/10.1007/s12350-018-01542-6

McBride, O. M., Joshi, N. V., Robson, J. M., MacGillivray, T. J., Gray, C. D., Fletcher, A. M., Dweck, M. R., van Beek, E. J., Rudd, J. H., Newby, D. E., & Semple, S. I. (2016, Apr). Positron Emission Tomography and Magnetic Resonance Imaging of Cellular Inflammation in Patients with Abdominal Aortic Aneurysms. *Eur J Vasc Endovasc Surg, 51*(4), 518-526. https://doi.org/10.1016/j.ejvs.2015.12.018

McDougald, W., Vanhove, C., Lehnert, A., Lewellen, B., Wright, J., Mingarelli, M., Corral, C. A., Schneider, J. E., Plein, S., Newby, D. E., Welch, A., Miyaoka, R., Vandenberghe, S., & Tavares, A. A. S. (2020, Mar). Standardization of Preclinical PET/CT Imaging to Improve Quantitative Accuracy, Precision, and Reproducibility: A Multicenter Study. *J Nucl Med, 61*(3), 461-468. https://doi.org/10.2967/jnumed.119.231308

Morel, O., Mandry, D., Micard, E., Kauffmann, C., Lamiral, Z., Verger, A., Chevalier-Mathias, E., Mathias, J., Karcher, G., Meneroux, B., Rossignol, P., & Marie, P. Y. (2015, Jul). Evidence of Cyclic Changes in the Metabolism of Abdominal Aortic Aneurysms During Growth Phases: ^{18}F-FDG PET Sequential Observational Study. *J Nucl Med, 56*(7), 1030-1035. https://doi.org/10.2967/jnumed.114.146415

Moss, A. J., Sim, A. M., Adamson, P. D., Seidman, M. A., Andrews, J. P. M., Doris, M. K., Shah, A. S. V., BouHaidar, R., Alcaide-Corral, C. J., Williams, M. C., Leipsic, J. A., Dweck, M. R., MacRae, V. E., Newby, D. E., Tavares, A. A. S., & Sellers, S. L. (2020, Nov 19). Ex vivo (18)F-fluoride uptake and hydroxyapatite deposition in human coronary atherosclerosis. *Sci Rep, 10*(1), 20172. https://doi.org/10.1038/s41598-020-77391-6

New, S. E., Goettsch, C., Aikawa, M., Marchini, J. F., Shibasaki, M., Yabusaki, K., Libby, P., Shanahan, C. M., Croce, K., & Aikawa, E. (2013, Jun 21). Macrophage-derived matrix vesicles: an alternative novel mechanism for microcalcification in atherosclerotic plaques. *Circ Res, 113*(1), 72-77. https://doi.org/10.1161/circresaha.113.301036

NG156. (2020). National Institute for Health and Care Excellence. Abdominal aortic aneurysm: diagnosis and management. NICE guideline NG156.

Retrieved Accessed 21 March 2020, from https://www.nice.org.uk/guidance/NG156

Oikonomou, E. K., Marwan, M., Desai, M. Y., Mancio, J., Alashi, A., Hutt Centeno, E., Thomas, S., Herdman, L., Kotanidis, C. P., Thomas, K. E., Griffin, B. P., Flamm, S. D., Antonopoulos, A. S., Shirodaria, C., Sabharwal, N., Deanfield, J., Neubauer, S., Hopewell, J. C., Channon, K. M., Achenbach, S., & Antoniades, C. (2018, Sep 15). Non-invasive detection of coronary inflammation using computed tomography and prediction of residual cardiovascular risk (the CRISP CT study): a post-hoc analysis of prospective outcome data. *Lancet, 392*(10151), 929-939. https://doi.org/10.1016/s0140-6736(18)31114-0

Oliveira, N. F. G., Gonçalves, F. B., Hoeks, S. E., Josee van Rijn, M., Ultee, K., Pinto, J. P., Raa, S. T., van Herwaarden, J. A., de Vries, J. P. M., & Verhagen, H. J. M. (2018, Dec). Long-term outcomes of standard endovascular aneurysm repair in patients with severe neck angulation. *J Vasc Surg, 68*(6), 1725-1735. https://doi.org/10.1016/j.jvs.2018.03.427

Oliveira-Pinto, J., Ferreira, R. S., Oliveira, N. F. G., Hoeks, S., Van Rijn, M. J., Raa, S. T., Mansilha, A., Verhagen, H. J. M., & Gonçalves, F. B. (2020, Jun). Total Luminal Volume Predicts Risk after Endovascular Aneurysm Repair. *Eur J Vasc Endovasc Surg, 59*(6), 918-927. https://doi.org/10.1016/j.ejvs.2020.02.011

Osborne-Grinter, M., Kwiecinski, J., Doris, M., McElhinney, P., Cadet, S., Adamson, P. D., Moss, A. J., Alam, S., Hunter, A., Shah, A. S. V., Mills, N. L., Pawade, T., Wang, C., Weir-McCall, J. R., Roditi, G., van Beek, E. J. R., Shaw, L. J., Nicol, E. D., Berman, D., Slomka, P. J., Newby, D. E., Dweck, M. R., Dey, D., & Williams, M. C. (2022, Aug 22). Association of coronary artery calcium score with qualitatively and quantitatively assessed adverse plaque on coronary CT angiography in the SCOT-HEART trial. *Eur Heart J Cardiovasc Imaging, 23*(9), 1210-1221. https://doi.org/10.1093/ehjci/jeab135

Palasubramaniam, J., Wang, X., & Peter, K. (2019, Aug). Myocardial Infarction-From Atherosclerosis to Thrombosis. *Arterioscler Thromb Vasc Biol, 39*(8), e176-e185. https://doi.org/10.1161/atvbaha.119.312578

Parodi, J. C., Palmaz, J. C., & Barone, H. D. (1991, Nov). Transfemoral intraluminal graft implantation for abdominal aortic aneurysms. *Ann Vasc Surg, 5*(6), 491-499. https://doi.org/10.1007/bf02015271

Patel, P. R., & De Jesus, O. (2023). CT Scan. In *StatPearls*. StatPearls Publishing

Patel, R., Sweeting, M. J., Powell, J. T., & Greenhalgh, R. M. (2016, Nov 12). Endovascular versus open repair of abdominal aortic aneurysm in 15-years'

follow-up of the UK endovascular aneurysm repair trial 1 (EVAR trial 1): a randomised controlled trial. *Lancet, 388*(10058), 2366-2374. https://doi.org/10.1016/s0140-6736(16)31135-7

Pawade, T. A., Cartlidge, T. R., Jenkins, W. S., Adamson, P. D., Robson, P., Lucatelli, C., Van Beek, E. J., Prendergast, B., Denison, A. R., Forsyth, L., Rudd, J. H., Fayad, Z. A., Fletcher, A., Tuck, S., Newby, D. E., & Dweck, M. R. (2016, Oct). Optimization and Reproducibility of Aortic Valve 18F-Fluoride Positron Emission Tomography in Patients With Aortic Stenosis. *Circ Cardiovasc Imaging, 9*(10), e005131. https://doi.org/10.1161/circimaging.116.005131

Powell, J. T., Sweeting, M. J., Thompson, M. M., Ashleigh, R., Bell, R., Gomes, M., Greenhalgh, R. M., Grieve, R., Heatley, F., Hinchliffe, R. J., Thompson, S. G., & Ulug, P. (2014, Jan 13). Endovascular or open repair strategy for ruptured abdominal aortic aneurysm: 30 day outcomes from IMPROVE randomised trial. *Bmj, 348*, f7661. https://doi.org/10.1136/bmj.f7661

Powell, J. T., Sweeting, M. J., Ulug, P., Blankensteijn, J. D., Lederle, F. A., Becquemin, J. P., & Greenhalgh, R. M. (2017, Feb). Meta-analysis of individual-patient data from EVAR-1, DREAM, OVER and ACE trials comparing outcomes of endovascular or open repair for abdominal aortic aneurysm over 5 years. *Br J Surg, 104*(3), 166-178. https://doi.org/10.1002/bjs.10430

Qin, Y., Wang, Y., Liu, O., Jia, L., Fang, W., Du, J., & Wei, Y. (2017, Mar). Tauroursodeoxycholic Acid Attenuates Angiotensin II Induced Abdominal Aortic Aneurysm Formation in Apolipoprotein E-deficient Mice by Inhibiting Endoplasmic Reticulum Stress. *Eur J Vasc Endovasc Surg, 53*(3), 337-345. https://doi.org/10.1016/j.ejvs.2016.10.026

Quintana, R. A., & Taylor, W. R. (2019, Feb 15). Cellular Mechanisms of Aortic Aneurysm Formation. *Circ Res, 124*(4), 607-618. https://doi.org/10.1161/circresaha.118.313187

Ritman, E. L. (2007, Oct 1). Small-animal CT - Its Difference from, and Impact on, Clinical CT. *Nucl Instrum Methods Phys Res A, 580*(2), 968-970. https://doi.org/10.1016/j.nima.2007.06.040

Sah, B. R., Husmann, L., Mayer, D., Scherrer, A., Rancic, Z., Puippe, G., Weber, R., & Hasse, B. (2015, Apr). Diagnostic performance of 18F-FDG-PET/CT in vascular graft infections. *Eur J Vasc Endovasc Surg, 49*(4), 455-464. https://doi.org/10.1016/j.ejvs.2014.12.024

Saida, T., Mori, K., Sato, F., Shindo, M., Takahashi, H., Takahashi, N., Sakakibara, Y., & Minami, M. (2012, Mar). Prospective intraindividual comparison of unenhanced magnetic resonance imaging vs contrast-enhanced computed tomography for the planning of endovascular abdominal

aortic aneurysm repair. *J Vasc Surg, 55*(3), 679-687. https://doi.org/10.1016/j.jvs.2011.09.091

Sakalihasan, N., Limet, R., & Defawe, O. D. (2005, Apr 30-May 6). Abdominal aortic aneurysm. *Lancet, 365*(9470), 1577-1589. https://doi.org/10.1016/s0140-6736(05)66459-8

Sakaue, T., Suzuki, J., Hamaguchi, M., Suehiro, C., Tanino, A., Nagao, T., Uetani, T., Aono, J., Nakaoka, H., Kurata, M., Sakaue, T., Okura, T., Yasugi, T., Izutani, H., Higaki, J., & Ikeda, S. (2017, Oct). Perivascular Adipose Tissue Angiotensin II Type 1 Receptor Promotes Vascular Inflammation and Aneurysm Formation. *Hypertension, 70*(4), 780-789. https://doi.org/10.1161/hypertensionaha.117.09512

Salata, K., Syed, M., Hussain, M. A., de Mestral, C., Greco, E., Mamdani, M., Tu, J. V., Forbes, T. L., Bhatt, D. L., Verma, S., & Al-Omran, M. (2018, Oct 2). Statins Reduce Abdominal Aortic Aneurysm Growth, Rupture, and Perioperative Mortality: A Systematic Review and Meta-Analysis. *J Am Heart Assoc, 7*(19), e008657. https://doi.org/10.1161/jaha.118.008657

Sampson, U. K., Norman, P. E., Fowkes, F. G., Aboyans, V., Song, Y., Harrell, F. E., Jr., Forouzanfar, M. H., Naghavi, M., Denenberg, J. O., McDermott, M. M., Criqui, M. H., Mensah, G. A., Ezzati, M., & Murray, C. (2014, Mar). Estimation of global and regional incidence and prevalence of abdominal aortic

aneurysms 1990 to 2010. *Glob Heart, 9*(1), 159-170. https://doi.org/10.1016/j.gheart.2013.12.009

Schanzer, A., Greenberg, R. K., Hevelone, N., Robinson, W. P., Eslami, M. H., Goldberg, R. J., & Messina, L. (2011, Jun 21). Predictors of abdominal aortic aneurysm sac enlargement after endovascular repair. *Circulation, 123*(24), 2848-2855. https://doi.org/10.1161/circulationaha.110.014902

Shen, Y. H., & LeMaire, S. A. (2017, Mar). Molecular pathogenesis of genetic and sporadic aortic aneurysms and dissections. *Curr Probl Surg, 54*(3), 95-155. https://doi.org/10.1067/j.cpsurg.2017.01.001

Sidloff, D. A., Gokani, V., Stather, P. W., Choke, E., Bown, M. J., & Sayers, R. D. (2014, Oct). Type II endoleak: conservative management is a safe strategy. *Eur J Vasc Endovasc Surg, 48*(4), 391-399. https://doi.org/10.1016/j.ejvs.2014.06.035

Singh, M., Ziganshin, B. A., & Elefteriades, J. A. (2018). Aortic Aneurysm. In R. S. Vasan & D. B. Sawyer (Eds.), *Encyclopedia of Cardiovascular Research and Medicine* (pp. 123-142). Elsevier. https://doi.org/https://doi.org/10.1016/B978-0-12-809657-4.99690-X

Spanos, K., Behrendt, C. A., Kouvelos, G., Giannoukas, A. D., & Kölbel, T. (2020, Aug 21). A new randomized controlled trial on abdominal aortic

aneurysm repair is needed. *J Vasc Surg*. https://doi.org/10.1016/j.jvs.2020.06.102

Stather, P. W., Wild, J. B., Sayers, R. D., Bown, M. J., & Choke, E. (2013, Oct). Endovascular aortic aneurysm repair in patients with hostile neck anatomy. *J Endovasc Ther, 20*(5), 623-637. https://doi.org/10.1583/13-4320mr.1

Suckow, B. D., Goodney, P. P., Columbo, J. A., Kang, R., Stone, D. H., Sedrakyan, A., Cronenwett, J. L., & Fillinger, M. F. (2018, Jun). National trends in open surgical, endovascular, and branched-fenestrated endovascular aortic aneurysm repair in Medicare patients. *J Vasc Surg, 67*(6), 1690-1697.e1691. https://doi.org/10.1016/j.jvs.2017.09.046

Sweeting, M. J., Thompson, S. G., Brown, L. C., & Powell, J. T. (2012, May). Meta-analysis of individual patient data to examine factors affecting growth and rupture of small abdominal aortic aneurysms. *Br J Surg, 99*(5), 655-665. https://doi.org/10.1002/bjs.8707

Syed, M. B., Fletcher, A. J., Forsythe, R. O., Kaczynski, J., Newby, D. E., Dweck, M. R., & van Beek, E. J. (2019, Nov). Emerging techniques in atherosclerosis imaging. *Br J Radiol, 92*(1103), 20180309. https://doi.org/10.1259/bjr.20180309

Syed, M. B. J., Fletcher, A. J., Debono, S., Forsythe, R. O., Williams, M. C., Dweck, M. R., Shah, A. S. V., Macaskill, M. G., Tavares, A., Denvir, M. A., Lim, K., Wallace, W. A., Kaczynski, J., Clark, T., Sellers, S. L., Masson, N., Falah, O., Chalmers, R. T. A., Tambyraja, A. L., van Beek, E. J. R., & Newby, D. E. (2022, Jul). (18)F-Sodium Fluoride Positron Emission Tomography and Computed Tomography in Acute Aortic Syndrome. *JACC Cardiovasc Imaging, 15*(7), 1291-1304. https://doi.org/10.1016/j.jcmg.2022.01.003

Syed, M. B. J., Fletcher, A. J., Dweck, M. R., Forsythe, R., & Newby, D. E. (2019, Nov). Imaging aortic wall inflammation. *Trends Cardiovasc Med, 29*(8), 440-448. https://doi.org/10.1016/j.tcm.2018.12.003

Takagi, H., Ando, T., & Umemoto, T. (2018, Mar). Abdominal Aortic Aneurysm Screening Reduces All-Cause Mortality: Make Screening Great Again. *Angiology, 69*(3), 205-211. https://doi.org/10.1177/0003319717693107

Taqueti, V. R., Di Carli, M. F., Jerosch-Herold, M., Sukhova, G. K., Murthy, V. L., Folco, E. J., Kwong, R. Y., Ozaki, C. K., Belkin, M., Nahrendorf, M., Weissleder, R., & Libby, P. (2014, Nov). Increased microvascularization and vessel permeability associate with active inflammation in human atheromata. *Circ Cardiovasc Imaging, 7*(6), 920-929. https://doi.org/10.1161/circimaging.114.002113

Tarkin, J. M., Dweck, M. R., Evans, N. R., Takx, R. A., Brown, A. J., Tawakol, A., Fayad, Z. A., & Rudd, J. H. (2016, Feb 19). Imaging Atherosclerosis. *Circ Res, 118*(4), 750-769. https://doi.org/10.1161/circresaha.115.306247

Tzolos, E., Bing, R., Andrews, J., MacAskill, M. G., Tavares, A. A. S., Macnaught, G., Clark, T., Mills, N. L., Fujisawa, T., Nash, J., Dey, D., Slomka, P. J., Koglin, N., Stephens, A. W., Deutsch, M. A., van Beek, E. J. R., Williams, M. C., Hermann, S., Hugenberg, V., Dweck, M. R., & Newby, D. E. (2023, Jun). Noninvasive In Vivo Coronary Artery Thrombus Imaging. *JACC Cardiovasc Imaging, 16*(6), 820-832. https://doi.org/10.1016/j.jcmg.2022.10.002

Tzolos, E., Bing, R., Newby, D. E., & Dweck, M. R. (2021, Aug 7). Categorising myocardial infarction with advanced cardiovascular imaging. *Lancet, 398*(10299), e9. https://doi.org/10.1016/s0140-6736(21)01329-5

Tzolos, E., & Dweck, M. R. (2020, Jul). (18)F-Sodium Fluoride ((18)F-NaF) for Imaging Microcalcification Activity in the Cardiovascular System. *Arterioscler Thromb Vasc Biol, 40*(7), 1620-1626. https://doi.org/10.1161/atvbaha.120.313785

Tzolos, E., Kwiecinski, J., Lassen, M. L., Cadet, S., Adamson, P. D., Moss, A. J., Joshi, N., Williams, M. C., van Beek, E. J. R., Dey, D., Berman, D. S., Dweck, M. R., Newby, D. E., & Slomka, P. J. (2020, Jun 11). Observer repeatability and interscan reproducibility of 18F-sodium fluoride coronary

microcalcification activity. *J Nucl Cardiol*. https://doi.org/10.1007/s12350-020-02221-1

Tzolos, E., McElhinney, P., Williams, M. C., Cadet, S., Dweck, M. R., Berman, D. S., Slomka, P. J., Newby, D. E., & Dey, D. (2021, Jan-Feb). Repeatability of quantitative pericoronary adipose tissue attenuation and coronary plaque burden from coronary CT angiography. *J Cardiovasc Comput Tomogr, 15*(1), 81-84. https://doi.org/10.1016/j.jcct.2020.03.007

Tzolos, E., Williams, M. C., McElhinney, P., Lin, A., Grodecki, K., Flores Tomasino, G., Cadet, S., Kwiecinski, J., Doris, M., Adamson, P. D., Moss, A. J., Alam, S., Hunter, A., Shah, A. S. V., Mills, N. L., Pawade, T., Wang, C., Weir-McCall, J. R., Roditi, G., van Beek, E. J. R., Shaw, L. J., Nicol, E. D., Berman, D. S., Slomka, P. J., Dweck, M. R., Newby, D. E., & Dey, D. (2022, Jun). Pericoronary Adipose Tissue Attenuation, Low-Attenuation Plaque Burden, and 5-Year Risk of Myocardial Infarction. *JACC Cardiovasc Imaging, 15*(6), 1078-1088. https://doi.org/10.1016/j.jcmg.2022.02.004

Ulug, P., Powell, J. T., Martinez, M. A., Ballard, D. J., & Filardo, G. (2020, Jul 1). Surgery for small asymptomatic abdominal aortic aneurysms. *Cochrane Database Syst Rev, 7*(7), Cd001835. https://doi.org/10.1002/14651858.CD001835.pub5

Vaidyanathan, S., Patel, C. N., Scarsbrook, A. F., & Chowdhury, F. U. (2015, Jul). FDG PET/CT in infection and inflammation--current and emerging clinical applications. *Clin Radiol, 70*(7), 787-800. https://doi.org/10.1016/j.crad.2015.03.010

van Schaik, T. G., Yeung, K. K., Verhagen, H. J., de Bruin, J. L., van Sambeek, M., Balm, R., Zeebregts, C. J., van Herwaarden, J. A., & Blankensteijn, J. D. (2017, Nov). Long-term survival and secondary procedures after open or endovascular repair of abdominal aortic aneurysms. *J Vasc Surg, 66*(5), 1379-1389. https://doi.org/10.1016/j.jvs.2017.05.122

Vaz, S., Falkmer, T., Passmore, A. E., Parsons, R., & Andreou, P. (2013). The case for using the repeatability coefficient when calculating test-retest reliability. *PLoS One, 8*(9), e73990. https://doi.org/10.1371/journal.pone.0073990

Vesey, A. T., Jenkins, W. S., Irkle, A., Moss, A., Sng, G., Forsythe, R. O., Clark, T., Roberts, G., Fletcher, A., Lucatelli, C., Rudd, J. H., Davenport, A. P., Mills, N. L., Al-Shahi Salman, R., Dennis, M., Whiteley, W. N., van Beek, E. J., Dweck, M. R., & Newby, D. E. (2017, Mar). (18)F-Fluoride and (18)F-Fluorodeoxyglucose Positron Emission Tomography After Transient Ischemic Attack or Minor Ischemic Stroke: Case-Control Study. *Circ Cardiovasc Imaging, 10*(3), e004976. https://doi.org/10.1161/circimaging.116.004976

Wall, C., Huang, Y., Le, E. P. V., Ćorović, A., Uy, C. P., Gopalan, D., Ma, C., Manavaki, R., Fryer, T. D., Aloj, L., Graves, M. J., Tombetti, E., Ariff, B., Bambrough, P., Hoole, S. P., Rusk, R. A., Jayne, D. R., Dweck, M. R., Newby, D., Fayad, Z. A., Bennett, M. R., Peters, J. E., Slomka, P., Dey, D., Mason, J. C., Rudd, J. H. F., & Tarkin, J. M. (2021, Sep). Pericoronary and periaortic adipose tissue density are associated with inflammatory disease activity in Takayasu arteritis and atherosclerosis. *Eur Heart J Open, 1*(2), oeab019. https://doi.org/10.1093/ehjopen/oeab019

Wanhainen, A., Hultgren, R., Linné, A., Holst, J., Gottsäter, A., Langenskiöld, M., Smidfelt, K., Björck, M., & Svensjö, S. (2016, Oct 18). Outcome of the Swedish Nationwide Abdominal Aortic Aneurysm Screening Program. *Circulation, 134*(16), 1141-1148. https://doi.org/10.1161/circulationaha.116.022305

Wanhainen, A., Verzini, F., Van Herzeele, I., Allaire, E., Bown, M., Cohnert, T., Dick, F., van Herwaarden, J., Karkos, C., Koelemay, M., Kölbel, T., Loftus, I., Mani, K., Melissano, G., Powell, J., Szeberin, Z., Esvs Guidelines, C., de Borst, G. J., Chakfe, N., Debus, S., Hinchliffe, R., Kakkos, S., Koncar, I., Kolh, P., Lindholt, J. S., de Vega, M., Vermassen, F., Document, R., Björck, M., Cheng, S., Dalman, R., Davidovic, L., Donas, K., Earnshaw, J., Eckstein, H. H., Golledge, J., Haulon, S., Mastracci, T., Naylor, R., Ricco, J. B., & Verhagen, H. (2019, Jan). Editor's Choice - European Society for Vascular Surgery (ESVS) 2019 Clinical Practice Guidelines on the Management of Abdominal

Aorto-iliac Artery Aneurysms. *Eur J Vasc Endovasc Surg, 57*(1), 8-93. https://doi.org/10.1016/j.ejvs.2018.09.020

Waton, S., Johal, A., Birmpili, P., Li, Q., Cromwell, D., Pherwani, A., O'Neill, R., & Boyle, J. (2020). *National Vascular Registry: 2020 Annual report.* https://www.vsqip.org.uk/reports/2020-annual-report/

Waton, S., Johal, A., Birmpili, P., Li, Q., Cromwell, D., Williams, R., & Pherwani, A. (2022). *National Vascular Registry: 2022 Annual report.* https://www.vsqip.org.uk/reports/2022-annual-report/

Wen, W., Gao, M., Yun, M., Meng, J., Yu, W., Zhu, Z., Tian, Y., Mou, T., Zhang, Y., Hacker, M., Li, S., Yu, Y., Li, X., & Zhang, X. (2022, 11 May 2022). In Vivo Coronary (18)F-Sodium Fluoride Activity. *JACC: Cardiovascular Imaging, 0*(online). https://doi.org/doi:10.1016/j.jcmg.2022.03.018

Whittington, B., Tzolos, E., Bing, R., Andrews, J., Lucatelli, C., MacAskill, M. G., Tavares, A. A. S., Clark, T., Mills, N. L., Nash, J., Dey, D., Slomka, P. J., Koglin, N., Stephens, A. W., van Beek, E. J. R., Smith, C., Dweck, M. R., Williams, M. C., Whiteley, W., Wardlaw, J. M., & Newby, D. E. (2023, Jul 13). Noninvasive In Vivo Thrombus Imaging in Patients With Ischemic Stroke or Transient Ischemic Attack. *Arterioscler Thromb Vasc Biol*. https://doi.org/10.1161/atvbaha.122.318204

Williams, M. C., Kwiecinski, J., Doris, M., McElhinney, P., D'Souza, M. S., Cadet, S., Adamson, P. D., Moss, A. J., Alam, S., Hunter, A., Shah, A. S. V., Mills, N. L., Pawade, T., Wang, C., Weir McCall, J., Bonnici-Mallia, M., Murrills, C., Roditi, G., van Beek, E. J. R., Shaw, L. J., Nicol, E. D., Berman, D. S., Slomka, P. J., Newby, D. E., Dweck, M. R., & Dey, D. (2020, May 5). Low-Attenuation Noncalcified Plaque on Coronary Computed Tomography Angiography Predicts Myocardial Infarction: Results From the Multicenter SCOT-HEART Trial (Scottish Computed Tomography of the HEART). *Circulation, 141*(18), 1452-1462. https://doi.org/10.1161/circulationaha.119.044720

Wilmink, A. B., Forshaw, M., Quick, C. R., Hubbard, C. S., & Day, N. E. (2002). Accuracy of serial screening for abdominal aortic aneurysms by ultrasound. *J Med Screen, 9*(3), 125-127. https://doi.org/10.1136/jms.9.3.125

Wu, J. C., & Nguyen, P. K. (2011, Aug 2). Imaging atherosclerosis with F18-fluorodeoxyglucose positron emission tomography: What are we actually seeing? *J Am Coll Cardiol, 58*(6), 615-617. https://doi.org/10.1016/j.jacc.2011.04.021

Xiong, W., Zhao, Y., Prall, A., Greiner, T. C., & Baxter, B. T. (2004, Feb 15). Key roles of CD4+ T cells and IFN-gamma in the development of abdominal aortic aneurysms in a murine model. *J Immunol, 172*(4), 2607-2612. https://doi.org/10.4049/jimmunol.172.4.2607

Youn, T., Al'Aref, S. J., Narula, N., Salvatore, S., Pisapia, D., Dweck, M. R., Narula, J., Lin, F. Y., Lu, Y., Kumar, A., Virmani, R., & Min, J. K. (2020, Feb). (18)F-Sodium Fluoride Positron Emission Tomography/Computed Tomography in Ex Vivo Human Coronary Arteries With Histological Correlation. *Arterioscler Thromb Vasc Biol, 40*(2), 404-411. https://doi.org/10.1161/atvbaha.119.312737